ACIBADEM MEHMET ALİ AYDINLAR UNIVERSITY

GRADUATE SCHOOL OF NATURAL AND APPLIED SCIENCES

PREPARATION OF BIOADHESIVE MICROPARTICLES CONTAINING DRUG-LOADED AND PEPTIDE CONJUGATED POLYMERIC MICELLES EFFECTIVE IN LUNG CANCER

ALİ BORA BAYIK

M.Sc. THESIS

DEPARTMENT OF BIOMATERIALS

SUPERVISOR

Assoc. Prof. Gülen Melike Demirbolat

SECONDARY SUPERVISOR

Assoc. Prof. Özgül Gök Özatay

İSTANBUL-2025

ACIBADEM MEHMET ALİ AYDINLAR UNIVERSITY

GRADUATE SCHOOL OF NATURAL AND APPLIED SCIENCES

PREPARATION OF BIOADHESIVE MICROPARTICLES CONTAINING DRUG-LOADED AND PEPTIDE CONJUGATED POLYMERIC MICELLES EFFECTIVE IN LUNG CANCER

ALİ BORA BAYIK

M.Sc. THESIS

DEPARTMENT OF BIOMATERIALS

SUPERVISOR

Assoc. Prof. Gülen Melike Demirbolat

SECONDARY SUPERVISOR

Assoc. Prof. Özgül Gök Özatay

İSTANBUL-2025

Department: Biomaterials
Program: Biomaterials Program
Thesis Title: Preparatıon Of Bıoadhesıve Mıcropartıcles Containing Drug-Loaded And Peptıde Conjugated Polymerıc Mıcelles Effectıve In Lung Cancer
Student's name and surname: Ali Bora Bayık
Date of Defence: 01/ 07/ 2025

This is to certify that I have examined this copy of the master thesis. I confirm that she/he prepared after fulfilling the specified requirements in the associated legislations before the final examining committee whose signatures are below.

		Signature
Jury Member (Supervisor of the Thesis)	Assoc. Prof. Gülen Melike Demirbolat Acibadem Mehmet Ali Aydinlar University, Faculty of Pharmacy, Department Of Pharmaceutical Technology, Department Of Pharmaceutical Technology	……..……
Jury Member (Second Supervisor of the Thesis)	Assoc. Prof. Özgül Gök Özatay Acibadem Mehmet Ali Aydinlar University, Faculty of Engineering and Natural Sciences, Department Of Biomedical Engineering, Biomedical Engineering Pr.	……..……
Jury Member	Assist. Prof. Ayşegül Kavas Acibadem Mehmet Ali Aydinlar University, Faculty of Engineering and Natural Sciences, Department Of Biomedical Engineering, Biomedical Engineering Pr.	……..……
Jury Member	Assist. Prof. Ebru Altuntaş Istanbul University, Faculty of Pharmacy, Department Of Pharmaceutical Technology, Department Of Pharmaceutical Technology	……..……
Jury Member	Assist. Prof. Ongun Mehmet Saka Ankara University, Faculty of Pharmacy, Department Of Pharmaceutical Technology, Department Of Pharmaceutical Technology	……..……

DECLARATION

I declare that this thesis work is my own work, I had no unethical behavior at any stages from the planning to the writing of the thesis, I obtained all the information in this thesis in accordance with academic and ethical rules, I cited all the information and comments that were not obtained with this thesis work, and I provided resources in the list of references. I also declare that there was no violation of any patents and copyrights during the study and writing of this thesis.

01/07/2025

Ali Bora Bayık

PREFACE AND ACKNOWLEDGEMENT

First of all, I would like to thank my supervisor Assoc. Prof. Dr. Gülen Melike Demirbolat for her patience and supportive attitude throughout the studies. What she has added to me by carrying out this study with me will always be etched in my memory. I would like to thank Assoc. Prof. Dr. Özgül Gök Özatay for her unwavering support throughout the studies. I would like to thank my mother (Nursel Kesercioğlu) and my valuable friends for their unwavering moral support throughout my master's degree.

I would like to express my sincere gratitude to The Scientific and Technological Research Council of Türkiye (TÜBİTAK). This master's thesis was supported by TÜBİTAK Directorate of Science Fellowships and Grant Programmes (BİDEB) 2211-C (Application Number:1649B022303568) priority Fields graduate scholarship program. Being a recipient of this scholarship is an honor, and I am truly thankful for the opportunity.

Also, this study was supported by Acıbadem Mehmet Ali Aydınlar University Scientific Research Projects Commission (ABAPKO, titled "Akciğer Kanserinde Etkili Ilaç Yüklü Polimerik Misel Içeren Biyoadhezif Mikropartiküllerin Geliştirilmesi", project no. ABAPKO 2022/02-05).

TABLE OF CONTENTS

LIST OF ABBREVIATIONS AND SYMBOLS

4E-BP1	Eukaryotic Translation Initiation Factor 4E-Binding Protein
ACN	Acetonitrile
ALK	Anaplastic lymphoma kinase
ATS	American Thoracic Society
CA	Cellulose acetate
CFC	Chlorofluorocarbon
CMC	Critical Micelle Concentration
CMT	Critical micelle temperature
COOH-PEG-PLA	Carboxylic acid-poly(ethylene glycol)-b-poly(D,L-lactide)
COPD	Chronic obstructive pulmonary disease
COP	Not listed (assumed typo or abbreviation missing full form)
DHFR	Dihydrofolate reductase
DIC	N,N'-Diisopropylcarbodiimide
DMF	N,N-Dimethylformamide
DNA	Deoxyribonucleic acid
DPI	Dry powder inhalers
DLS	Dynamic light scattering
EC	Ethylcellulose
EE (%)	Encapsulation efficiency

Eq	Equation
ERS	European Respiratory Society
EPR	Enhanced permeability and retention
EVE	Everolimus
FT-IR	Fourier Transform Infrared Spectroscopy
GPC	Gel Permeation Chromatography
GnRH	Gonadotropin-releasing hormone
HFA	Hydrofluoroalkane
HPMC	Hydroxypropyl methyl cellulose
IARC	International Agency for Research on Cancer
MC	Methylcellulose
MDI	Metered-dose inhalers
MPs	Microparticles
mPEG-PLA	Methoxy poly(ethylene glycol)-b-poly(L-lactide)
mTOR	Mechanistic target of rapamycin
Na-CMC	Sodium carboxymethylcellulose
NHS-PEG-PLA	N-Hydroxysuccinimide ester-poly(ethyleneglycol)-b-poly(D,L-lactide)
NSCLC	Non-small cell lung cancer
PBS	Phosphate buffered saline
PCL	Polycaprolactone

PDI	Polydispersity index
PEG	Polyethylene glycol
PET	Positron emission tomography
PLA	Polylactic acid
PLGA	Poly(lactic-co-glycolic acid)
PMs	Polymeric micelles
PY (%)	Production yield
RGD	Arginine-glycine-aspartic acid
RGDK	Arginine-glycine-aspartic acid-lysine
SCLC	Small cell lung cancer
SD	Standard deviation
SEM	Scanning electron microscopy
SLF	Simulated Lung Fluid
TEM	Transmission electron microscopy
THF	Tetrahydrofuran
UV-Vis	Ultraviolet–Visible Spectroscopy
WHO	World Health Organization

LIST OF FIGURES

LIST OF IMAGES

LIST OF TABLES

SUMMARY

Preparation of Bioadhesive Microparticles Containing Drug-Loaded and Peptide Conjugated Polymeric Micelles Effective In Lung Cancer

Lung cancer is one of the cancers with the highest mortality risk. Everolimus is a rapamycin analog and is an immunosuppressant and anti-cancer agent. Everolimus is characterized by low bioavailability in oral administration and low patient compliance in IV administration. Polymeric micelles stand out as drug delivery systems with their ability for active targeting and high loading capacities. Microparticular microparticles suitable for pulmonary delivery with bioadhesive properties such as HPMC provide many advantages. Within the scope of the thesis study, it was aimed to develop everolimus loaded RGD conjugated polymeric micelle integrated HPMC microparticles. Within the scope of the thesis, everolimus was encapsulated in polymeric micelles containing two different functional groups. RGD peptide was conjugated to the micelle containing the third functional group. RGD conjugation was successfully performed. Drug-loaded micelles were obtained in targeted sizes, monodisperse and stable. Micelle integrated HPMC microparticles were produced by spray drying method. The produced dry powder produced in sizes that are effective in pulmonary delivery. The bioadhesive properties of HPMC microparticles in artificial lung fluid were demonstrated and in vitro swelling behaviour was investigated. As a result, RGD conjugated polymeric micelle integrated HPMC microparticles with potential for use in the treatment of lung cancer were developed in this thesis.

Keywords: Targeted drug delivery system, Polymeric micelles, Microparticles, Lung cancer, Everolimus

ÖZET

Akciğer Kanserinde Etkili İlaç Yüklü ve Peptit Konjuge Polimerik Misel İçeren Biyoadhezif Mikropartiküllerin Geliştirilmesi

Mortalite riski en çok olan kanser türlerinden biri akciğer kanseridir. Everolimus bir rapamisin analoğu olup immunosüpresan ve anti-kanser bir ajandır. Everolimus oral verilişte düşük biyoyararlanıma sahip olmakla birlikte IV uygulamalarda düşük hasta uyuncu ile karakterizedir. Polimerik miseller ilaç taşıcı sistemler olarak aktif hedeflendirmeye açık yapısı ve yüksek yükleme kapasiteleri ile ön plana çıkmaktadır. HPMC gibi biyo-adhezif özellikler gösteren pulmoner verilişe uygun mikropartiküler birçok avantaj sağlar. Tez çalışması kapsamında everolimus yüklü RGD konjuge polimerik misel entegre HPMC mikropartiküllerinin geliştirilmesi hedeflenmiştir. Tez kapsamında iki farklı fonksiyonel grup içeren polimerik misele everolimus enkapsüle edilmiştir. Üçüncü fonksiyonel grubu içeren misele RGD peptidi konjuge edilmiştir. RGD konjugasyonu başarıyla gerçekleştirilmiştir. İlaç yüklü miseller hedeflenen boyutlarda, monodispers yapıda ve stabil olarak elde edilebilmiştir. Misel entegre HPMC mikropartikülleri püskürtürek kurutma metotu üretilmiştir. Üretilen kuru toz pulmoner verilişte etkin olan boyutlarda üretilebilmiştir. HPMC mikropartiküllerinin yapay akciğer sıvısında biyoadhezif özelliği gösterilmiş ve in-vitro şişme davranışları incelenmiştir. Sonuç olarak, tez çalışmasında akciğer kanseri tedavisinde kullanılmaya potansiyel olan RGD konjuge polimerik misel entegre edilmiş HPMC mikropartiküller geliştirilmiştir.

Anahtar Sözcükler: Hedeflendirilmiş ilaç taşıma sistemi, Polimerik misel, Mikropartikül, Akciğer Kanseri, Everolimus

1. INTRODUCTION AND AIM

Cancer is a widespread disease whose prevalence has increased with the increase in life expectancy resulting from medical advances in the last century. Cancer has been seen in all age groups and its progression varies according to the region and organ affected . Despite the advent of diverse treatment approaches such as chemotherapy, radiotherapy and surgery, cancer remains one of the diseases with the highest mortality rates. Lung cancer is among the most deadly forms of the disease. It accounts for 19% of cancer deaths worldwide and 3% of all deaths. Two main types of lung cancer have been identified: non-small cell lung cancer (NSCLC) and small cell lung cancer (SCLC).

Everolimus is a rapamycin analogue with anticancer and immunosuppressive properties, from the class of first-generation mTOR inhibitors. In 2009, it was approved by the United States Food and Drug Administration (FDA) for the treatment of renal cell carcinoma. Its effectiveness and safety have been reported in individuals with previously treated non-small cell lung cancer (NSCLC). However, when administered orally, it exhibits a high protein binding rate and low bioavailability due to its first-pass effect in the liver. It is frequently administered parenterally in the treatment of CSCLC, but adverse effects such as fatigue, abnormal bleeding, jaundice and dyspnea can reduce patient compliance.

Polymeric micelles are one of the carrier materials used in targeted drug delivery systems. The prominent features of polymeric micelles are that they form micelles spontaneously in the solvent and that their various forms allow active targeting against tumors via amino acid groups. It is possible to form copolymeric structures with polymeric micelles. These structures form two separate functional compartments defined as core and shell. The outer shell is responsible for in vivo pharmacokinetic properties, while the inner core is responsible for drug entrapment, stability and drug release properties. While hydrophobic drugs are encapsulated in the core, the surface can be modified according to desired properties, an advantage unique to polymeric micelles.

Inhalation technology is one of the treatment methods employed in the management of certain pathologies as a drug delivery system. The pulmonary route of administration of drugs with the so-called dry powder inhaler provides certain advantages. These advantages include the ability to achieve the desired effect at a much lower dose due to the wide tissue distribution in the lungs, the first pass effect in the liver in the systemic route if the targeted site of the therapeutic effect is the lung, bypassing obstacles such as oral absorption, decreasing bioavailability.

Bioadhesion is the binding of synthetic or natural polymers to a biological substrate. The use of bioadhesive biopolymers in targeted drug systems has many advantages. Increased absorption by prolonging the residence time of the drug, increased absorption due to more blood flow and blood flow velocity, prevention of the first pass effect, prevention of degradation in the gastrointestinal tract, increased patient compliance with easier administration compared to parenteral route, faster onset of action compared to oral administration, etc.

Microparticles are spherical particles consisting of proteins or synthetic polymers with an average particle size ranging from 1 to 50 μm. Microparticles produced using biopolymers with bioadhesive properties can be loaded with anticancer drugs and applied as microspheres to reduce the toxic effects of the relevant drugs and controlled release of the drugs can be realized.

Two different strategies are utilised to target drug delivery systems to specific tissues. The passive targeting strategy is based on the natural accumulation of drug carrier systems in highly permeable tissues, such as tumours and tissues with poor lymphatic drainage. In active targeting, ligands such as antibody peptides with affinity for the receptors of the targeted cells are used on the surface of the carrier. In this manner, carrier systems bind specifically to the target cell and perform effective transport.

The aim of this thesis is to develop a formulation to increase the bioavailability of everolimus and thus its effectiveness in treatment. The formulation combines nanotechnological approaches with controlled/altered and targeted release systems. It

is based on the encapsulation of everolimus in an innovative drug delivery system and its design as microparticles that can adhere to the lung mucosa. The system designed in the thesis study constitutes an unprecedented combination in the relevant literature with regard to both its composition and the purpose of its development.

2. BACKGROUND

2.1. Cancer and Lung Cancer

Cancer is a disease characterised by uncontrolled and abnormal cell division, with a tendency to spread to external tissues such as the liver, brain and bone via lymph and blood circulation, which may result in mortality. Lung cancer, otherwise known as bronchogenic carcinoma, is defined as malignancies arising from the lung parenchyma. The incidence and mortality rates of lung cancer are increasing, due to a variety of environmental and genetic factors. Environmental factors can be categorised into numerous sub-factors, including chemical factors (e.g. smoking, alcohol, asbestos), physical factors (e.g. ultraviolet rays, radon gas), and biological factors (e.g. Helicobacter pylori, human papillomavirus). Genetic predispositions can be summarised as follows: they are constituted by inherited disorders and changes in tumour suppressor genes (1). According to data published by the International Agency for Research on Cancer (IARC) of the World Health Organization (WHO), approximately 20 million new cancer cases and 9.7 million cancer-related deaths were reported worldwide in 2022. As demonstrated in Figure 2, among all other cancer types, lung cancer has the highest incidence (2).

Lung cancer is the most common type of cancer resulting in death, with a mortality rate of 18.4%. The elevated mortality rate in comparison to other cancerous afflictions can be attributed to the following factors: the late stages of diagnosis, the challenges associated with treatment, and the prevalence of metastasis in other regions (3). The frequency of diagnosis by gender indicates that this is the most commonly diagnosed cancer in men and the leading cause of cancer-related deaths. In women, it is the third most frequently diagnosed cancer type, following breast and colon cancer (4). Since the 1920s, there has been an upward trend in the incidence of the condition among men. Among women, however, the same tendency has only become apparent since the 1960s. The causes of this discrepancy are twofold: increased consumption of tobacco products and greater exposure to air pollution. A variety of factors have been identified as contributing to the development of lung cancer, including passive smoking, exposure to asbestos and radon gas, chronic obstructive pulmonary disease, recurrent

inflammation in the lung, sequelae in the lung, and exposure to chemicals such as polycyclic aromatic hydrocarbons, chromium, nickel, and organic arsenic compounds produced by the combustion of organic materials. Furthermore, patients diagnosed with head and neck cancer, in addition to those with a personal or family history of lung cancer, are considered to be genetically predisposed (5).

2.1.1. Subtypes of Lung Cancer

In the past, the classification of lung cancer was based on immunohistologic principles, namely the staining of biopsy and cytology specimens taken from lung tissue with various staining materials, and the subsequent examination of these samples under a light microscope. Recent advancements in the molecular biology, coupled with the identification of drugs tailored to specific lung cancer subtypes, have prompted a revised pathological classification of lung cancer. This revision was determined by a consensus of the International Association for the Study of Lung Cancer (IASLC), the American Thoracic Society (ATS), and the European Respiratory Society (ERS) (6-7). According to the most recent classification system promulgated by the World Health Organization (WHO), lung cancer is categorised as either small cell lung cancer (SCLC) or the heterogeneous group of non-small cell lung cancer (NSCLC), which includes squamous cell carcinoma, adenocarcinoma and large cell carcinoma (8).

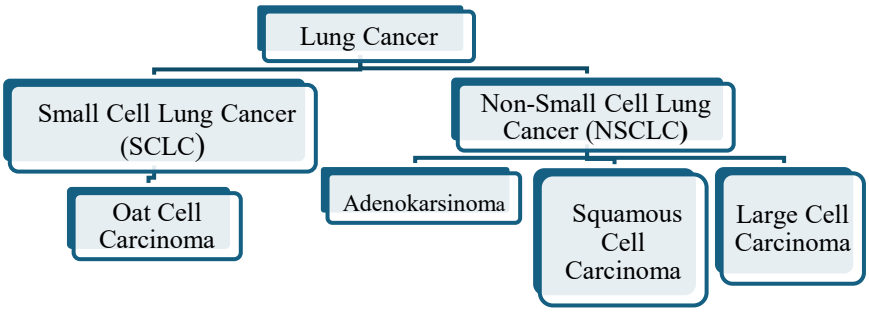

Figure 2.1. Classification of Lung Cancer (8)

2.1.1.1. Small Cell Lung Cancer (SCLC)

Small Cell Lung Cancer (SCLC) represents 15% of all lung cancers and is characterised by an aggressive progression, predominantly affecting smokers (8). The prognosis for this condition is often poor, due to the tendency of the cancer to metastasize rapidly and to grow quickly. SCLC cells are characterised by their round or oval shape, diminutive size and minimal cytoplasm. Immunopathologically, mutations in p53 and Rb tumour suppressor genes occur frequently in SCLC, contributing to the uncontrolled continuation of the cell cycle and tumour development (8, 9). Furthermore, the expression of programmed death ligand 1 (PD-L1) is found to be minimal in SCLC, thus indicating a potential limited response to immunotherapies (9).

2.1.1.2. Non-Small Cell Lung Cancer (NSCLC)

It is the second main type of lung cancer, which accounts for approximately 80-85% of all lung cancers and has various histologic subtypes (8). Since the disease is diagnosed in advanced stages, five-year survival rates are low. There are three subtypes of NSCLC; adenocarcinoma, squamous cell carcinoma and large cell carcinoma. Adenocarcinoma accounts for approximately 40% of NSCLC cases. Although it is the most commonly diagnosed cancer type in non-smokers, it is also highly associated with smoking (10). Adenocarcinomas usually form glandular structures. Their nuclei are prominent and oval or round nuclei are characterized by abundant cytoplasm (11). Genetically, mutations in EFGR and KRAS genes are observed at approximately the same rate (10). Translocations in the anaplastic lymphoma kinase (ALK) gene are found in 2-7% of lung adenocarcinomas and are sensitive to targeted therapies.

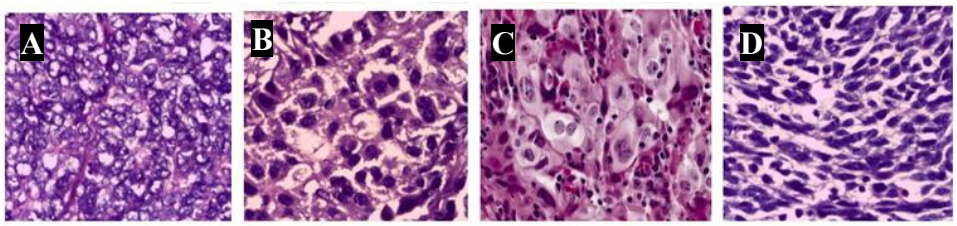

Figure 2.2. Microscopic images of lung cancers a) small cell b) adenocarcinoma c) squamous cell carcinoma d) large cell carcinoma

2.2. Treatment of Lung Cancer

Chemotherapy, radiotherapy, immunotherapy, immunotherapy, nanomedicine and surgical applications are widely used methods in the treatment of lung cancer (13). Treatment methods can be categorized into three different types: conventional therapy, molecular targeted therapy and nanocarrier-based therapy (14). Different approaches such as hormone therapy and biological agents can be used alone or in combination to support conventional or other methods (13,15). A number of problems and needs encountered in conventional treatment have led to the emergence of molecular targeted therapy and methods using nanocarrier systems (15).

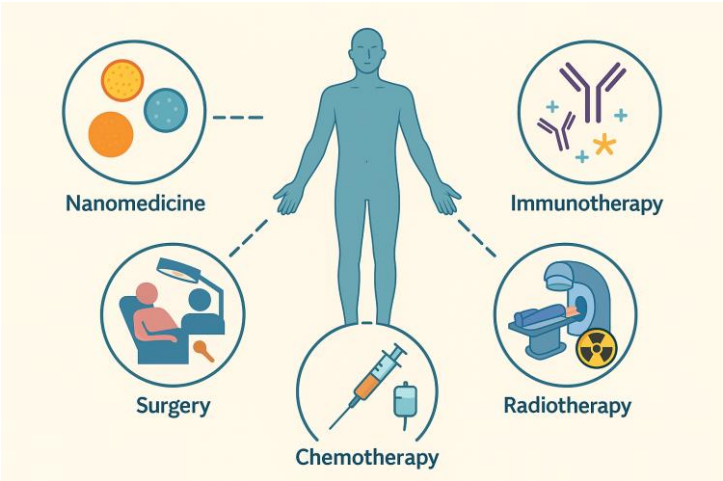

Figure 2.3 Therapeutic Approaches in the Treatment of Lung Cancer (14)

2.2.1. Conventional Treatment Methods

The application of surgical methods in the treatment of lung cancer was the first documented instance of this. The first successful pneumonectomy was performed in the early 20th century, and this procedure subsequently became the milestone of treatment. In the second half of the 20th century, following the discovery that radiotherapy was effective, especially in cases where surgical intervention was not appropriate, this method became the standard until the emergence of chemotherapy (16). Following the 1970s discovery of effective chemotherapeutic agents, these three methods have been used in combination until the present day (17).2

2.2.1.1. Chemotherapy

Chemotherapy was first tested for lung cancer in the 1950s, but methotrexate and actinomycin D were not effective. Cisplatin was discovered in the 1970s and by the 1980s it was standard to use it with other drugs. Antineoplastic or anticancer drugs are agents that function by aiming to halt the proliferation of malignant cells (19). Antineoplastic agents, which vary in terms of mechanism of action and side effect profiles, affect cancer cells as well as cells that often need rapid division. This is the basis of their side effect profile (20). The following table provides a comprehensive overview of the adverse effects commonly associated with anticancer drugs.

Table 2.1. Side effect profiles of anticancer agents (20)

Effected System	Side Effect
Hematological System	Significant decline in regularly proliferating cells (e.g. leukocytes, platelets, erythrocytes).
Gastrointestinal System	Symptoms such as nausea, vomiting, stomatitis, mucositis and diarrhea.
Skin	Symptoms such as nausea, vomiting, stomatitis, mucositis and diarrhea.
Reproductive System	There may be a temporary decrease in fertility due to the toxic effect on gonadal cells.
Immune System	Immunosuppression may occur as a result of immune cells not being able to multiply.
Liver and Kidney	Some agents may cause hepatotoxicity and nephrotoxicity in long-term treatments.

At present, antineoplastic drugs employed in the treatment of lung cancer encompass a range of drug groups, which are classified according to their mechanism of action. These include alkylating agents, antimetabolites, plant-based drugs, antitumour antibiotics, hormones and hormone antagonists, and other drugs (18).

Alkylating agents: The first agent in this class, mechlorethamine, was approved by the FDA in 1949 and was a milestone in the clinical use of alkylating agents (21). The mechanism of action of these agents involves the formation of covalent bonds with nucleophilic sites in DNA, thereby inhibiting cell division (22). The target site is the N7 location in DNA, with the mechanism of action involving the triggering of apoptosis through the formation of cross-links and DNA breaks (23).

Antimetabolites: These agents, which inhibit cell growth in a variety of ways, are highly effective against rapidly dividing cancer cells since they target cells that actively synthesise DNA in the S phase of the cell cycle. The mechanism of action of these agents involves the inhibition of the synthesis or utilisation of purine and pyrimidine bases, thereby reducing the nucleotide pool. Consequently, the synthesis of deoxyribonucleic acid (DNA) and ribonucleic acid (RNA) is halted, or defective products are formed. Folate antagonists, which are classified as antimetabolites, function by reversibly inhibiting the formation of tetrahydrofolate, a critical component in the synthesis of purines and thymidylates. This inhibition is achieved by targeting the enzyme dihydrofolate reductase (DHFR).

Plant-derived anticancer agents: Plant-derived anticancer drugs have an important place in the treatment of cancer and are divided into various subclasses according to their mechanism of action (24). Vinca alkaloids, one of the microtubule inhibitors belonging to this class, are obtained from Catharanthus Roseus, which is an endemic plant native to Madagascar (25). Vinca alkaloids effects by binding to microtubule proteins from inside the cell and preventing mitotic spindle formation (26). Vincristine and vinblastine are agents belonging to this group (27). Taxanes, another microtubule inhibitor, are obtained from the plant Taxus Brevifolia (25). Taxanes aggressively promote the polymerization of microtubules in the cell. This leads to intracellular stabilization of microtubules and triggers apoptosis (26). Agents such as paclitaxel and

docetaxel belong to this class. These agents are used in the treatment of breast, lung, and ovarian cancers (27). Epipodophyllotoxins, which are topoisomerase inhibitors and another type of plant-derived antineoplastic, are derived from the plant Podophyllum Peltatum (25). The mechanism by which topoisomerase II is inhibited is through the action of these agents, which consequently impedes the process of DNA replication. The use of these drugs has been demonstrated in the treatment of testicular and small cell lung cancers (27). Epipodophyllotoxins, which are topoisomerase inhibitors and another type of plant-derived antineoplastic, are derived from the plant Podophyllum Peltatum (25). The inhibition of DNA replication by causing inhibition of topoisomerase II enzyme. They are used for testicular and small cell lung cancers (26). Camptothecin derivative compounds, a subgroup of topoisomerase inhibitors, are obtained from the plant Camptotheca acuminata (25). Their mechanism of action is similar to epipodophyllotoxins and camptothecin-derived compounds act by inhibition of topoisomerase I enzyme. The agents are mainly used in the treatment of ovarian and colon cancers (26). Protein synthesis inhibitors, which are the last subgroup of plant-derived antineoplastic drugs, contain homoharringtonine. It is obtained from the plant named Cephalotaxus harringtonii (25). It acts by inhibiting protein synthesis in ribosomes. It is used in the treatment of chronic myeloid leukemia (26).

Antitumor Antibiotics: Agents isolated to be used in the treatment of infections caused by microorganisms were started to be used with the discovery that anticancer effects were present (22). In the medical field of cancer treatment, the utilisation of this group of drugs is not primarily due to their antibiotic properties, but due to their cytotoxic characteristics (28). Antitumor antibiotics are categorised into four distinct subgroups: anthracyclines, actinomycins, bleomycin and mitomycin derivatives. Agents such as doxorubicin and daunorubicin are classified as anthracyclines, and their mechanism of action involves the disruption of the double-stranded structure of DNA by entering the interhelical spaces of cell DNA (29). Actinomycins function by inhibiting the RNA polymerase enzyme. Bleomycin sulfate has been shown to form a complex with iron ions within the cell. This complex then oxidises in the presence of oxygen, resulting in the formation of single- or double-stranded DNA breaks (S. Consequently, these disruptions result in the obstruction of the G2 phase of the cell

cycle, thereby hindering proliferation (30). The treatment has been used in cases of testicular cancer, Hodgkin lymphoma and head and neck tumours (28). Mitomycin C functions as a pro-drug. The active form of the substance, which is its metabolite, has been observed to form chain cross-links with alkylation reactions on DNA. The cross-links formed have been shown to inhibit DNA replication (30). Its usage is frequently observed in gastrointestinal tumours, including, but not restricted to, gastric cancer, bladder cancer and pancreatic adenocarcinoma (28).

Hormones and Hormone Antagonists: They been demonstrated to be directly related to hormonal activity. The mechanism of action of hormones and hormone agonists involves the regulation of hormone signals and the inhibition of proliferation in tumour cells (31). These agents are considered the primary treatment modality for breast, prostate, endometrial (uterine) and thyroid cancers (32). These hormones are categorised into various groups, including glucocorticoid hormones, estrogens, gonadotropin-releasing hormone (GnRH), estrogen antagonists, progestins, and antiandrogens (31).

2.2.1.2. Radiotherapy

It is a treatment method based on the principle of stopping the growth of the tumor or shrinking and destroying the tumor by causing damage to the DNA of malignant cells using ionizing radiation (33). It became widespread in cancer treatment in the second half of the twentieth century after Wilhem Conrad Röntgen discovered the existence of X-rays in 1895 (34). It has been used in combination with chemotherapy since the 1980s and is still an important pillar of treatment (35). Radiotherapy, which is used for curative, adjuvant and palliative purposes, continues to maintain its importance with the development of devices that can be applied with different techniques. Although radiotherapy was initially used for palliative purposes in lung cancer in the 1950s, it was later introduced for curative use in various subtypes and different stages of lung cancer. Today, chemotherapy, immunotherapy and radiotherapy continue to be used in combination (36).

2.2.1.3. Surgery

The surgical method in the treatment of cancer has a long history dating back to ancient times. At the end of the 19th century, with the development of asepsis and antisepsis methods, surgical operations became quite safe and systematic use in the treatment of cancer became possible (37). Currently, surgery in cancer treatment is usually included in a multidisciplinary approach. Surgical intervention is performed according to the stage, type and patient-related factors (38). Surgery, which has an important place in the treatment of lung cancer, continues to be applied curatively and palliatively. Lobectomy or segmentectomy is one of the main applications in NSCLC stage I and stage II patients (39). In combination with surgery followed by chemotherapy, it has become standard to eliminate microscopic malignant tissues and metastases missed during surgical intervention (40). In late stage patients, surgical interventions are frequently used for palliative purposes. Palliative surgery aims at symptomatic treatment. Applications such as opening the airways or dilating obstructions are emphasized to relieve the patient (41).

2.2.2. Molecular Targeted Therapy

A detailed understanding of the pathogenesis of cancer and advances in genetic and molecular biology have made it possible to use molecular targeted therapy in cancer treatment (42). Molecular targeted therapy approved by the US Food and Drug Administration (FDA) in the treatment of lung cancer has been reported to give promising results (43). Molecularly targeted agents act on cancer cells through surface antigens, growth-factors and growth receptors or signal transduction pathways during cell division. As a result of this effect, it is aimed to stop the cell cycle, induce apoptosis, suppress angiogenesis and prevent a possible metastasis (44). One of the biggest challenges in molecular targeted therapy is resistance to treatment over time. With the understanding of resistance mechanisms and the addition of different strategies to treatment, it is expected that more effective results can be obtained from treatment (45). The agents used in molecular targeted therapy are subcategorized according to their mechanisms of action. The classification includes kinase inhibitors,

proteasome inhibitors, mTOR inhibitors, PARP inhibitors, CDK4/6 inhibitors and monoclonal antibodies (46).

Table 2.2. Subclassification of Molecular Targeted Agents (46)

Subclass	Mechanism of Action
Kinase Inhibitors	Inhibit tyrosine kinases or serine/threonine kinases involved in intracellular signaling, thereby blocking cell growth and
Proteasome Inhibitors	Prevent the degradation of proteins, leading to accumulation of toxic proteins and induction of apoptosis.
mTOR Inhibitors	Inhibit the mTOR pathway, suppressing cell growth, angiogenesis, and protein synthesis.
PARP Inhibitors	Inhibit PARP enzymes involved in DNA repair, leading to accumulation of DNA damage and cancer cell death
CDK4/6 Inhibitors	Block cyclin-dependent kinases 4 and 6, which control cell cycle progression from G1 to S phase, thereby inhibiting cell division
Monoclonal Antibodies	Bind to specific antigens on the cell surface, triggering immune-mediated cell death or blocking intracellular signaling pathways.

2.2.2.1. mTOR Inhibitors

mTOR, a protein from the serine/threonine kinase family, is involved in the regulation of cellular responses. It exists in two different forms, mTORC1 and mTORC2, as a multiprotein complex in the cell. It is involved in activities such as cell growth and proliferation, protein-lipid synthesis, suppression of autophagy, and suppression of apoptotic signals through various signaling pathways (47). In diseases such as cancer, diabetes, obesity, cardiovascular diseases, mTOR pathways may not function properly and over-activation of cellular signaling pathways linked to mTOR may directly or indirectly cause tumor development (48). mTOR inhibitors have been used therapeutically since the isolation of rapamycin (sirolimus) from Streptomyces hygroscopicus bacteria. It was initially used for its immunosuppressant and antifungal properties. In the following process, inhibitory effects of rapamycin on mTOR were

demonstrated and agents such as temsirolimus, everolimus and ridaforolimus, which are analogs of rapamycin (sirolimus), were introduced in clinical use (49).

Everolimus

Everolimus is an analog of rapamycin, a type of mTOR inhibitor (50). Everolimus is structurally obtained by introducing the hydrosiethyl group at the 40th carbon of rapamycin into selective alkylation or esterification reactions. As a result of this reaction, oral bioavailability of the molecule is increased (51). Oral bioavailability is approximately 30-35% and maximum plasma concentration is reached within 1-2 hours. Metabolization occurs in the liver via the CYP3A4 pathway. It binds to 74% of plasma proteins. It is largely excreted with feces (52). The mechanism of action of everolimus is realized in many different ways. Everolimus binds to the binding protein called FKP12 inside the cell and the complex formed causes disruption in some signals transmitted via mTORC1. Inhibition of mTORC1 leads to inactivation of proteins called 4E-BP1 (Eukaryotic Translation Initiation Factor 4E-Binding Protein). Inhibition of mTORC1 prevents the phosphorylation of the enzyme S6K1 (Ribosomal protein S6 kinase beta-1). This leads to suppression of the transition from G1 to S phase during mitosis. Another effect is that inhibition of mTOR inhibits the formation of VEGF (vascular endothelial growth factor), which provides the angiogenesis needed by tumor cells in hypoxic conditions. Inhibition of mTOR, which is involved in the suppression of autophagy in cells, triggers the autophagic process and facilitates apoptosis. Since everolimus is a selective inhibitor only against mTORC1, mTORC2 activity responsible for the organization of the cytoskeleton continues (53-54). This may lead to the resistance in long-term treatment patients against everolimus (55). Immunosuppressive effects of everolimus occur due to its anti-cancer properties. Since it also causes a strong suppression in the proliferation of T cells, it is widely used for organ rejection after organ transplantation (56). Although it is mostly administered orally in clinical practice, it is also administered parenterally for experimental studies (57). When administered orally, side effects similar to the side effects of antineoplasmic drugs are generally observed, while the risk of systemic toxicity is significantly increased in parenteral administration (58). Everolimus has been approved by the FDA for the treatment of renal cell carcinoma, breast cancer and

advanced neuroendocrine tumors (59). Although it is not yet approved for the treatment of lung cancer, phase II and III trials are ongoing, especially for the treatment of NSCLC (60).

2.3. Nanomedicine and Nanocarrier Systems

Nanomedicine can broadly be defined as the application of nanotechnological approaches and methods for the diagnosis, monitoring, prevention, and treatment of diseases (63). In late 20th century, the integration of nanotechnology in medicine, initially within the domain of targeted drug delivery systems and subsequently expanding into areas such as contrast agents, biosensors, and tissue engineering (64).

In comparison with established conventional treatment approaches, nanomedicine offers a number of benefits throughout the therapeutic process. When employed as drug delivery systems, it allows for the targeted delivery of active pharmaceutical ingredients. This is significant benefit in the context of cytotoxic treatments, such as chemotherapy. Furthermore, nanocarrier systems permit the controlled and time-dependent release of therapeutic agents, thereby enabling extended dosing intervals. The enhancement of the solubility of drugs with suboptimal bioavailability has the potential to result in clinically significant outcomes (65). Consequently, these advantages contribute not only to enhanced treatment efficacy but also to improved patient compliance (66).

It is anticipated that nanocarrier systems will demonstrate properties including elevated drug loading capacity, protracted circulation time, diminished toxicity to healthy tissues, and augmented anti-tumour activity (67).

2.3.1. Nanocarriers in Cancer Treatment

Nanocarriers such as polymeric nanoparticles, liposomes, niosomes and polymeric micelles with different structures and compositions are widely researched and have clinical applications, especially in cancer treatments (63). The first clinically used nanocarrier system was approved by the FDA in 1995 for use in cancer treatment.

The product marketed under the name Doxil® contains pegylated liposomes loaded with doxorubicin (68). The clinical use of Doxil® was a turning point for nanocarrier systems. The introduction of Doxil® moved nanocarrier systems from an experimental approach to a discipline that can be used safely and effectively in the clinic (69). The introduction of Doxil® into clinical use encouraged the introduction of many nanoparticle-based formulations, and in the following years, systems such as Abraxane® (albumin-bound paclitaxel) and Genexol-PM (paclitaxel-loaded polymeric micelle) found a place in the market (68,70).

2.4. Polymeric Micelles

Polymeric micelles are biocompatible nanosized structures that spontaneously form spherical or ellipsoidal structures when certain conditions are provided in aquatic environments with the structure of amphiphilic block co-polymers (71). In the late 1960s, they came to the forefront as drug carrier systems with their amphilic structures and self-organisable properties. In the 1980s, experimental studies using polymeric micelles as drug carrier systems in cancer treatment were reported (72).

2.4.1. Structure of Polymeric Micelles

Polymeric micelles can be composed of block copolymers with various architectures. The most commonly used structures include di-block (A-B), tri-block (A-B-A), and graft copolymers. These structural differences significantly influence the properties of the micelles. The hydrophobic block of the copolymer plays a critical role in determining biocompatibility, stability, drug loading capacity, and release profile, whereas the hydrophilic shell is responsible for properties such as active targeting, ligand attachment, and steric stabilization (73). Diblock copolymers, composed of two distinct polymeric segments covalently bonded together, typically consist of one hydrophilic and one hydrophobic block. Upon micellization, they most often form core–shell structures (73). These systems are widely used in drug delivery and passive targeting applications (74). Their sizes are within the nanometer range (10–100 nm), which is suitable for drug transport. Due to their low critical micelle concentrations (CMC), they can maintain stability under in vivo conditions. Moreover,

they are relatively easy to synthesize (73,75). Commonly used combinations include polyethylene glycol (PEG) as the hydrophilic shell and polymers such as polylactic acid (PLA), polycaprolactone (PCL), or poly(lactic-co-glycolic acid) (PLGA) as the hydrophobic core components (73).

Triblock copolymers may have an A-B-A or B-A-B structure, in which one of the blocks is hydrophobic and the other is hydrophilic. These copolymers maintain their amphiphilic characteristics. A widely used example is the Pluronic® (PEO–PPO–PEO) triblock copolymer. A significant advantage of triblock copolymers is their ability to form stimuli-responsive systems. They can exhibit controlled release behavior in response to environmental triggers such as temperature, pH, solubility changes, morphology, or shape transitions (73,76).

Graft copolymers, which have a brush-like morphology, are formed by attaching polymer chains with distinct characteristics to the side chains of a main backbone. The grafted polymers can be hydrophilic or hydrophobic in nature (73). This architecture endows graft copolymers with several advantages, including high drug loading capacity, enhanced potential for surface modification, and redox-responsive drug release profiles (77).

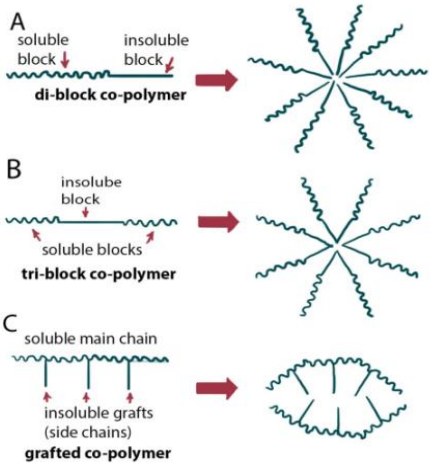

Figure 2.4. Micelle Formation Mechanism from Copolymers (77) A) Di-block co-polymers, B) Tri-Block co-polymers, C) Grafted co-polymer

2.4.2. Formation of Polymeric Micelles

Amphiphilic unimers that constitute micelles can exist as polymeric chains under certain conditions. In aqueous solutions, they spontaneously form micelles when the temperature and concentration exceed specific thresholds (78). Micelle formation occurs as a result of entropy-driven processes (79). The temperature at which micellization begins is referred to as the critical micelle temperature (CMT), while the concentration at which micelles start to form is known as the critical micelle concentration (CMC) (80). The formation of micelles is governed by a decrease in free energy (79). The hydrophobic segment of the block copolymer tends to avoid the aqueous environment and assembles into a micellar core, whereas the hydrophilic segment interacts with water through hydrogen bonding. The formation of hydrogen bonds leads to a reduction in free energy in the system. This excess energy facilitates the aggregation of hydrophobic segments via Van der Waals interactions, ultimately resulting in micelle formation (80).

2.4.2.1. Critical Micelles Concentration

The critical micelle concentration (CMC) is one of the most important parameters in the formation of polymeric micelles and in evaluating their colloidal stability. It refers to the minimum concentration at which block copolymers are able to form micelles. The CMC value depends on several characteristics of the copolymers that constitute the polymer. Among these, the hydrophilic-to-hydrophobic block ratio significantly influences the CMC. When the hydrophilic block is disproportionately longer than the hydrophobic block, micelle formation becomes more difficult, resulting in an increased CMC (81). In addition, factors such as solution temperature and solvent properties also affect the CMC value (82).

In drug delivery applications, especially for intravenous administration, an average dilution of up to 25-fold is expected in the bloodstream (83). Therefore, a low CMC value is desirable; in other words, it is crucial for micelles to remain stable and intact above their CMC after dilution, in order to reach the target site and release the drug effectively. If the concentration drops below the CMC, micelles dissociate into

monomers, rendering the targeted delivery unsuccessful and drug transport ineffective. On the other hand, micelle formulations prepared at concentrations far above the CMC often lead to aggregation. In intravenous applications, aggregated micelles can cause vascular blockage and thrombus formation; thus, it is essential for micelles to have a monodisperse structure (84).

The CMC value is typically measured using surface tensiometry and fluorescence probe techniques. In surface tensiometry, the CMC is determined based on the principle that surface tension decreases with increasing concentration until a plateau is reached, where no further reduction in surface tension is observed (85).

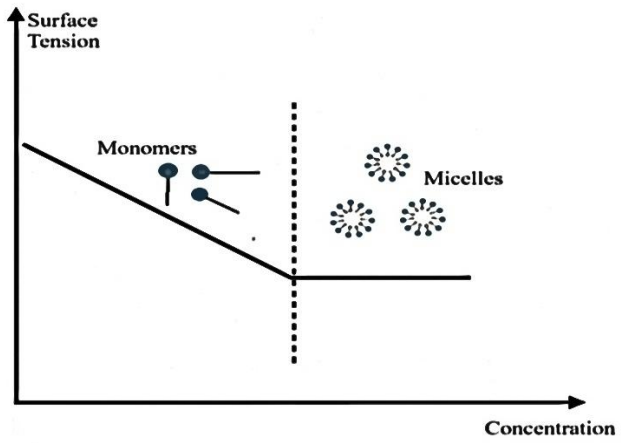

Figure 2.5. Relation between critical micelles concentration and surface tension (86)

2.5. Pulmonary Drug Delivery Systems

Pulmonary drug delivery is a non-invasive and efficient administration route that enables the direct delivery of therapeutic agents to the lungs. It can be employed in the treatment of both systemic and local diseases (88). This method provides significant advantages in the treatment of diseases such as asthma, chronic obstructive pulmonary disease (COPD), pneumonia, and lung cancer (88,89). Unlike oral administration, pulmonary delivery bypasses the gastrointestinal tract and hepatic metabolism, thereby avoiding the first-pass effect observed with certain drugs. This allows the desired therapeutic effect to be achieved with lower doses (90).

The pulmonary route provides a large surface area for absorption (~100 m^2), which facilitates high bioavailability and a rapid onset of therapeutic action. Its efficacy in both local and systemic diseases makes it a promising strategy for effective treatment of pulmonary disorders with reduced side effects (90,91). Additionally, controlled drug release through carrier systems can reduce dosing frequency (91). Since it is non-invasive compared to parenteral routes, patient compliance and comfort are considerably improved (92).

However, pulmonary drug delivery also has certain disadvantages. Effective drug deposition heavily depends on the patient's ability to properly use inhaler devices. Improper usage may result in insufficient drug delivery to the target site, negatively affecting treatment outcomes. This issue is particularly common in elderly, disabled, and pediatric patients. Moreover, biological barriers in the lungs pose challenges to pulmonary drug delivery. Body fluids present in the lungs (such as mucus, surfactant, interstitial fluid, and alveolar fluid) as well as non-humoral immune components may inactivate the drug before it reaches the target region (93–95).

2.5.1. Deposition of Particles In The Respiratory Region

In pulmonary drug delivery systems, the deposition of drug-loaded particles in the respiratory region is of critical importance for therapeutic success (96). The effectiveness of regional deposition is influenced by several factors, the most crucial of which is the aerodynamic behavior of the carrier particles. Additionally, patient-dependent factors such as inhalation rate, inhaled volume, breath-holding duration, and breathing morphology significantly affect deposition efficiency (96,97).

Particle deposition in the respiratory tract occurs via different mechanisms, including impaction, sedimentation, and diffusion (97). In impaction, particles traveling with the airstream during inhalation deviate from the airflow trajectory and collide with airway surfaces at points where airflow changes direction, provided they possess sufficient momentum. Larger particle size, higher particle density, and increased airflow velocity promote impaction. Particles larger than 5 μm are typically deposited in the upper respiratory tract through this mechanism (98).

Sedimentation-based deposition relies on gravitational forces and occurs predominantly in the lower airways, where airflow is minimal. The residence time of air in the pulmonary tract directly influences sedimentation efficiency; longer residence times allow more particles to settle. For this mechanism, particles ranging between 1–5 μm are considered optimal (98).

Diffusion-mediated deposition involves particles smaller than 1 μm undergoing Brownian motion. As particle size approaches 0.5 μm, the tendency for Brownian motion increases. These ultrafine particles can reach the deepest regions of the lungs. Their random collisions with gas molecules in the airstream result in Brownian diffusion-based deposition. The two most influential factors for this mechanism are particle size and the residence time within the respiratory tract (98,99).

2.5.2. Inhalation Devices

Inhalation devices are medical tools designed to deliver active pharmaceutical ingredients directly to the lungs, thereby exerting a localized therapeutic effect (100). Although the invention of modern inhalers dates back to the 19th century, their widespread clinical use began in the 1950s with the introduction of metered-dose inhalers (MDIs). Inhalation devices can generally be classified according to formulation type, dose control mechanism, and mode of administration (101).

2.5.2.1. Metered-Dose Inhalers (MDIs)

Metered-dose inhalers (MDIs) are pressurized, multi-dose, and portable inhalation devices that deliver a specific dose of medication in aerosol form using a propellant gas. Formulations may include solvents, co-solvents, and lubricating agents (102). The drug is usually formulated as a solution or suspension and aerosolized via propellants such as hydrofluoroalkane (HFA) (103). Chlorofluorocarbon (CFC) propellants were formerly used but were discontinued due to their environmental harm (102). MDIs offer advantages such as consistent and metered dosing, portability, and rapid onset of action. However, a key limitation is the need for coordination between actuation and

inhalation. Additionally, the propellant may trigger a cough reflex, potentially impeding drug deposition in the lungs (103).

2.5.2.2 Nebulizers

Nebulizers generate aerosols by dispersing fine liquid droplets in a carrier gas and are administered to patients via a mask. They are primarily used in hospital settings, particularly for patients with limited mobility, difficulty operating other devices, or those requiring high drug doses (102). Compared to other inhalation devices, nebulizers offer several advantages: they allow continuous inhalation, minimizing user error, and provide deep lung penetration due to slow, prolonged drug delivery. Unlike other devices with dose limitations, nebulizers can administer relatively high drug doses and accommodate a wide range of formulations, including antibiotics, corticosteroids, bronchodilators, and mucolytics (104). Disadvantages include their lack of portability (especially in the case of jet nebulizers), noise production, and treatment times typically ranging from 10 to 15 minutes. Because the device is often not patient-specific, proper sterilization post-use is essential, adding to the workload and cost (102,104).

2.5.2.3. Dry Powder Inhalers (DPIs)

Dry powder inhalers (DPIs) are devices that deliver drugs in powdered form and are activated by the patient's inhalation effort (102). The active ingredient is often blended with a carrier substance such as lactose, which helps improve powder flow, increase volume, and transport fine drug particles (105). DPIs provide an important alternative to MDIs and nebulizers due to their improved stability, absence of environmentally harmful propellants, and ease of use (103). The dry powder formulation offers high stability and ease of storage. Unlike MDIs, DPIs do not require hand-breath coordination and are easily activated by passive inhalation, making them suitable for patients with sufficient inspiratory effort (103,106). They are also more cost-effective to produce and allow for repeatable dosing (107). However, DPIs have drawbacks, including the potential for powder agglomeration in humid environments, which can affect flow properties and homogeneity, thus complicating manufacturing.

Formulations containing lactose may also cause symptoms in lactose-intolerant individuals (103). Various DPI designs exist: some require inserting single-dose gelatin capsules into the device, while others store doses in blister packs. Multi-dose devices use a reservoir mechanism that measures and delivers the appropriate dose (108).

2.6. Microparticles

Microparticles are spherical, solid microcarriers with sizes ranging from 1 to 1000 μm. They can be formed in various bulk structures, either biodegradable or non-biodegradable within the body, and contain the active pharmaceutical ingredient dispersed at either a molecular or macroscopic level (109). The encapsulated active agent within microparticles may exist in solid form, or as part of a solution, suspension, or emulsion (110). Microparticles are generally categorized into two types: microcapsules and microspheres. In microcapsules, the active substance is surrounded by a polymeric shell, whereas in microspheres, the active substance is homogeneously distributed throughout the polymeric matrix of the particle. These systems are capable of enabling controlled drug release and can be administered through oral, parenteral, or pulmonary routes (111).

Microparticles are used as drug delivery systems in both conventional and innovative pharmaceutical applications (112). They offer several pharmacokinetic and pharmacodynamic advantages. Compared to traditional drug delivery methods, microparticles provide enhanced bioavailability, improved stability, longer shelf life, therapeutic efficacy with lower doses, a milder side effect profile, and the possibility of controlled release and targeting. Moreover, their ability to encapsulate and deliver multiple drugs simultaneously allows for synergistic effects (111–112). However, despite these advantages, microparticles also present certain drawbacks, such as challenges in large-scale production, the risk of drug degradation during the loading process, and the potential inability to precisely control drug release rates, even though they are intended for controlled delivery (112).

2.6.1. Pulmonary Applications of Microparticles

Microparticles are one of the most remarkable drug delivery systems employed for pulmonary drug administration. Different microparticle-based systems are already in clinical use (113). For microparticles to be suitable for pulmonary delivery, microparticles have to provide physicochemical and biopharmaceutical criteria. The most fundamental requirement is that the material composing the microparticle must be biocompatible and preferably biodegradable (112). If biocompatibility is not achieved, the particles may induce inflammatory responses, systemic or cellular toxicity, or immunological reactions (114).

In pulmonary delivery, the aerodynamic diameter of the carrier system is of critical importance for effective deposition in the targeted anatomical region. Therefore, particle size optimization during formulation and characterization is essential. It has been observed that particles of different sizes deposit in distinct regions of the respiratory system. Particles larger than 10 μm tend to be trapped in the nasopharyngeal region and do not reach the lungs. Particles with diameters between 5–10 μm usually deposit in the trachea and large bronchi. Those between 1–5 μm accumulate in the small bronchi and bronchioles, and are thus considered optimal for targeting the lower respiratory tract. Although particles smaller than 1 μm can reach the alveolar region, they are often exhaled before exerting a therapeutic effect and thus are generally ineffective (115).

In addition to influencing deposition, particle size also affects the humoral immune response. Particles larger than 10 μm are typically cleared by the mucociliary system, whereas particles smaller than 1 μm are rapidly phagocytosed by alveolar macrophages, significantly reducing the bioavailability of the active substance (115). Other physical parameters such as shape, density, and surface charge also influence the transport and deposition behavior of the particles. However, particle size remains the most critical determinant (98). Another key requirement for microparticles intended for pulmonary use is sterilizability. They must be resistant to sterilization methods such as autoclaving or gamma irradiation (116). Furthermore, the suitability

for large-scale industrial production is also crucial for ensuring commercial sustainability and clinical applicability of the formulation (117).

2.6.2. Polymers Used in the Preparation of Microparticles

Natural or synthetic polymers are used in the preparation of microparticles. Natural polymers include biochemical materials such as lipids, amino saccharides, proteins, and sugars (118). Synthetic polymers used in production can be categorized into two groups based on their degradability: biodegradable and non-biodegradable (119).

Both natural and synthetic polymers offer distinct advantages over one another. The primary advantages of natural polymers include the non-toxic degradation products they yield, high stability, controlled particle size distribution, high encapsulation efficiency for water-soluble drugs, and mucoadhesive properties, particularly when applied via the pulmonary route. However, natural polymers also have several disadvantages compared to synthetic ones: difficulties in obtaining them in high purity, limited physicochemical tunability, sensitivity to temperature and pH changes, and, though rare, the potential to trigger inflammatory responses.

On the other hand, synthetic polymers has advantage such as; easy synthesis, modifiability, reproducibility, and the ability to achieve optimal controlled release profiles. Nevertheless, they may also bring some limitations, such as higher production costs, more complex manufacturing processes, and potential toxicity of their degradation products (120).

Cellulose Derivatives

Cellulose is a biodegradable polysaccharide that is found frequently in nature and can be consumed as food (121). Cellulose is chemically a straight chain homopolymer consisting of D-glucopyranose units linked by β(1→4) glycosidic bonds. Since there are three hydroxyl groups on glucose units, it is open to chemical modification (122). Its general chemical formula is $(C_6H_{10}O_5)_n$ (123). Methylcellulose (MC), one of the

most widely used cellulose derivatives as drug carrier microparticles, is a water-soluble, semi-synthetic derivative that forms a gel with temperature. Another one, sodium carboxymethylcellulose (Na-CMC), is anionic and water soluble. It shows mucoadhesive properties. It is often effective in the transport of hydrophilic agents. Ethylcellulose (EC) is preferred in delayed agent release systems due to its water insoluble barrier against water. It is effective in the transport of lipophilic agents. Cellulose acetate (CA) is a semi-synthetic cellulose derivative. It is obtained based on partial and complete replacement of hydroxyl groups on cellulose between acetyl groups. This synthesis by acetylation reaction affects the water solubility of cellulose acetate, hydrophobicity increases as acetylation increases. It shows thermoplastic properties and its permeability to gases and water becomes selective thanks to its semi-permeable structure (124). Detailed information about hydroxypropyl methyl cellulose (HPMC) has given in the below.

Hydroxypropyl Methylcellulose (HPMC)

Hydroxypropyl methylcellulose (HPMC) is produced by substituting some of the hydroxyl groups in cellulose with methyl and hydroxypropyl groups. The methyl groups are introduced via esterification with methyl chloride, while the hydroxypropyl groups result from nucleophilic ring-opening of propylene oxide in an alkaline environment (125). HPMC is a non-ionic, semi-synthetic polymer with improved water solubility compared to cellulose, owing to the increased hydrophilicity conferred by the hydroxypropyl groups (126). These modifications provide HPMC with functional properties such as viscous gel formation. Its pH-independent solubility allows its use in drug delivery systems targeting various body sites. Hydrophilic drugs are more easily encapsulated, while the use of hydrophobic drugs may require stabilizing agents (127). HPMC-based microparticles can achieve encapsulation efficiencies of up to 50% (128).

HPMC microparticles have low density, which allows their aerodynamic diameter to remain within the desired 1–5 μm range, even if their geometric size is relatively large advantage for pulmonary delivery (125,128). Furthermore, HPMC ensures optimal particle morphology, including shape, surface structure, and internal

architecture (129). Its mucoadhesive properties extend the residence time of microparticles at mucosal surfaces, potentially enhancing bioavailability and enabling controlled release optimization (128,129).

2.7. Drug Targeting In Drug Delivery Systems

Targeting in drug delivery systems is used to direct therapeutic agents to desired cells or tissues, particularly to reduce systemic toxicity if the agent is cytotoxic, while also increasing therapeutic efficacy. Targeting is classified into two main strategies: passive and active targeting (130).

2.7.1. Passive Targeting

In passive targeting, the carrier systems mus3t meet certain physical and chemical criteria to accumulate in the desired regions. Parameters such as particle size, surface charge, surface modifications, shape, and stability are important for accumulation in the targeted site (131). First described in 1986, the EPR effect (Enhanced Permeability and Retention effect) is a biological phenomenon observed in tumor tissues and certain autoinflammatory diseases (132). It is the mechanism that allows carrier systems to accumulate in tissues and cells via passive targeting. Passive targeting is based on the accumulation of nanocarriers within the tumor microenvironment due to unique characteristics not typically present in healthy tissues. The nature of tumor tissues facilitates the accumulation of carrier systems in the desired area. Tumor tissues, due to irregular and rapid vascularization, exhibit fenestrations in their vessel walls where nanoparticles can accumulate, leading to the permeability effect. The retention effect occurs because of the poor lymphatic drainage in tumor tissues, allowing carrier systems to remain in the target region for longer periods and accumulate (133).

Table 2.3. Factors affecting EPR effect in passive targeting (131)

Property of the particle	**Preferred feature**
Size (Diameter)	The optimum range is between 10-200 nm. <10 nm particles are eliminated by the kidneys, cannot reach the target area. >200 nm particles mononuclear phagocyte system (MPS) are captured and phagocytosed by the MPS.
Surface Charge	Preferably notr or slightly negative charge.
Shape and Elasticity	Spherical and elasticizable particles
Stability	Unless not maintain stability they may degrade before reaching the targeted area.
Surface Modifications (Non-active targeting)	Pegylation can improve the desired properties.

However, passive targeting has limitations in terms of specificity. The characteristics that enable the EPR effect vary significantly between regions and among patients, which can lead to treatment failures. The density of extracellular matrix components around the tumor, the hypoxic environment, or unexpectedly effective lymphatic drainage can prevent particle accumulation in the intended region. In some cases, particles may accumulate outside the target area in healthy cells and tissues, causing off-target cytotoxicity (134).

2.7.2. Active Targeting

To overcome the limitations of passive targeting strategies, active targeting strategies have been developed. Active targeting is achieved by modifying the surface of drug delivery systems with ligands such as peptides or antibodies that have high affinity for receptors strongly expressed on the surface of cells in the target tissue (135). As a result of the interaction between the ligand added to the drug delivery system and the receptors on the target cells, the system is internalized into the cell via receptor-mediated endocytosis. The interaction between the ligand and receptor occurs in several steps (136). First, molecular recognition and approach take place based on factors such as shape, charge, and hydrophilicity. This is followed by binding through weak interactions such as hydrogen bonding, Van der Waals forces, and electrostatic interactions. In response to the signal generated by binding, a cellular response is

initiated, and the system is internalized via receptor-mediated endocytosis. The properties of the targeted receptor and the ligand used are important for the success of targeting (136,137). Some characteristics that the receptor and ligand should exhibit include: the receptor should be strongly expressed in the target cells while being weakly expressed in other cells; after ligand-receptor binding, the receptor should be able to generate a signal that triggers internalization of the delivery system; and the ligand should have a high binding affinity for the receptor. Partial binding events can lead to failure in targeting. If the ligand also has affinity for other receptors, its low specificity can cause off-target effects, thus specificity is important (138). Additionally, the ligand should exhibit biocompatibility in systemic circulation and possess high stability. Combining effective active targeting strategies with passive targeting offers several advantages. When applied to cancer treatment, such strategies can significantly reduce the side effects of the active compounds, improving patient comfort and compliance (139). However, active targeting also has its own limitations. An inflammatory response may develop against some peptide-based ligands, or the peptide structure may undergo enzymatic degradation and be destroyed. Moreover, if the target receptor is not equally expressed across all target cells, treatment efficacy may be significantly reduced due to the heterogeneous response (140).

2.7.2.2. Ligands Used In Active Targeting

Different structures are used as ligands in active targeting. Selecting a ligand, criteria such as specificity, biocompatibility, ease of conjugation, and support for intracellular uptake are considered. Commonly used ligands include monoclonal antibodies, peptides, folic acid, monosaccharides, and aptamers (141).

RGDK Peptide

Arginine-glycine-aspartic acid-lysine (RGDK) is a modified derivative of the classical arginylglycylaspartic acid (RGD) peptide (142). RGD was first described in the early 1980s by Ruoslahti and Pierschbacher as the minimal recognition sequence within fibronectin required for cell binding (143). Since its discovery, RGD has been used in various fields. In drug discovery, it has enabled the development of drugs for

cancer and cardiovascular diseases by elucidating the molecular basis of integrin binding mechanisms. RGD's high affinity and selectivity for integrin αVβ3 receptors have also been exploited in PET (Positron Emission Tomography) imaging, which is used for cancer diagnosis and monitoring treatment response (144). Additionally, it is a widely used short peptide sequence in drug delivery systems targeted to tumor cells. The addition of lysine (K) to the classical RGD sequence facilitates its conjugation to delivery systems. The most common conjugation technique is covalent bonding. In this method, conjugation occurs through a functional group such as amine, carboxyl, or thiol via chemical cross-linkers like succinyl amide or maleimide, binding the peptide to the surface of the delivery system. The effectiveness of RGD-conjugated delivery systems in targeting tumor cells has been confirmed by numerous preclinical studies. Although some studies have advanced to phase I/II clinical trials, there is still a need for optimization of critical parameters (145).

3. MATERIALS AND METHODS

3.1. Materials

Name of The Chemical	Cat No, Brand, Country
Methoxy poly(ethylene glycol)-b-poly(L-lactide) (5k-10k)	900656, Sigma-Aldrich, USA
Carboxylic acid-poly(ethylene glycol)-b-poly(D,L lactide) (5k-16k)	909300, Sigma-Aldrich, USA
N-Hydroxysuccinimideester-poly(ethyleneglycol)-b-poly(D,L lactide) (5k-16k)	909874, Sigma-Aldrich, USA
Pluronic F-127	P2443, Sigma-Aldrich, USA
Brij98™	34718, Acronica Organics, Belgium
Gelucire® 48/16	Gattefossé, France
Everolimus	SML2282, Sigma-Aldrich, USA
(Hydroxypropyl)methyl cellulose (HPMC)	9004-65-3, Sigma-Aldrich, USA
Lactose Monohydrate	Inhalac® 500, Meggle GmbH & Co. KG, Germany
Ethanol	34852-M, Sigma-Aldrich, USA
Acetonitrile (ACN)	34998, Sigma-Aldrich, USA
Chloroform	366927, Sigma-Aldrich, USA
Ethylacetate	34858, Sigma-Aldrich, USA
Tetrahydrofuran (THF)	439215, Sigma-Aldrich, USA
Dimetil Sülfoksit (DMSO)	34869, Sigma-Aldrich, USA
2-propanol (IPA)	34863, Sigma-Aldrich, USA
PBS Tablets	A09-2051-100, Aniara Diagnostica, Inc, USA
L-Arginine	194626, MP Biomedicals LLC, USA
Glysine	11446551, MP Biomedicals LLC, USA
L-Lysine	19022425, MP Biomedicals LLC, USA
L-Aspartic acid	02100809, MP Biomedicals LLC, USA
Piperidine	822299, Sigma-Aldrich, USA
N,N'-Diisopropylcarbodiimide (DIC)	D125407, Sigma-Aldrich, USA
Ethyl cyanohydroxyiminoacetate (Oxyma)	233412, Sigma-Aldrich, USA
Diethly ether	309966, Sigma-Aldrich, USA
Dimetilformamid (DMF)	648531, Sigma-Aldrich, USA
Rink Amide Protide Resin	R003-B, CEM Corporation, USA

3.2 Methods

3.2.1. Critical Micelles Concentration For Polymeric Micelles

The micelle concentration to encapsulate Everolimus (EVE, SML2282, Sigma Aldrich, USA) was determined using the pendant drop method in a tensiometer device (Attension ThetaLite, Biolin Scientific, Sweeden). For this purpose, samples prepared with three different types of polymers (mPEG-b-PLA, COOH-PEG-b-d-PLA, NHS-PEG-PLA) were analyzed. Briefly in this method, drug free polymeric micelles were dispersed in water and samples were prepared at various concentrations. The surface tension (mN/m) of the drug-free polymeric micelle samples was measured using the pendant drop method. The decrease in surface tension with increasing concentration (ug/mL) was then graphed. The intersection point of the line equations drawn in the two regions where the surface tension was observed to decrease linearly on the graph was determined and the concentration corresponding to the intersection point was accepted as the critical micelle concentration.

3.2.2. Critical Micelles Concentration For Surfactants

The surfactants targeted to be used to further reduce the critical micelle concentrations of polymeric micelles were Pluronic F-127 (P2443) to be added in different ratios to distilled aqueous d(H_2O) dispersions of polymeric micelles, The critical micelle concentrations of three different surfactants Sigma Aldrich, USA), Brij™ 98 (10117553, Thermo Scientific, USA) and Gelucire® (Polyoxyl-32 stearate) (9011-21-6, Gattefosse, France) were determined by the same method as for polymeric micelles. Table 3.1 shows the concentrations of the prepared surfactants samples.

Table 3.1. Concentrations of Surfactants Dispersions

Concentrations of Surfactant (Pluronic F-127) (mg/mL)	Concentrations of Surfactant (Brij98™) (µg/mL)	Concentration of Surfactant (Gelucire®) (µg /mL)
0,025	0,1	5
0,005	5	10
0,1	10	15
0,25	15	20
0,5	20	25
5	30	50
10	50	70
25	100	100
50	200	200
100	300	
250	400	

3.2.2.1. Preparation of Pluronic F-127 Samples

250 mg of Pluronic® F-127 was weighed and dissolved in 1 mL chloroform. The resulting solution was kept in a fume hood overnight and then the chloroform was evaporated to obtain a thin film. The film was dispersed by adding 1 mL of distilled water d(H_2O). The dispersion was vortexed for 1 min and then kept in a water bath at room temperature. As a result of this process, a stock solution with a concentration of 250 mg/mL was obtained and samples of different concentrations were prepared with the necessary dilutions using the stock solution.

3.2.2.2 Preparation of Brij™ 98 Samples

1 mg of Brij™ 98 was weighed and dissolved in 1 mL of chloroform. The resulting solution was kept in a fume hood overnight and a thin film was formed by evaporation of chloroform. The film was dispersed by adding 1 mL of distilled water d(H_2O). The resulting stock solution of 1 mg/mL was used to prepare the samples to be used for the measurements by making the necessary dilutions.

3.2.2.3. Preparation of Gelucire® Samples

200 mg of Gelucire® 48/16 was weighed and dissolved in 1 mL chloroform. The prepared solution was kept in a fume hood overnight to evaporate the chloroform and a thin film was formed. The obtained film was dispersed by hydrating with 1 mL of distilled water d(H_2O). The dispersion obtained in this way was used as a stock solution and samples of different concentrations were prepared by making the necessary dilutions.

3.2.3. Critical Micelles Concentration For mPEG-PLA PMs Mixtures

Aqueous dispersions of surfactants (Pluronic F-127, Brij™ 98, Gelucire®) at various concentrations were mixed with micelles at a ratio of 1:2. Micelles and surfactant mixtures were prepared by thin-film method and aqueous dispersions of surfactants were mixed with aqueous dispersions of surfactants to obtain measurement samples.

Table 3.2. Concentrations of mPEG-PLA and surfactants mixtures

Concentration of mPEG-PLA-PMs	Concentration of (Pluronic F-127) (µg/mL)	Concentration of Samples (Brij98™) (µg/mL)	Concentration of Samples (Gelucire®) (µg/mL)
10	5	5	5
15	7,50	7,50	7,50
20	10	10	10
30	15	15	15
40	20	20	20
50	25	25	25
75	37,5	37,5	37,5
100	50	50	50
125	62,5	62,5	62,5
150	75	75	75

3.2.4. Preparation of Polymeric Micelles

To produce polymeric micelles (PMs), 3 different types of PEG-b-PLA copolymer were used: metoxy, carboxylic acid, and N-hydroxy succinimide ester. These 3 different types carry the same PEG-b-PLA main skeleton. In terms of structure, the methoxy group is a group that does not carry a functional group in its structure, in other words, it is a group that does not have the ability to bond (146). The carboxylic acid substituted form is an intermediate polymeric product and is included in the use of N-hydroxy succinimide ester derivative PEG-b-PLA. N-hydroxy succinimide ester is the functional group that can conjugate with RGDK.

All formulations were produced by thin film hydration method. Critical micelle concentrations (CMC) for three different polymer types were determined and drug loaded PMs were produced by selecting a concentration above the critical micelle concentration. The production process briefly includes the following steps; dissolution of the polymer in organic solvent, evaporation of the organic solvent to obtain a thin film layer, hydration of the thin film and formation of polymeric micelles by self-assembly. In total, 6 different formulations were prepared as follows.3

a) Drug-free Methoxy poly (ethylene glycol)-*b*-poly(L-lactide) micelles
b) EVE-loaded Methoxy poly (ethylene glycol)-*b*-poly(L-lactide) micelles
c) Drug-free Carboxylic acid-poly (ethylene glycol)-*b*-poly (D,L lactide) micelles
d) EVE-loaded Drug free Carboxylic acid-poly (ethylene glycol)-*b*-poly (D,L lactide) micelles
e) 3N-Hydroxysuccinimide ester-poly(ethyleneglycol)-b-poly(D,Llactide) micelles
f) RGDK Conjugated EVE Loaded Carboxylic acid-poly (ethylene glycol)-*b*-poly (D,L lactide) micelles

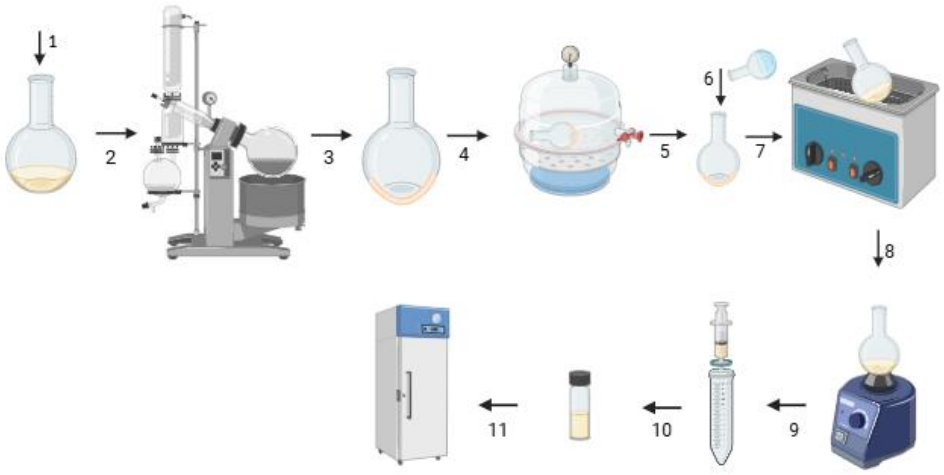

Figure 3.1. Steps of polymeric micelles production with thin hydration method

To list the steps in Figure 1; (1) dissolving the polymeric micelles in chloroform and placing them in a round bottom flask. (2) evaporation of the organic solvent (chloroform) in a rotary evaporator. (3) thin film formation. (4) overnight incubation of the thin film in a vacuum desiccator to remove organic solvent residues. (5-6) Hydration of the thin film with distilled water at 25 °C. (7) Sonication of the formulation in an ultrasonic water bath set at 50 °C. (8) Vortexing of the formulation in a vortex shaker. (9) Filtration with a 0.45 µm syringe filter. (10) Transfer of the formulation into a glass vial. (11) Storage of the formulation at +4 °C for characterization. The production method is explained in detail below.

3.2.4.1. Preparation of Drug free PMs

Methoxy poly(ethylene glycol)-b-poly(L-lactide)b (mPEG-PLA) micelles (5k-10k, 900656, Sigma-Aldrich, USA), carboxylic acid-poly (ethylene glycol)-b-poly (D,L lactide) (COOH-PEG-PLA) (5k-16k, 909300, Sigma-Aldrich, USA) and N-Hydroxy succinimide ester-poly (ethylene glycol)-b-poly (D,L lactide) (NHS-PEG-PLA) (5k-16k, 909874, Sigma-Aldrich, USA) the drug free versions of three different diblock co-polymers prepared with thin hydration method. PMs were produced at a concentration of 40 µg/L which is above the critical micelle concentration. Chloroform (366927, Merck, Germany) was used as the organic solvent to form thin films from

polymeric micelles. 2 mg of polymer was weighed and dissolved in 50 mL of 99.8% GC chloroform (366927, Merck, USA). Then, chloroform was evaporated in a rotary evaporator (100 rpm, 65 °C, 300 mbar) for 90 min to obtain a thin film. The thin film was stored in a vacuum desiccator overnight to remove chloroform residues. It was hydrated with 50 mL of 25 °C distilled water d(H_2O) and sonicated in an ultrasonic water bath pre-set to 50 °C for 30 min. It was kept in the vortex mixer for 1 min. It was stored in the refrigerator for further analysis.

3.2.4.2. Preparation of EVE-loaded PMs

2 mg of EVE was weighed and dissolved in 5 mL of tetrahydrofuran (THF, 360589, Sigma Aldrich, 99.00%, USA). 2 mg of mPEG-b-PLA and COOH-PEG-PLA dissolved in 50 mL of chloroform were added to the solution and the same method as in section 3.2.1 was followed.

3.2.5. Synthesis of RGDK peptide

RGDK peptide was synthesized with The Liberty Blue Automated Microwave Peptide Synthesizer (CEM Corporation, USA). The synthesis scale was arranged to 0,1 mmol and C terminus was adjusted as amide end. 0,143 mg Rink Amide Protide resin (R003-B, CEM Corporation, USA) was previously weighed, left to swell in dimethylformamide (DMF, 200-679-5, Merck, USA) prior to peptide synthesis. >%99 N,N′-Diisopropylcarbodiimide (DIC,8.03649, Sigma Aldrich, USA) was used as an activator and its solution was prepared by adding 0.5 mL DIC in 5.5 mL DMF. For activator base, Ethyl cyanohydroxyiminoacetate (Oxyma, 233412, Sigma Aldrich, USA) was used and prepared in 3 mL DMF. Also, piperidine was prepared by mixing 5 mL of it with 20 mL DMF. After placing each amino acid, DIC, oxyma, resin, piperidine and DMF in appropriate bottles, the peptide synthesis was initiated. The reaction proceeded and after it finished the peptide was cleaved from the resin part with Razor Peptide Cleavage System (CEM Corporation, USA). The cleavage cocktail consists of 4.75 mL of trifluoroacetic acid (TFA 108262, Merck USA), 125 µL of %98 triisopropylsilane (TIS, 23378, Sigma Aldrich, USA) and 125 µL of distilled water d(H_2O). The cleavage was conducted at 38°C for 30 minutes. The cleaved peptide was

precipitated in cold diethyl ether (346136, Merck, USA) and then centrifuged two times at 8000 rpm for 5 minutes. After centrifugation, diethyl ether was decantated and peptide was left to dry under vacuum. The peptide ready for storage was stored at -20°C for micelle conjugation.

3.2.6. Purification of EVE Loaded PMs

EVE-loaded mPEG-b-PLA and COOH-PEG-b-d-PLA micelles were purified by gel permeation chromatography (GPC) with sephadex resin (PD MiniTrap™ G-25, 28-9180-07, Cytiva, UK). Prior to purification, the formulations were used directly without passing through a PES membrane syringe filter with a pore diameter of 0.45 μm. Purification was performed by gravity flow method. To prepare the columns for use, 3.0 mL of distilled water d(H_2O) was first added to remove the buffer solution in the kit and the column was equilibrated by repeating this process two more times. Then, 1 mL of EVE-loaded PMs sample was loaded onto the column. After the first elution step, 1.5 mL of distilled water was added to the column and this fraction was collected with the micelles label. Then, 1.5 mL of distilled water was again added to the column to obtain free (unencapsulated) everolimus and the resulting fraction was collected separately.

3.2.7. Optimization of HPMC MPs

In the optimization studies of microparticles, the properties of the formulation and the production parameters used in the production were cross-characterized in order to reveal the effect of various factors on the size, morphology, production efficiency and reproducibility, bio-adhesion properties of the microparticle. With the formulation and production parameters selected as a result of optimization studies, encapsulation of drug-loaded polymeric micelles into microparticles was carried out. The parameters used in the formulation and production parameters are as follows.

3.2.7.1. Parameters Used in Formulation Optimization

In the production of particles to be produced by spray-drying method, the increase in the total solid content in the solution makes the droplets formed during atomization during production more dense, thus increasing the size of the particles formed as a result of production (147). However, similarly, if the concentration is decreased by increasing the volume of solvent used, the droplets will contain less solid particles and the particle diameter will decrease after the drying process (148, 149). On the other hand, microparticles obtained with very low concentrations may show a fragile structure and their morphology may not provide the desired properties. The use of auxiliary substances in the formulation may reduce the crystallization of the active substance in various cases and provide a more homogeneous structure, or it may cause an increase in particle size due to an increase in the proportion of solids in the solution (149).

The amount of HPMC selected as the microparticle forming agent, the volume of distilled water (H_2O) selected as the solvent, the concentration of HPMC in the solution, and the presence and amount of lactose monohydrate used as an excipient in the formulation were determined as variables in the optimization of the formulation.

3.2.7.2. Optimization of Process Parameters

Spray-drying method was chosen for the production of microparticles. Spray-drying method is a scalable technology in which liquid formulations are rapidly dried with hot air and then sprayed with a noozle to form solid particles (150). The production parameters applied during production with this method have a direct impact on the targeted properties of the microparticles. Production parameters can be listed as inlet temperature, gas pressure, pump rate, aspirator rate, noozle diameter, outlet temperature.

In order to produce particles with the targeted morphology and size, the production parameters were determined by considering the studies in the literature where water

(aqueous medium) (H_2O) was used as solvent and HPMC as particle former (147,148,149).

During the optimization, the pump rate (%) parameter was selected as a variable to optimize the production in terms of repeatability and particle size and distribution. According to the chart obtained from the user manual of the device used in production (Mini Spray Dryer B-290®), the relationship between the percentage pump rate feed flow is as follows.

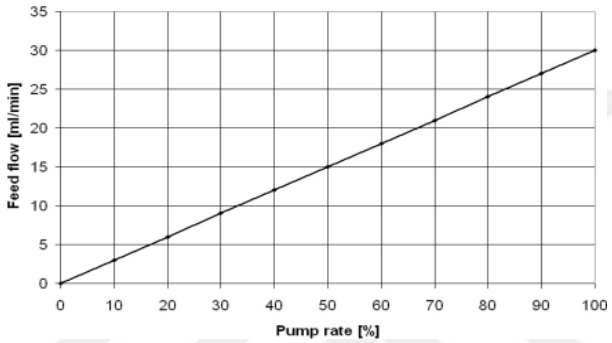

Figure 3.2. Relation Between Pump Rate (%) and Feed Flow (mL/min) (151)

3.2.8. Preparation of HPMC Solution

The amount of HPMC, solvent volume and solution concentration (% v/w) were first optimized to determine the formulation with the most suitable properties to encapsulate the drug-loaded PMs. Preparation of the solution; the amount of HPMC intended to be used was weighed (0.15, 0.3, g) and the required amount of distilled water d(H_2O) (100, 200 and 400 mL) was added. The mixture was kept on a magnetic stirrer at 25 °C for 24 hours to completely dissolve the HPMC in distilled water. The formulations containing only HPMC prepared for optimization purposes are as follows. The formulations were prepared multiple times on different days under identical conditions for reproducibility tests.

Table 3.3. Properties of HPMC solutions

Formulation Number	Amount of HPMC (gr)	Solvent Volume (mL)	% (w/v) concentration
1	0,15	100	% 0,15
2	0,3	100	% 0,3
3	0,3	200	% 0,15
4	0,3	400	% 0,075

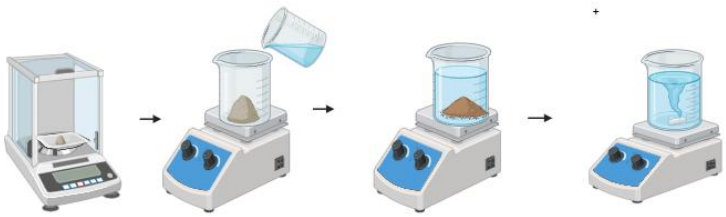

Figure 3.3. Preparation of HPMC Solutions

3.2.9. Spray-Drying Process of HPMC Solutions

HPMC solutions were spray dried in a Mini Spray Dryer B-290® (BÜCHI Labortechnik AG, Switzerland). Among the production parameters, pump rate (%) was set as a variable for optimization studies. Spray drying was performed under the following conditions: inlet temperature was set to 130 °C, with an outlet temperature maintained around 60 °C. The peristaltic pump rate was adjusted to % (8,10 and 20) which equals to 2.4, 3, 6 mL/min respectively (151), the aspirator rate was set to 100% (~ 35 m3/h, gas flow rate) and the atomizing air flow (rotameter) was maintained at 40 mm which equals to 473 L/h. A two-fluid nozzle (0.7 mm diameter) was used in nozzle cleaner mod. The spray drying process is completed, the device is turned off according to the instructions and left to cool the dry powder collected in the collection from container carefully.

Table 3.4 Experimental conditions used for the optimization studies

Number of the Formulation		**1**	**2**	**3**	**4**	**5**	**6**	**7**
Process Paremeters	Pump Rate (%)	20%	10%	10%	20%	10%	20%	%10
	Inlet Temperature (°C)	130 °C	130 °C	130 °C	130 °C	130°C	130 °C	130 °C
	Aspirator (%)	100%	100%	100%	100%	100%	100%	100%
	Rotameter (Flow Meter) (mm)	40 mm	40 mm	40 mm	40 mm	40 mm	40 mm	40 mm
Formulation Conditions	Amount of HPMC (gr.)	0,3 gr.	0,3 gr.	0,3 gr.	0,3 gr.	0,3 gr.	0,15 gr.	0,15 gr.
	Solvent Volume (mL)	100 mL	100 mL	200 mL	200 mL	400 mL	400 mL	200 mL
	% (w/v) concentration	0,30%	0,30%	0,15%	0,15%	0,30%	0,037%	0,075

After completing characterization studies (size and size distribution, morphology, adhesion tests, adhesion tests, production efficiency) on six different formulations, everolimus-loaded PMs integration was carried out on the formulation showing the most suitable properties. Production yields (%) were also calculated for each formulation produced.

3.2.10. Optimization of Amount of Lactose

During the spray drying process, the deposition of substances with adhesive properties (HPMC) on the column walls was observed in the column where the drying process took place. The inclusion of low-adhesive excipients such as lactose in the formulation helps to increase production efficiency by reducing the stickiness of the product during the process and allowing more product to reach the collection container (152). Lactose monohydrate (InhaLac® 500, Meggle Pharma, USA) was included in the formulation to increase production efficiency and to improve the flow profile of the powder to be obtained.

Optimization of the amount of lactose to be used in the formulation was carried out after the optimizations on the production parameters (pump rate) and the main formulation (amount of substance, solvent volume, concentration) were completed. Four different formulations containing only lactose, lactose and HPMC mixtures were

prepared for the optimization study. The method of preparation of the formulations was the same as the method of preparation of HPMC solutions. The formulations containing only lactose were prepared by weighing certain amounts of lactose (0.3 g and 0.9 g), adding 200 mL of distilled water d(H_2O) and allowing it to dissolve completely in a magnetic stirrer at 25°C for 24 hours. Lactose and HPMC containing formulations; certain amounts of lactose (0.3 g and 0.9 g) and 0.3 g of HPMC were weighed and 200 mL of distilled water d(H_2O) was added and allowed to dissolve completely in a magnetic stirrer at 25°C for 24 hours.

Table 3.5. Conditions of Prepared Formulations for Excipient (Lactose) Optimization

Number of the Formulation		**1**	**2**	**3**	**4**
Process Paremeters	Pump Rate (%)	10%	10%	10%	10%
	Inlet Temperature (°C)	130 °C	130 °C	130 °C	130 °C
	Aspirator (%)	100%	100%	100%	100%
	Rotameter (Flow Meter) (mm)	40 mm	40 mm	40 mm	40 mm
Formulation Conditions	Amount of Lactose (gr.)	0,3 gr.	0,3 gr.	0,9 gr.	0,9 gr.
	Amount of HPMC (gr.)	0,3 gr.	0	0,3 gr.	0
	Solvent Volume (mL)	200 mL	200 mL	200 mL	200 mL
	% (w/v) HPMC concentration	0,15%	0,00%	0,15%	0,00%
	% (w/v) Lactose concentration	0,15%	0,15%	0,45%	0,45%
	% (w/v) Total	0,30%	0,30%	0,60%	0,45%

The prepared formulations were subjected to spray drying process under the conditions given in the table (Pump Rate: 10%, Inlet Temp. :130 °C, Aspirator 100%, Rotameter: 40 mm). After the characterization studies (size distribution, morphology, adhesion tests, production efficiency) were completed on the dry powder obtained as a result of production, the amount of lactose to be used in the formulation was determined.

3.2.11. Integration of EVE Loaded PMs Into HPMC MPs

EVE-loaded polymeric micelles (EVE-PMs) were integrated into HPMC microparticles (MPs) by in-process loading method. As a result of optimization studies on production parameters and formulation components, the most suitable formulation for encapsulation of EVE-loaded PMs was determined. Necessary adjustments were made in the formulation according to the final mixture to be formed before the spray drying process. In this context, three separate productions were carried out using three different polymer types (mPEG-PLA, COOH-PEG-PLA and RGDK-NHS-PEG-PLA). All production parameters except the polymer type used were kept constant. The PMs dispersions were prepared four times more concentrated to compensate for the dilution that would occur when added to the HPMC-lactose solution. At the same time, to keep the total volume of the HPMC-lactose solution constant, the PMs dispersion was prepared in a reduced volume (25% less) by the volume in the final mixture. Table 3.6 shows the adjustments made to the formulations to create the final mixture.

Table 3.6. Formulation Regulation for Final Mixture

EVE loaded PMs Formulation		**HPMC – Lactose Solution Formulation**	
First Volume	50 mL	**First Volume**	150 mL
Final Volume (In Mixture)	200 mL	**Final Volume (In Mixture)**	200 mL
First PMs Concentration	200 ug/L	**First Concentration % (w/v) (HPMC + Lactose)**	% 0,75
Final PMs Concentration	40 ug/L	**Final Concentration % (w/v) (HPMC + Lactose)**	%0,6

The following figure illustrates the production steps; (1) The loaded micelle and HPMC and lactose solution were collected in a single beaker. (2) Stirred in a magnetic stirrer at 25 °C for 24 h. (3) Spray dried under optimized conditions (Pump Rate: 10%, Inlet Temp. :130 °C, Aspirator 100%, Rotamer: 40 mm).

Figure 3.4 Steps of Preparation of Encapsulation of EVE Loaded PMs into MPs

3.2.12. Characterization of Polymeric Micelles

3.2.12.1. Size Distribution

The size distribution of 3 different versions of drug free and EVE-PMs (unfiltered and 0,45 µM PES membrane filtered) **(mPEG-PLA, COOH-PEG-PLA, NHS-PEG-PLA)** was determined by the mean hydrodynamic diameter using DynoPro Nanostar (Wyatt Technology, USA) which uses dynamic light scattering (DLS) as a measurement technique. For the analysis, 80 µL of the PM dispersion was placed into a DLS cuvette. The measurement was carried out through 10 consecutive runs, each preceded by a 5-second equilibration period. Particle size results were expressed as the mean value accompanied by the standard deviation (± SD).

3.2.12.2. Zeta Potential

The surface charge of the was drug free and EVE-PMs (unfiltered and 0,45 µM PES membrane filtered) determined by the zeta potential using LiteSizer 500 (Anton Paar, Austria) which DLS as a measurement technique. Samples are introduced into omega cuvettes (#225288, Anton Paar, Austria) for measurement. The measurements were performed for dispersions (water) at 0.8903 cP viscosity and 1.3303 refractive index parameters, at 25 ± 0.1 °C, in 20 run with 3 replication.

3.2.12.3. Particle Concentration Determination of EVE-PMs

Particle concentration measurements were performed using a Dyno-Pro Nanostar instrument (Wyatt Technology). Measurements were performed on mPEG-PLA and COOH-PEG-PLA micelle samples loaded with EVE only. Before the measurement, the instrument was subjected to calibration procedures. First, the offset value of the instrument was determined with distilled water used as a dispersant for the micelles. After calibration, the measurements were performed using a 2 µL JC-710 (Wyatt Technology, USA) quartz cuvette.

3.2.13. Morphology

3.2.13.1. Scanning Electron Microscopy (SEM)

The surface morphology, shape and size homogeneity of the produced PMs (mPEG-PLA, COOH-PEG-PLA, RGD-PEG-PLA) and EVE-PMs (loaded mPEG-PLA, COOH-PEG-PLA) analyzed using scanning electron microscope (SEM) (Thermoscientific, Quattro S SEM). SEM analysis was performed at +4°C, 15000 kV power, vacuum mode ($4.58 \times 10^{-4}\ Pa$) after micelles were dried by placing them on aluminum foil and placing copper strips on the edges to increase conductivity.

3.2.13.2. Transmission Electron Microscopy (TEM)

Morphological characterization of EVE-PMs (loaded mPEG-PLA, COOH-PEG-PLA) was supported by Transmission Electron Microscopy (TEM) (FEI, Thermo Fisher Scientific Talos L120C). For the analysis, one drop of each sample was taken and carefully dropped onto carbon-coated copper grids. Imaging was performed in bright-field mode at 120 kV.

3.2.14. Calibration Curve for Everolimus

0.54 mg EVE was weighed and dissolved in 1.4 mL (0,385 mg/mL) Acetonitrile (ACN) (100030, Merck, USA) to form a stock solution. Then, the solutions of EVE prepared in the range of 1.72- 41.3 mg/mL by dilution from the stock solution were measured absorbance values at 278 nm wavelength by UV-Vis spectrophotometer and the change according to the concentration was graphed as shown in Figure 3.5.

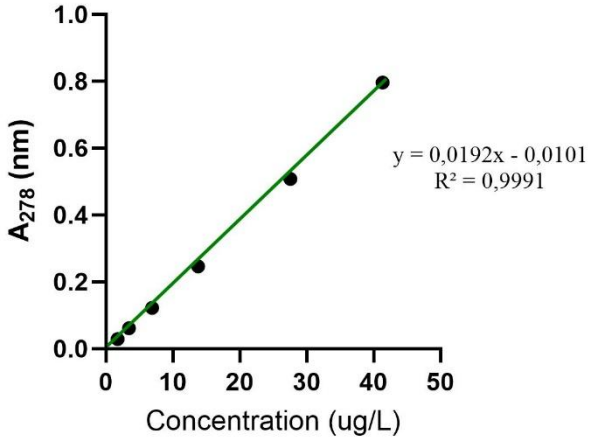

Figure 3.5. Calibration Curve for EVE

3.2.15. Determination of Encapsulation Efficiency

EVE quantification was determined by indirect method. Quantification of free (unencapsulated) EVE loaded micelles separated by GPC method was performed separately. Measurements were performed using a UV-Vis spectrophotometer (840-210600, Thermo Fischer, USA). A 1.5-fold dilution factor was applied for the samples. Measurements were performed in Thermo Scientific™ Semi-Micro Cell Quartz cuvettes. 200 uL of both samples were taken, dissolved in 500 uL ACN and placed in the cuvettes. The amount of EVE loaded into the micelles and the amount of free everolimus were calculated using the measured absorbance values and the previously prepared standard calibration curve equation. The encapsulation efficiency (EE) of the micelles was calculated in % according to Equation 1.

$$Drug\ EE(\%) = \left(\frac{encapsulated\ drug\ amount}{initially\ added\ drug\ amount}\right) \times 100$$

3.2.16. Functional Group Analysis of RGDK-NHS-PEG-PLA micelles

Fourier Transform Infrared Spectroscopy (FT-IR) (114640, Perkin Elmer, USA) was used to confirm the conjugation of the RGD peptide to the PEG-PLA structure. The measurements were performed with the ATR accessory method and the spectra were recorded in the wave number range 4000-500 cm^{-1}. The synthesized RGD peptide (RGDK), polymer (NHS-PEG-PLA) and RGD-PEG-(b)-PLA samples obtained after conjugation were analyzed. The success of the conjugation process was evaluated based on the characteristic functional group vibration bands.

3.2.17. Characterization of Microparticles

3.2.17.1. Size Distribution

Particle size distribution of dry powder microparticles was performed in Wet Dispersion Mode using a Mastersizer® 2000 (Malvern Instruments, UK). Analyses were performed at a temperature of 25 ± 0.1 °C with three replicates for each sample. Prior to the measurement, background measurements were performed with distilled water d(H_2O), ethanol and isopropyl alcohol (IPA), respectively. The formulations were grouped according to the excipients they contained; microparticles containing only HPMC, microparticles containing a combination of HPMC and lactose and microparticles containing only lactose. Microparticles containing HPMC only were dispersed in isopropyl alcohol (IPA). The dispersion medium had a refractive index of 1.377 and a viscosity of 2.43 cP. The refractive index of HPMC was set to 1.530 and the absorption value to 0.01. During the dispersion of HPMC and lactose-containing formulations in IPA, it was observed that lactose sedimented rapidly. Therefore, ethyl acetate (109623, Merck, USA) was used for the dispersion of lactose-containing and lactose microparticles. The dispersion medium parameters for ethyl acetate were entered into the system as refractive index 1.372 and viscosity 0.45 cP. The refractive index of lactose was determined as 1.538.

3.2.17.2. Morphology

Light Microscope Analysis

The surface morphology and appearance of the dry powder microparticles were examined using a light microscope (Carl Zeiss Microscopy GmbH, Germany). A small amount of the microparticle samples was dispersed with 100 µL IPA sprinkled on the slide and covered with cover glass. Samples were observed directly under the microscope and micrographs were taken at different magnifications (10× 20× and 40×) to observe the particle shape and to confirm particle size analysis.

Scanning Microscope Analysis (SEM)

The surface morphology, shape and size homogeneity of the produced MPs analyzed using scanning electron microscope (SEM) (Thermoscientific, Quattro S SEM). SEM analysis was performed at +4°C, 10000 kV power, low vacuum mode ($8.25 \times 10^{-4}\ Pa$) after placing copper strips on the edges to increase conductivity.

3.2.17.3. Adhesion Test

Preparation of Artificial Lung Fluid and PBS Buffer

To prepare the simulated lung fluid (SLF) solution, the formulation used by Twinning et. Al. (2005) was used to prepare the simulated lung fluid (SLF) solution. The required amount of ingredients were weighed and mixed in 100 mL of distilled water at 25 °C for 12 hours on a magnetic stirrer to obtain a clear solution. A 100 mL solution of PBS (saline) (P4417, Sigma Aldrich, USA) was prepared using a single tablet. Measurements were performed by wetting a small amount of powder for each formulation with 10 µL of SLF and PBS solution. The ingredients used in the formulation are shown in the table below.

Table 3.7 Components used in the preparation of simulated lung fluid

Component	Concentration (g/L)
Sodium chloride (NaCl)	6,43
Sodium bicarbonate ($NaHCO_3$)	2,60
Calcium acetate monohydrate	0,40
Calcium chloride ($CaCl_2$)	0,37
Magnesium acetate tetrahydrate	0,21
Magnesium chloride	0,20
Potassium dihydrogen phosphate (KH_2PO_4)	0,27
Dipotassium sulfate (K_2SO_4)	0,17
Citric acid ($C_6H_8O_7$)	1,15
Bovine serum albumin (Fraction V)	0,20
Benzalkonium chloride	0,05

3.2.17.4. Determination of Angel of Repose

Angle of repose is the peak angle of the conical pile formed by the dust particles when they are freely shed, which is formed due to the cohesion and friction behavior of the dust particles with each other. An increase in the angle of repose indicates an increase in the friction and cohesion forces between the particles. High levels of these two forces adversely affect the fluidity of dust particles (153,154). Bulk angle measurements of powder particles were performed only on particles containing HPMC. Since samples from a single batch were insufficient for measurement, HPMC particles produced on different days (different batches) were combined and measured. A round flat surface was prepared with a substrate covered with millimeter paper. Then, enough powder particles to form a conical pile were released vertically with a funnel about 10 cm above the millimeter paper covered surface. The base diameter and height of the conical stack were measured with a ruler. The angle of the pile was calculated using the trigonometric tangent equation.

3.2.17.5. Swelling Ratio

The swelling tests of the produced micelles free HPMC microparticles were carried out separately in PBS and pure water d(H2O) in the range of 0-240 min. in a light microcope. Images were measured in 20x micrograph, images of a selected particle under the microscope image were recorded in the measured time interval and swelling ratios in terms of size were calculated.

4. RESULTS

4.1 Optimization and Characterization of Polymeric Micelles

4.1.1 Determination of PMs Critical Micelles Concentration (CMC)

In order to determine the critical micelle concentration (CMC) of micelles obtained from mPEG-PLA, COOH-PEG-PLA, NHS-PEG-PLA polymers, surface tension (ST) values of µg/mL samples at various concentrations (5,10,15,15,20,20,30,40,50,50,75,100,125,150,200) were plotted as a linear graph depending on concentration - surface tension. Since the concentration values of the samples prepared for measurement were relatively close to each other, the concentration values were taken logarithmically, a significant curve between the surface tension did not emerge. Therefore, the CMC concentration values were determined by calculating the intersection point of two different lines drawn over the points where the surface tension varied linearly.

For mPEG-PLA PMs, the range of four samples (10, 12, 15, 20 µg/mL) was selected on the x-axis where the linear change was evident in the plotting of the line, and the range of three samples (50, 75, 100 µg/mL) was selected in the plotting of the second line. In Figure 4.1. the first-order line equations for the selected points and the correlation coefficient (R^2) are shown.

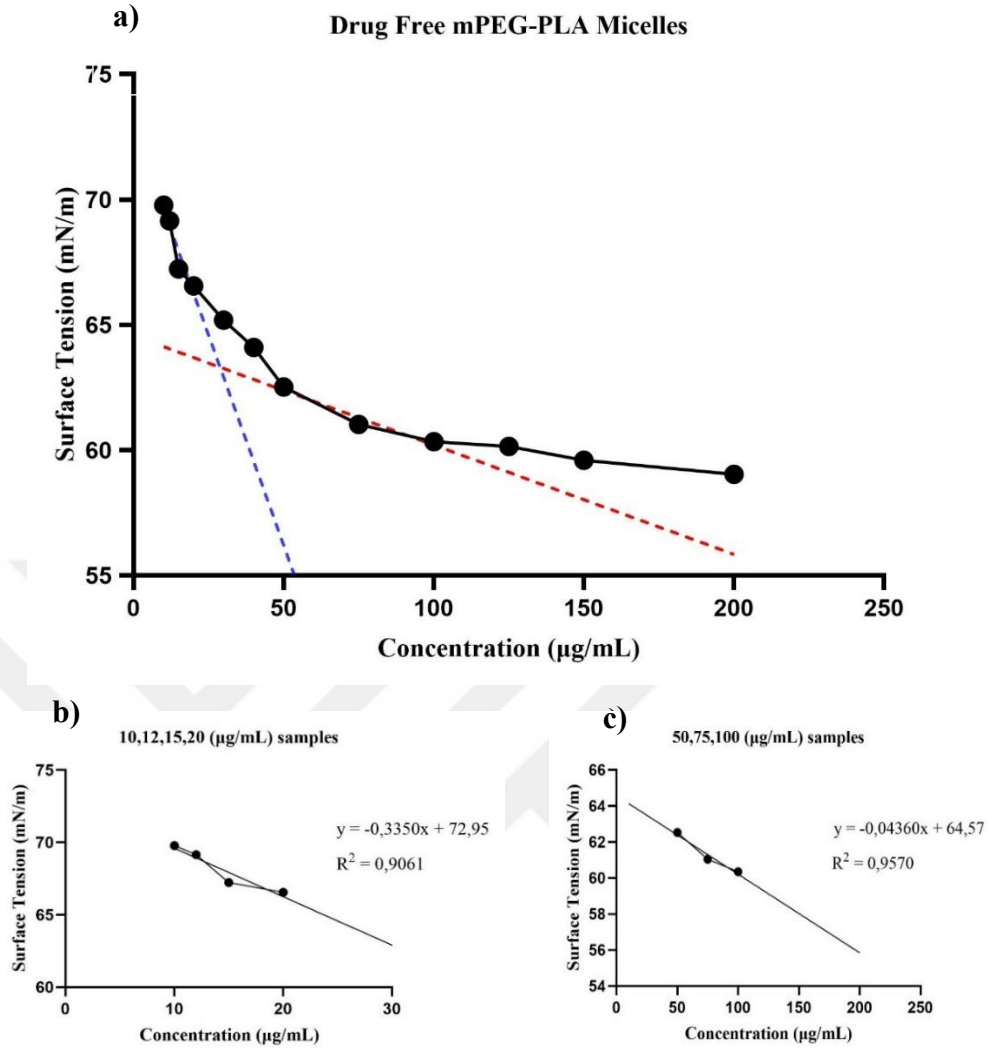

Figure 4.1. a) Surface tension – concentration graph of drug free mPEG-PLA samples, **b)** Surface tension – concentration graph of 10,15,20 µg/mL drug free mPEG-PLA samples, **c)** Surface tension – concentration graph of 50,75,100 µg/mL drug free mPEG-PLA samples

For COOH-PEG-PLA PMs, the first three points on the x-axis for the first line (10,15,20 µg/mL) and the second line (50,75,100 µg/mL) concentrations were selected. The equations of the lines are shown in Figure 4.2 with the correlation coefficients.

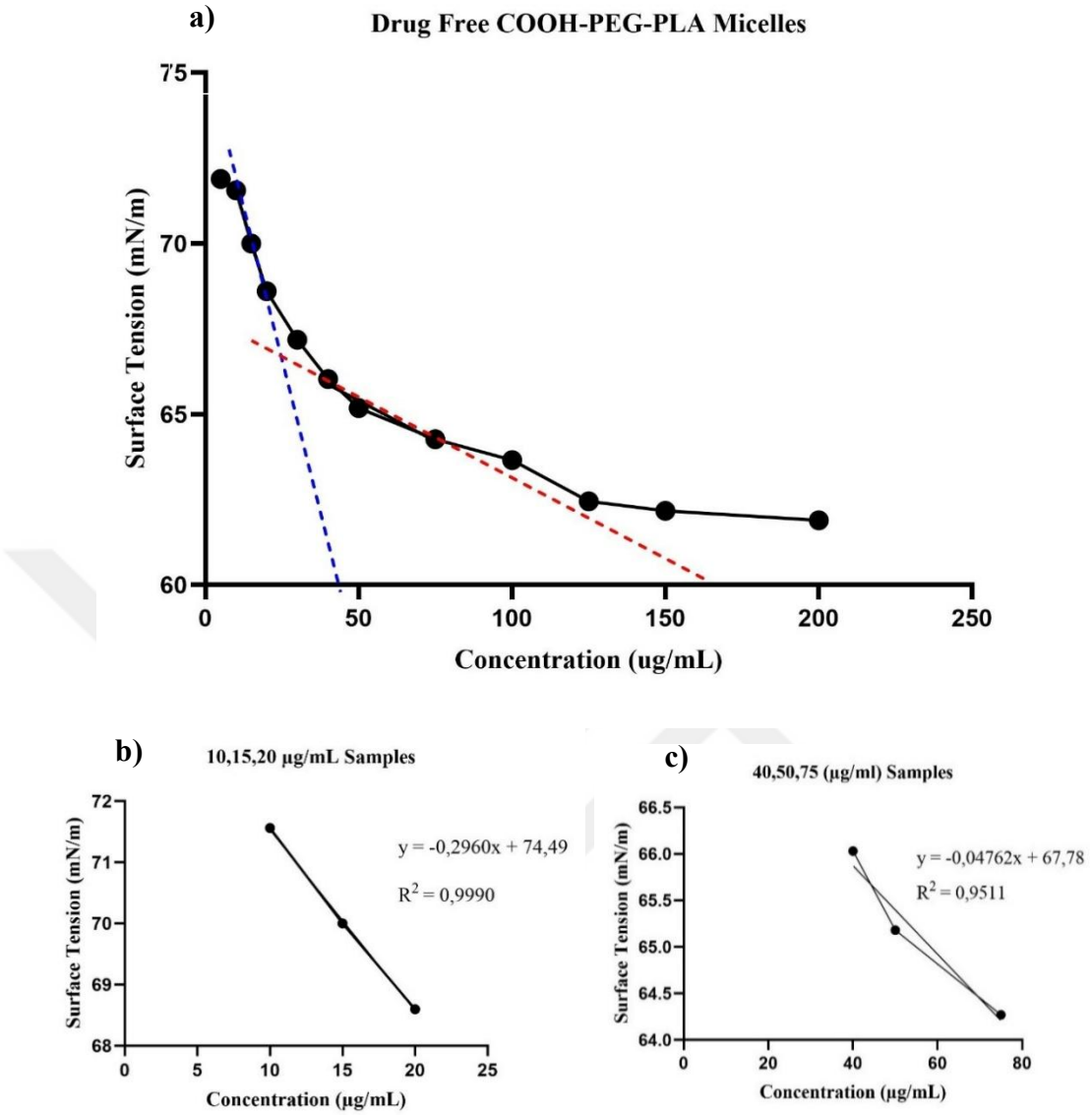

Figure 4.2. a) Surface tension – concentration graph of drug free COOH-PEG-PLA samples, b) Surface tension – concentration graph of 10,15,20 µg/mL drug free COOH-PEG-PLA samples, c) Surface tension – concentration graph of 40,50,75 µg/mL drug free COOH-PEG-PLA samples

For NHS-PEG-PLA PMs, the first line was selected from the range (10,15,20 µg/mL) and the second line was selected from the range (40,50,75 µg/mL). The equations of the lines are shown with their correlation coefficients.

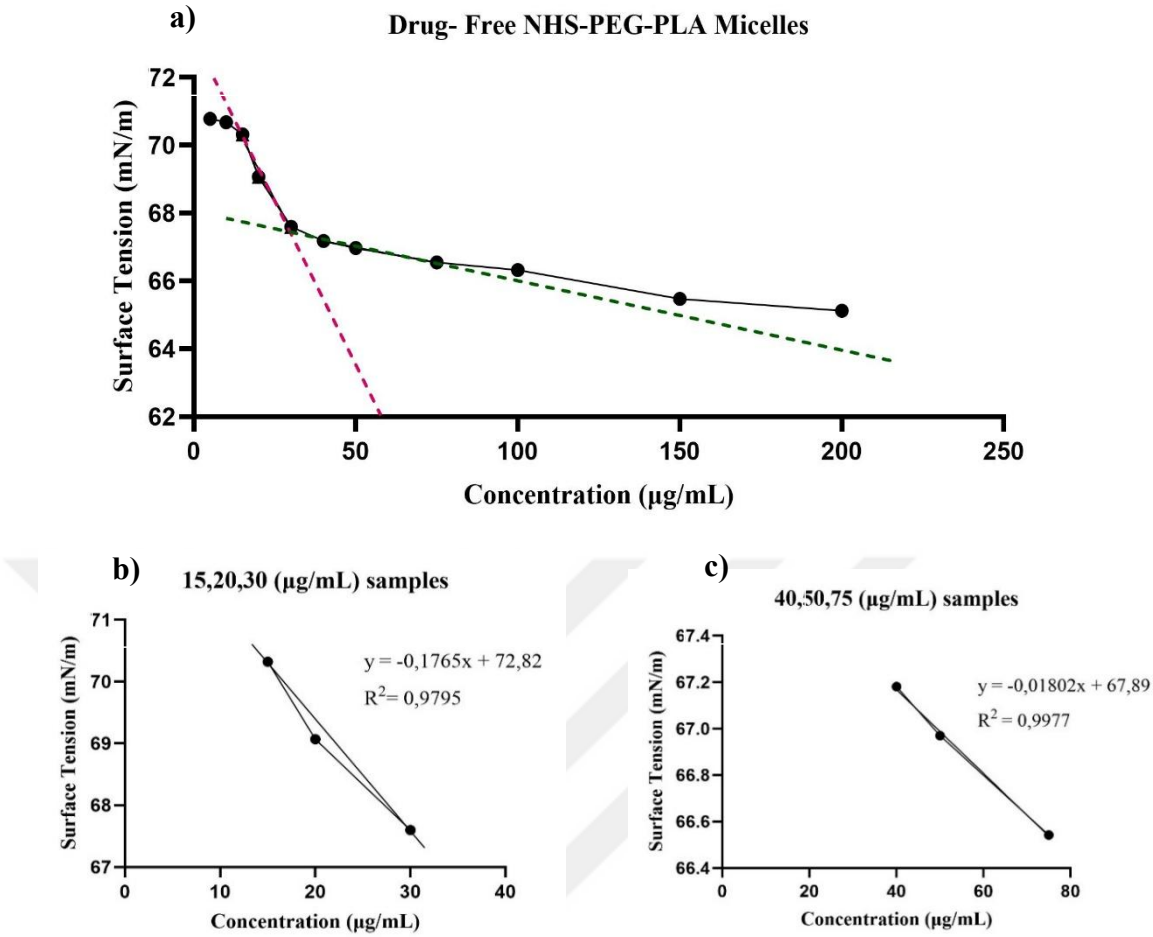

Figure 4.3. a) Surface tension – concentration graph of drug free NHS-PEG-PLA samples, **b)** Surface tension – concentration graph of 15,20,30 µg/mL drug free NHS-PEG-PLA samples, **c)** Surface tension – concentration graph of 40,50,75 µg/mL drug free NHS-PEG-PLA samples

The ordinate value calculated by solving the equation with two unknowns for the drawn lines was taken as the CMC value. The value found was compared with polymeric micelles obtained from the same polymers (different kDa) in the literature and it was concluded that the CMC value obtained was significant. Table 4.1. shows the calculated CMC values in µg/mL (ppm) and millimolar (mM), the molecular weights (g/mol) of the polymers and the concentration at which the active substance (EVE) was encapsulated.

Table 4.1 Calculated CMC values of 3 types of polymeric micelles

Micelle Type	Molecular Weight (g/mol)	Mean Molecular Weight (g/mol)	Calculated CMC (µg/mL) Value	Calculated CMC (mM) Value	EVE Loaded Concentration (µg/mL)
mPEG-PLA	5000-10.000	7500	28,75	3.83	40
COOH-PEG-PLA	5000-16.000	10.500	27,02	2.57	40
NHS-PEG-PLA	5000-16.000	10.500	31,10	2.96	-

As a result of the calculated CMC value, it was found appropriate to load everolimus at a concentration of 40 µg/mL, which is above the critical micelle concentration.

4.1.2 Determination of Surfactants Critical Micelles Concentration

In order to reveal the effect of surfactants on CMC values of polymeric micelles, critical micelle concentrations of three different surfactants (Pluronic F-127, Brij98™ and Gelucire®) were calculated.

In the surface tension measurements of Pluronic F-127, since the surface tension did not show a significant change in the measurements performed in the selected concentration range (5, 10, 15, 20, 30, 40, 50, 75, 100, 125, 200 µg/mL) in polymeric micelles and other surfactants and the CMC value obtained from the literature (950-1000 ppm) was higher than the other measured samples (Brij98 and Gelucire), the concentration range of the measurements was kept wider. For Pluronic F-127, measurements were carried out on samples with concentrations of (0.025, 0.005, 0.1, 0.25, 0.5, 5, 10, 25, 50, 100, 250, 500) mg/mL.

Figure 4.4. shows the graphs generated for Pluronic F-127. The range of (0.25, 0.5, 5 mg/mL) for the first line and (10, 50, 100 mg/mL) for the second line were selected

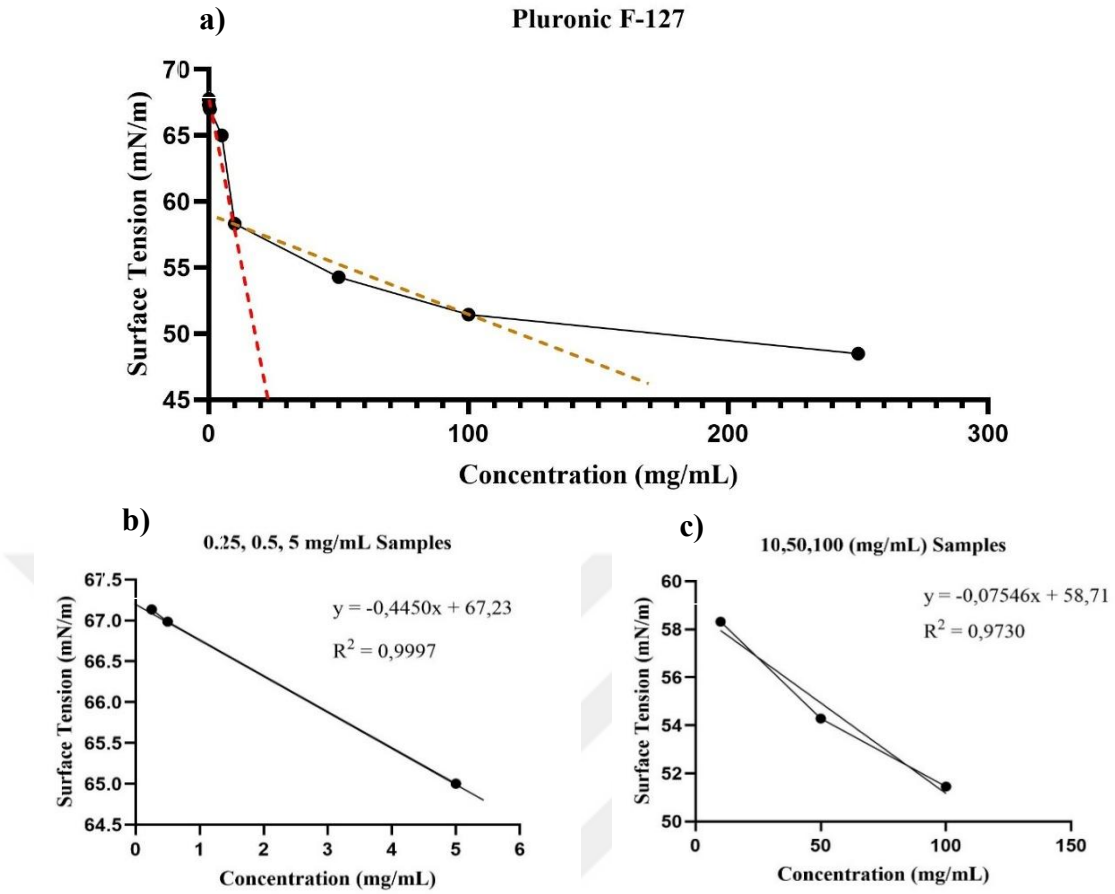

Figure 4.4 a) Surface tension – concentration graph of Pluronic F-127 samples, **b)** Surface tension – concentration graph of 0,25,0,5,5 mg/mL pluronic F-127 samples, **c)** Surface tension – concentration graph of 10,50,100 mg/mL pluronic F-127 samples

Measurements were performed in the concentration range (0.1, 0.5, 1, 5, 10, 15, 20, 30, 50, 100, 200, 300, 400 µg/mL) in the samples handled with Brij98™. Figure X shows the graphs of the measurements performed with Brj98™. The range (5,10,15 µg/mL) was chosen for the first line drawn and the range (50,100,200 µg/mL) was chosen for the second line drawn.

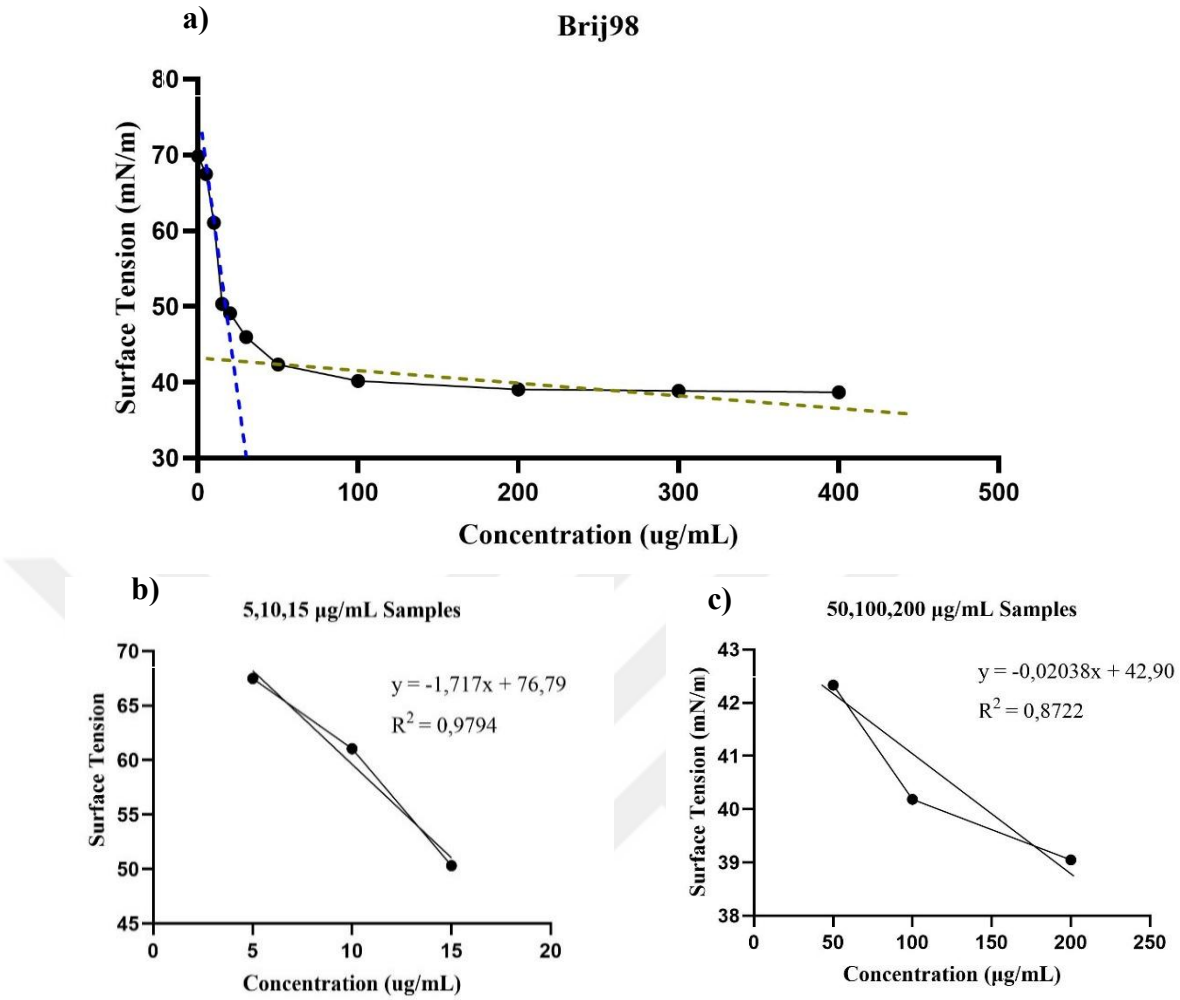

Figure 4.5. a) Surface tension – concentration graph of brij98 samples**, b)** Surface tension – concentration graph of 5,10,15 µg/mL brij98 samples **c)** Surface tension – concentration graph of 50,100,200 µg/mL brij98 samples

The measurements performed with the samples obtained with Gelucire® were performed in the concentration range (5, 10, 15, 20, 25, 50, 70, 100, 200 µg/mL). Figure 4.5 shows the graphs for the measurements performed with Brj98™. The range (5,10,15 µg/mL) was chosen for the first line drawn and the range (50,100,200 µg/mL) was chosen for the second line drawn.

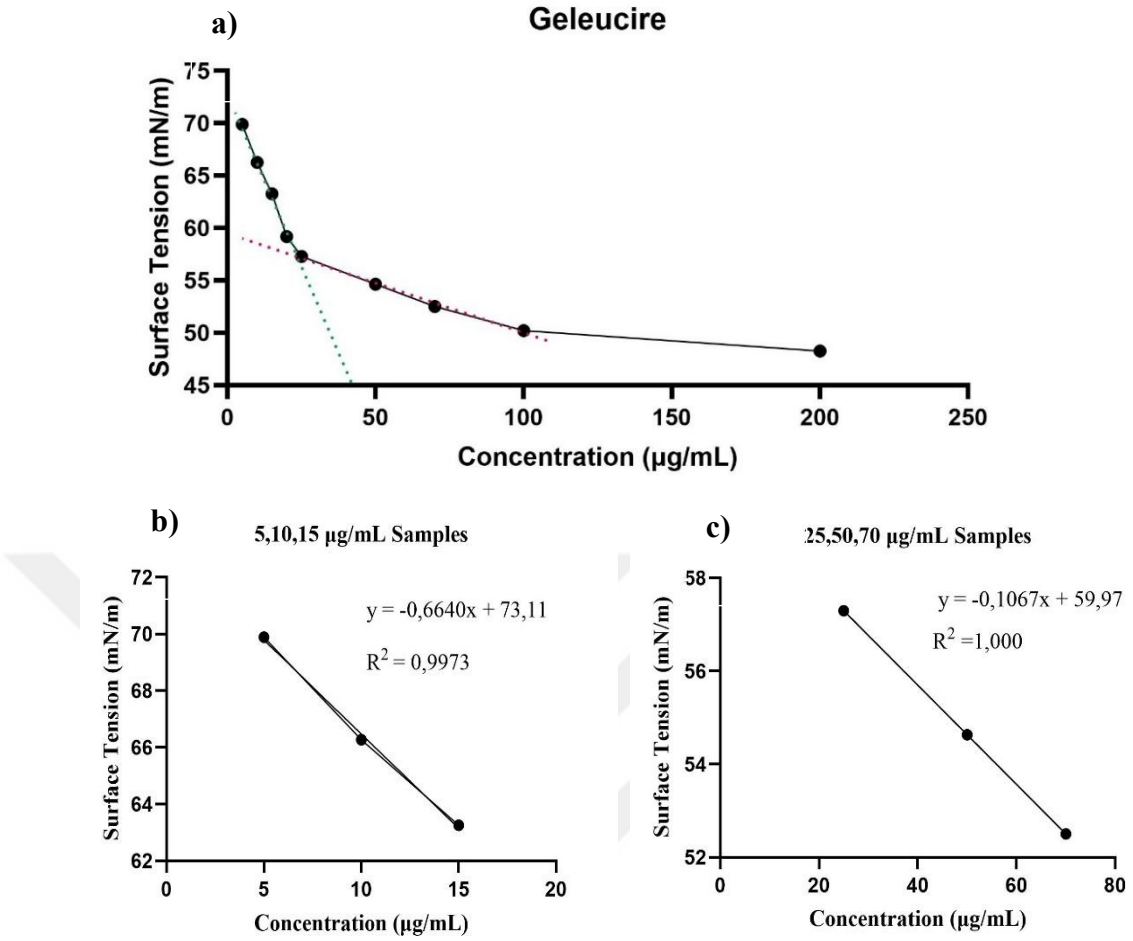

Figure 4.6. a) Surface tension – concentration graph of gelucire samples **b)** Surface tension – concentration graph of 5,10,15 µg/mL gelucire samples **c)** Surface tension – concentration graph of 25,50,70 µg/mL brij98 samples

Table 4.2. Calculated CMC values of surfactants

Surfactant Type	Mean Molecular Weight	Calculated CMC (µg/mL) Value	Calculated CMC (mM) Value	Literature CMC (µg/mL) Value
Pluronic F-127	12.600 g/mol	23050	1.83 mM	950-1000 (155)
Brij98™	1149,55 g/mol	20,05	0.01744 mM	28,75 (156)
Gelucire®	1766 g/mol	25,02	0.0142 mM	153 ± 31 (157)

4.1.2 Determination of Surfactants and Polymeric Micelles Mixtures Critical Micelles Concentration

In the samples obtained from the mixture of mPEG-PLA and pluronic F-127 (1:2 ratio), mPEG-PLA was used at a concentration range of (10,15,20,30,40,50,50,75,100,125,150,200 µg/mL) and pluronic F-127 was used at a concentration of (5, 7.5, 10, 15, 15, 20, 25, 37.5, 50, 62.5, 75, 100 µg/mL). Figure X shows the graphs of the measurements of the mixture. The range of (15-7.5, 20-10, 30-15 µg/mL) for the first line and (50-25, 75-37.5, 100-50) for the second line were chosen to represent the first concentration of mPEG-PLA and the second concentration of Pluronic F-127, respectively. CMC value for mPEG-PLA and pluronic F-127 mixtures 30,05 µg/mL.

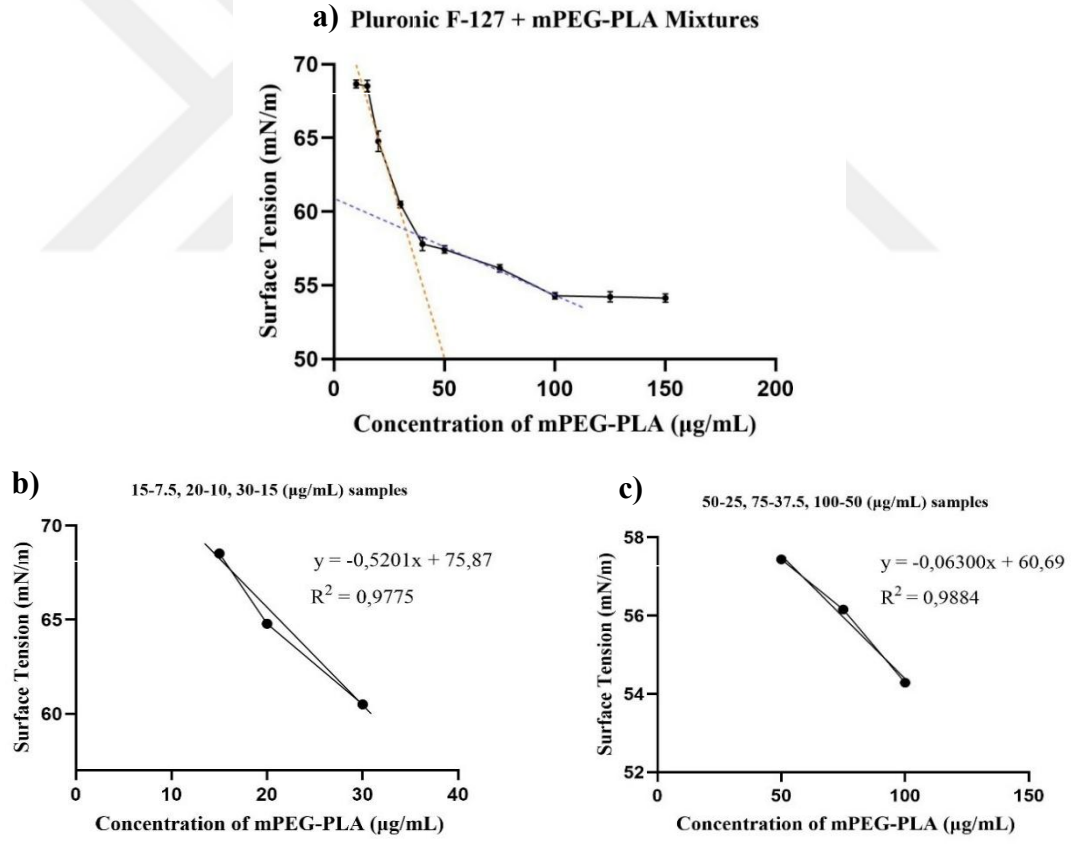

Figure 4.6. a) Surface tension – concentration graph of pluronic F-127 and mPEG-PLA mixture samples, **b)** Surface tension – concentration graph of 15-7.5, 20-10, 30-15 µg/mL mPEG-PLA and pluronic F-127 mixture samples, **c)** Surface tension – concentration graph of 50-25, 75-37.5, 100-50 µg/mL mPEG-PLA and pluronic F-127 mixture samples

In the samples obtained from mPEG-PLA and brij98 mixtures, the expected different linear decrease between surface tension and concentration could not be observed in the graph drawn. Therefore, CMC value could not be calculated for this mixture. Figure 4.7 shows that the surface tension continuously decreases. It is thought that this situation is not suitable for measuring the CMC value of the pendant drop method due to the high aggregation in the micellar structure.

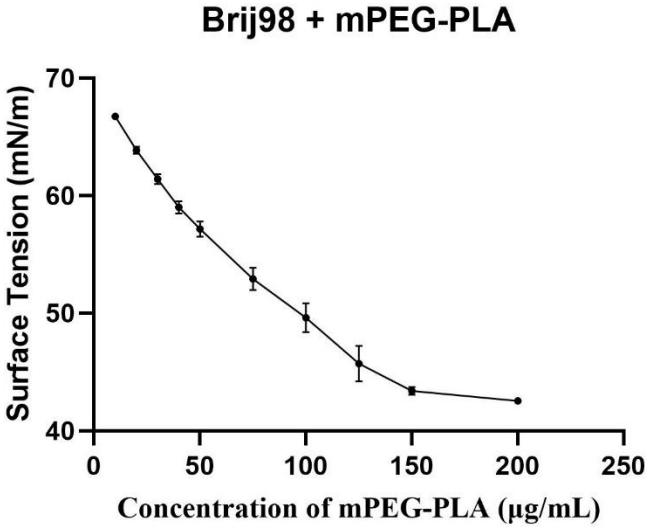

Figure 4.7. Surface tension – concentration graph of mPEG-PLA and brij98 mixtures

In the samples obtained from mPEG-PLA and gelucire mixtures, the expected different bi-linear decrease between surface tension and concentration could not be observed in the graph drawn. Therefore, CMC value could not be calculated for this mixture. Figure 4.8. shows that the surface tension continuously decreases similarly in brij98-PM mixtures graph.

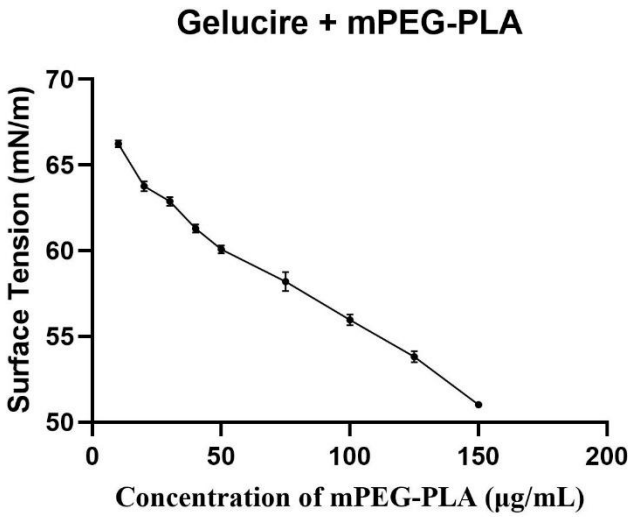

Figure 4.8. Surface tension – concentration graph of mPEG-PLA and gelucire mixtures

4.2 Characterization of Polymeric Micelles

4.2.1 Mean Size, Zeta Potential, PDI Determination of Drug Free PMs

The average size, zeta potential and polydispersity index of methoxy, carboxy and succinyl amide ester micelles obtained from three different derivatives of PEG-PLA are shown. In the measurement results, the values belonging to the peak with the highest intensity value are shown. Table 4.3. shows the values for mPEG-PLA. Within the scope of the thesis, it was aimed to produce micelles with dimensions below 100 nm and PDI value lower than 30% and monodisperse zeta potential value above ±10 mV.

It was observed that the PDI value of the sample of 40 µg/mL, the concentration at which the active substance (EVE) encapsulation of mPEG-PLA was performed, was higher than the target. It is observed that the zeta potential and size results are within the target limits.

Table 4.3. Mean size, zeta potential, molecular weight, %PD and %intensity values of drug free mPEG-PLA PMs.

Concentration (µg/mL)	Filtered Radius (nm)	Zeta Pot. (mV)	Mw-R (kDa)	%PD	%Intensity
20	93.0 ± 1.32	−15,4 ± 0,3	135676.1	32.39	89.5
30	198.9 ± 2.82	−32,7 ± 2,9	804850.3	85.9	28,00
40	96.3 ± 3.75	−17,3 ± 3,7	147227.0	62.79	98.7
50	191.2 ± 2.68	−9,3 ± 2,0	733665.5	20,65	92.0
75	70.3 ± 3.49	−37,6 ± 5,4	70585.5	30,86	90.3
100	66.9 ± 4.12	− 29,7 ± 1,8	62786.2	38,61	55.0
125	112.6 ± 2.71	−47,0 ± 1,6	212406.5	29,47	70.9
150	66.2 ± 2.06	− 18,4 ± 6,6	61265.2	14.14	98.7
200	61.6 ± 3.14	−33,9 ± 0,7	51892.4	25.69	80.3

For COOH-PEG-PLA micelles, the targeted properties in terms of size, zeta potential and polydispersity were obtained for the sample at 40 µg/mL concentration where EVE encapsulation occurred.

Table 4.4. Mean size, zeta potential, molecular weight, %PD and %intensity values of drug free COOH-PEG-PLA PMs.

Concentration (µg/mL)	Filtered Radius (nm)	Zeta Pot. (mV)	Mw-R (Kda)	%PD	%Intensity
20	52.4 ± 2.97	−18,8 ±2,404	35500.2	27.76	86.2
30	91.2 ± 2.74	−16,1 ± 1,3	129808.9	88.12	73.9
40	73.4 ± 3.15	− 17,400 ± 0,600	78087.6	13.85	100.0
50	101.7 ± 6.47	−22,8 ± 3,0	167505.3	41.24	98.3
75	64.5 ± 5.41	−24,1 ± 2,7	57666.2	93.3	93.3
100	113.4 ± 2.18	−30,233 ± 10,169	216215.6	63.77	93.5
125	83.5 ± 1.79	−31,7 ± 3,4	105528.8	49.25	98.9
150	286.4 ± 4.74	−42,6 ± 1,5	1887418.1	46.83	100.0

NHS-PEG-PLA micelles; although direct EVE encapsulation was not performed, conjugated RGD-PEG-PLA micelles were characterized to give an idea. The values for NHS-PEG-PLA are shown in Table 4.5.

Table 4.5. Mean size, zeta potential, molecular weight, %PD and %intensity values of drug free NHS-PEG-PLA PMs.

Concentration (µg/mL)	Filtered Radius (nm)	Zeta Pot. (mV)	Mw-R (kDa)	%PD	%Intensity
20	78.8 ± 4.12	− 35,6 ± 3,7	627204.7	39.96	82.0
30	106.1 ± 1.11	− 16,5 ± 1,7	184887.7	39.96	91.2
40	118.5 ± 7.68	− 28,4 ±2,1	239409.5	45.47	98.0
50	100.2 ± 3.84	−22,8 ± 3,0	161913.4	41.80	97.7
75	91.8 ± 2.41	−24,1 ± 2,7	131634.2	16.57	100.0
100	102.5 ± 2.67	−34,0 ± 2,7	170559.1	43.61	85.6
125	106.8 ± 3.15	−31,7 ± 3,4	187771.7	83.74	100.0
150	85.6 ± 4.85	−42,6 ± 1,5	111806.4	35.16	95.1

4.2.2 Mean Size, Zeta Potential, PDI, Particle Concentration Determination of EVE-PMs

Everolimus (EVE) encapsulated mPEG-PLA and COOH-PEG-PLA micelles at a concentration of 40 ug/mL were characterised in terms of size, zeta potential, polydispersity index and particle concentration. Table 4.6 shows the values for EVE-PMs (mPEG-PLA, COOH-PEG-PLA).

Table 4.6. Mean size, zeta potential, %PD, unfiltered and filtered particle concentration values of drug free COOH-PEG-PLA PMs.

Micelle Type	Sample Conc. (µg/mL)	Filtered Mean Radius (nm)	Zeta Pot. (mV)	%PD	Unfiltered Particle Conc. (1/mL)	Filtered Particle Conc. (1/mL)
mPEG-PLA	40	75.10 ± 2.50	−13,211 ± 1,1	12.20	$1{,}1 \times 10^{8}$	$3{,}17 \times 10^{5}$
COOH-PEG-PLA	40	92.43 ± 1.79	− 15,4 ± 1,9	10,88	$2{,}79 \times 10^{6}$	$4{,}99 \times 10^{4}$

Since the targeted monodispersity could not be achieved in the PDI results of drug-free mPEG-PLA micelles, the samples of EVE-loaded micelles were measured twice by passing through a 0.45 µM filter. While the size results were close to drug-free micelles, PDI and zeta potential values were produced within the targeted range. As a result of filtration, approximately 350-fold decrease in particle concentration was

observed for mPEG-PLA and 55-fold decrease for COOH-PEG-PLA. Size distribution graphs for EVE-PMs are shown below.

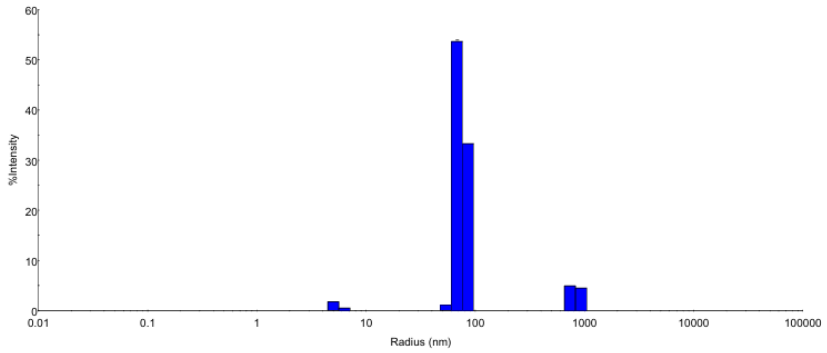

Figure 4.9. Size distribution of EVE loaded **mPEG-PLA Micelles**

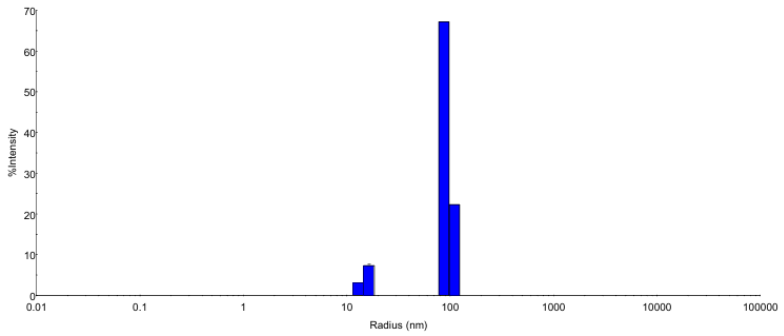

Figure 4.10. Size distribution of EVE loaded COOH-PEG-PLA Micelles

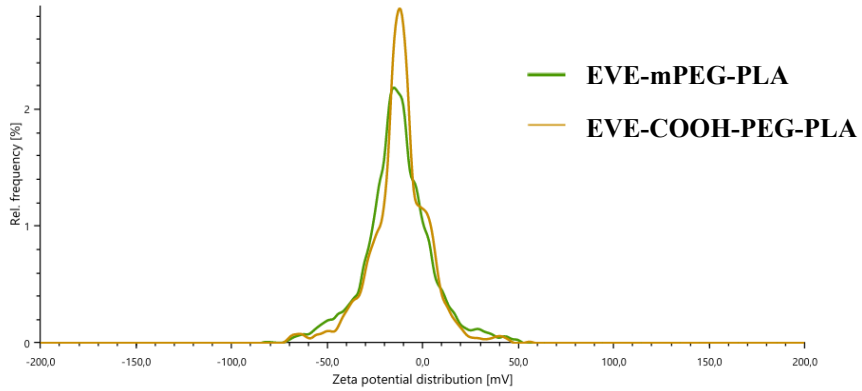

Figure 4.11. Zeta potential measurements of EVE-mPEG-PLA Micelles and EVE-COOH-PEG-PLA Micelles

4.2.3 Mean Size, Zeta Potential, PDI Determination of PMs and Surfactant Mixtures

Aqueous dispersions obtained from thin films of mPEG-PLA PMs and surfactant (Pluronic F-127, Brij98™, Gelucire®) mixtures were characterized in terms of average size and PDI. In the tables where the results are shown, the peak with the highest intensity value is shown. The average size and PDI values of polymeric micelles of surfactants were evaluated. Table 4.7. shows the values for Pluronic F-127 and mPEG-PLA and their blends. An increase in the size of unfiltered particles was observed when Pluronic F-127 was added. After filtration of the samples (0.45 μM), a wide range in PD values was observed, although the results were close in size.

Table 4.7. Unfiltered and filtered diameter, %PD and %intensity values of mPEG-PLA and pluronic F-127 mixtures

Conc.(μg/mL) (mPEG-PLA)	Conc. (μg/mL) Pluronic F-127	Unfiltered Diameter (nm)	Filtered Diameter (nm)	Filtered Samples %PD	%Intensity
15	7,5	423.3 ± 11.41	112.1 ± 2.12	36.24	96.3
20	10	206.9 ± 12.58	119.9 ± 1.99	22.57	69.7
30	15	1161.5 ± 10.60	146.4 ± 3.02	71.18	86.1
40	20	182.2 ± 4.12	117.3 ± 2.90	5,20	74.0
50	25	782.0 ± 17.46	114.4 ± 3.13	25.98	71.8
75	37,5	264.9 ± 13.42	107.5 ± 4.02	9,42	34.6
100	50	749.1 ± 14.25	45.1 ± 0.92	80.34	98.1
125	62,5	475.6 ± 12.28	127.5 ± 4.74	121.72	56.1
150	75	259.9 ± 9.47	118.1 ± 3.81	14.87	61.0
200	100	429.0 ± 10.63	101.6 ± 4.01	8,86	93.6

Significant improvements in PDI value were observed in the results obtained from Brij98™ and mPEG-PLA mixtures, especially at lower concentrations. However, there was a significant increase in particle size compared to surfactant-free mPEG-PLA micelles. Filtration process was not performed since the samples showed a monodisperse structure.

Table 4.8. Unfiltered diameter, %PD and %intensity values of mPEG-PLA and brij98 mixtures

Conc.(µg/mL) (mPEG-PLA)	Conc. (µg/mL) Brij98™	Diameter (nm)	%PD	%Intensity
15	7,5	182.3 ± 2.92	13.82	42.1
20	10	229.7 ± 4.67	11,29	37,60
30	15	484.7 ± 2.77	12,09	45.2
40	20	452.6 ± 6.46	12,08	53.1
50	25	199.7 ± 3.22	17.74	53.9
75	37,5	303.4 ± 4.10	48.52	74.8
100	50	149.1 ± 1.89	11,65	96.6
125	62,5	209.1 ± 3.61	21.39	71.8
150	75	389.0 ± 4.44	82.63	55.9
200	100	162.5 ± 1.26	10,27	57.0

While an increase in particle size was observed in Gelucire® and mPEG-PLA blend, both monodisperse and polydisperse structures were observed in PDI values. There was a significant increase in particle sizes compared to the surfactant-free micelles.

Table 4.9. Unfiltered diameter, %PD and % intensity values of mPEG-PLA and gelucire mixtures

Conc.(µg/mL) (mPEG-PLA)	Conc. (µg/mL) Geleucire®	Diameter (nm)	%PD	%Intensity
15	7,5	767.0 ± 12.48	85.6	14,4
20	10	631.6 ± 9.42	13,06	57.4
30	15	661.0 ± 10.01	85.48	93.8
40	20	386.9 ± 7.95	47.15	77.9
50	25	555.2 ± .6.89	75.92	97.8
75	37,5	245.8 ± 5.32	11,91	42.2
100	50	524.8 ± 7	11,94	91.9
125	62,5	358.1 ± 3.58	51.56	76.6
150	75	379.8 ± 4.64	46.20	83.0
200	100	361.2 ± 3.97	14.49	91.1

4.3 Morphologic Structure of Polymeric Micelles

4.3.1 Scanning Electron Microscopy

SEM micrographs of drug free PMs (**mPEG-PLA**, **COOH-PEG-PLA**, **NHS-PEG-PLA)** samples are shown in Figure 4.12., Figure 4.13 and Figure 4.14 Images were taken from micelles prepared at a concentration of 40 µg/mL.

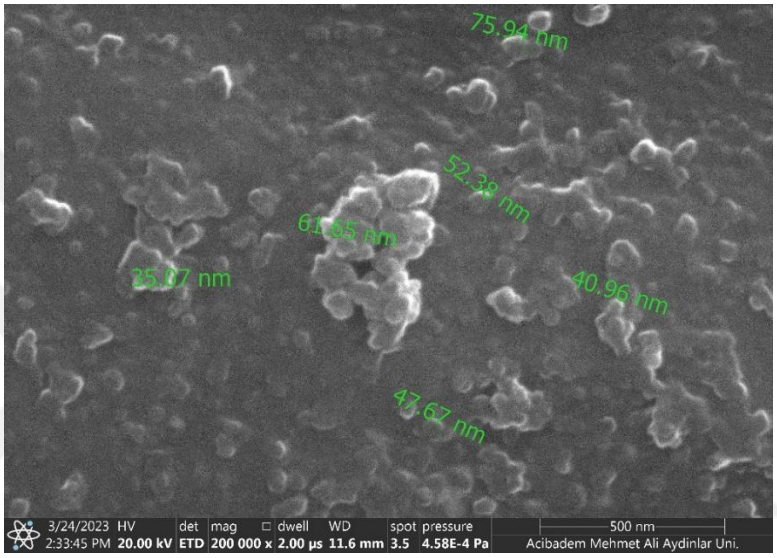

Figure 4.12. SEM micrograph of drug free mPEG-PLA micelles

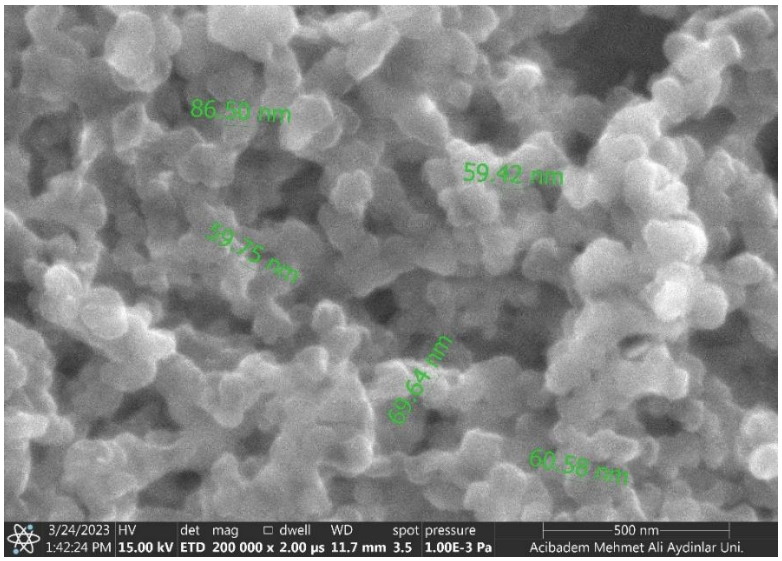

Figure 4.13. SEM micrograph of drug free COOH-PEG-PLA micelles

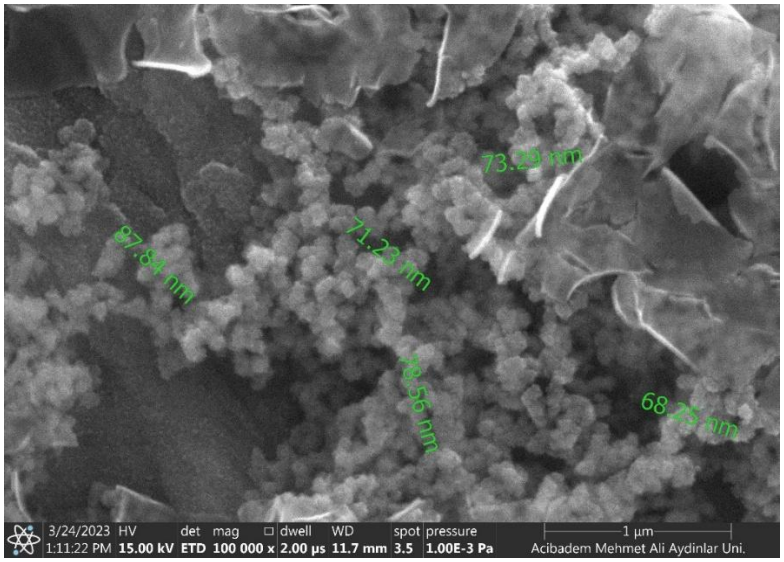

Figure 4.14. SEM micrograph of drug free NHS-PEG-PLA micelles

The micrographs obtained as a result of SEM analysis show that the polymeric micelles have the expected spherical morphology and quite monodisperse structure. In addition, the dimensions measured by SEM support the dimensions measured by DLS.

4.3.2 Tranmission Electron Microscopy

TEM imaging was performed on EVE-mPEG-PLA, drug free mPEG-PLA and drug free COOH-PEG-PLA micelles. EVE-mPEG-PLA, drug free mPEG-PLA and drug free COOH-PEG-PLA are shown in Figure 4.15, Figure 4.16 and Figure 4.17, respectively.

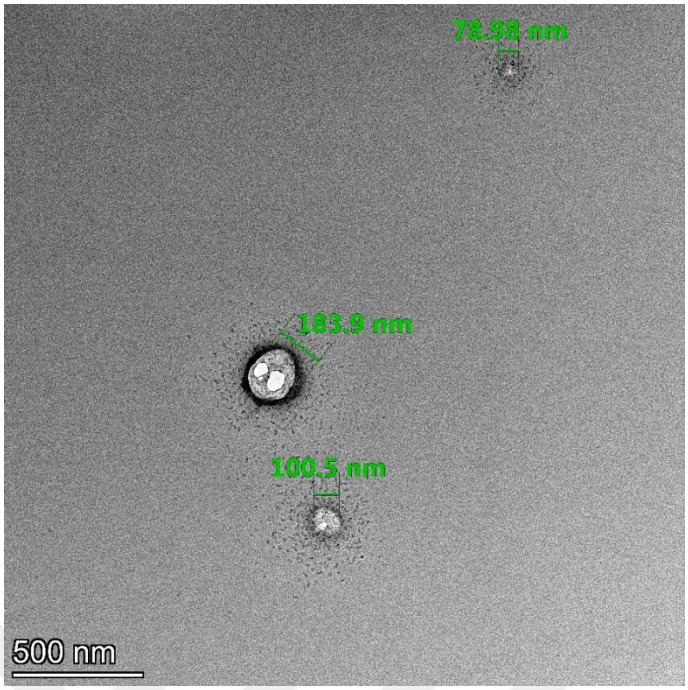

Figure 4.15. TEM micrograph of EVE-mPEG-PLA micelles

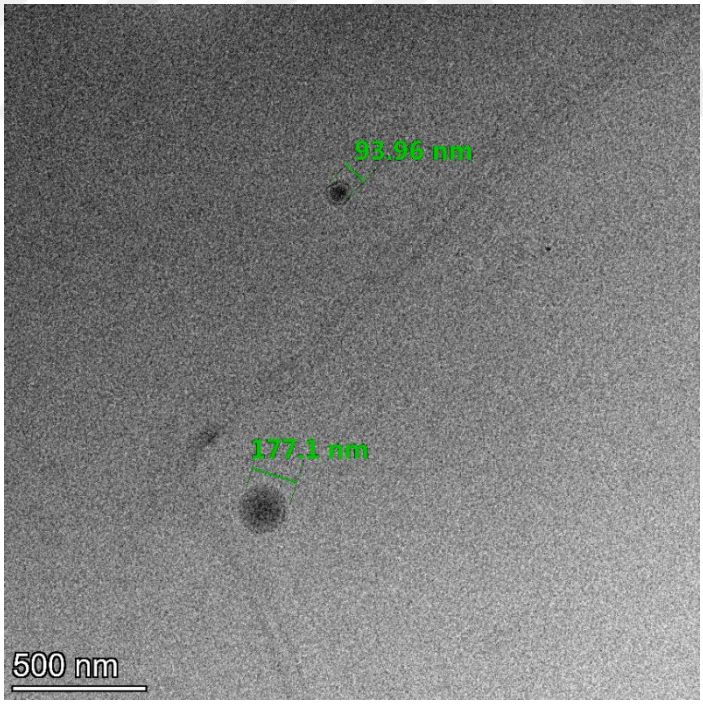

Figure 4.16. TEM micrograph of drug free mPEG-PLA micelles

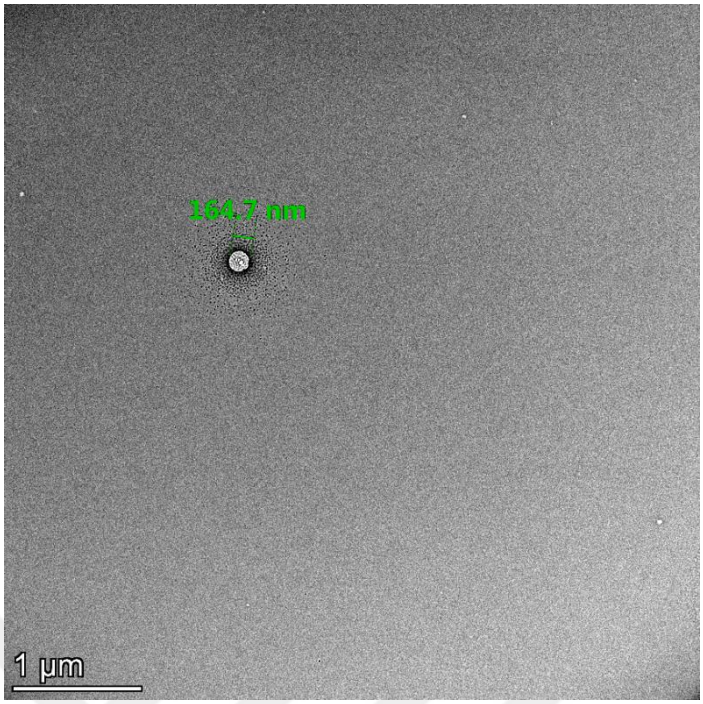

Figure 4.17. TEM micrograph of drug free COOH-PEG-PLA micelles

If the TEM micrographs of the three samples are evaluated it is seen that the samples have a spherical morphology. However, the dimensions of the samples measured by TEM confirm the dimensions measured by DLS.

4.4. Encapsulation Effiency

The absorbance value of EVE-mPEG – PLA micelles compared with calibration curve before drawn and the encapsulation effiency (E.E.) for EVE-mPEG – PLA micelles determined as %60,61. The aimed E.E. for study was %50 and it achieved.

4.5. FT-IR Spectroscopy Analysis of RGD Conjugated PEG-PLA Micelles

FT-IR spectroscopy was used to examine the success of conjugation of RGD(K) peptide to NHS-PEG-PLA micelles. Comparative FT-IR spectra of RGD, NHS-PEG-PLA and RGD-PEG-PLA are given in Figure 4.18.

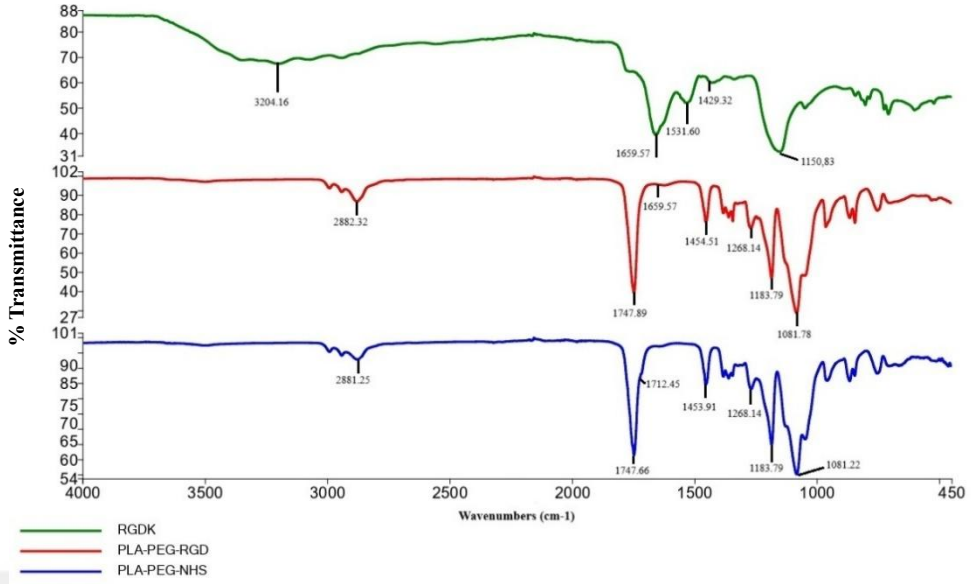

Figure 4.18. FT-IR Spectrums of RGD(K), RGD-PEG-PLA and NHS-PEG-PLA respectively.

Table 4.10 shows the stretching bands and approximate wave numbers for RGD, NHS-PEG-PLA and RGD-PEG-PLA. In the spectrum for RGD, the band for the first peptide bond (C=O stretch) is shown at 1650 cm^{-1} and the band for the second peptide bond (N-H bending) is shown at 1540 cm^{-1}. These two peptide bonds were expected to be observed in the structure of the RGD-PEG-PLA spectrum after conjugation. The free amine group band (N-H stretch) observed at 3300 cm^{-1} is expected to disappear after conjugation. This is because there is no longer a free amine group in the structure formed after conjugation. In the spectrum of NHS-PEG-PLA, it was observed that the band at 1710 cm^{-1} of the (C=O) stretch from the NHS ester carbonyl bond was not observed after RGD conjugation due to the loss of ester bonds. The formation of bands at 1650 cm^{-1} and 1540 cm^{-1} in the spectrum of RGD-PEG-PLA after conjugation and the absence of the (C=O) stretch from the ester carbonyl bond at 1710 cm^{-1} indicate that the conjugation was successful.

Table 4.10. Wave numbers measured in FT-IR according to samples and their corresponding functional groups

Sample	Approximate Wave Number (cm^{-1})	Functional Group and Stretch
RGD (K)	1650 cm^{-1}	C=O stretch, peptide bond
	3300 cm^{-1}	N–H stretch, free amin groups
	1400 cm^{-1}	COO^- symmetric stress
	1540 cm^{-1}	N-H bending second peptide bond
NHS-PEG-PLA	1710 cm^{-1}	NHS ester carbonyl (C=O) stretch
	1100–1150 cm^{-1}	C-O-C stretch, ether bond from PEG chain
	1750 cm^{-1}	C=O ester carbonyl group from PLA segment
	2870–2940 cm^{-1}	CH_2 stretch from PEG and PLA
RGD- PEG -PLA	1750 cm^{-1}	C=O ester carbonyl group from PLA segment
	1100–1140 cm^{-1}	C-O-C stretch, ether bond from PEG chain
	1650 cm^{-1}	C=O stretch, peptide bond
	1540 cm^{-1}	N-H bending second peptide bond

4.6. Optimization and Characterization of HPMC MPs

4.6.1. Optimization Studies

Optimization studies were carried out on the formulation and the pump rate parameter from the production parameters. Table 4.11. shows the seven formulations prepared for optimization studies and the pump rate parameter used during production. In this thesis, it is aimed to produce dry powder particles with an average size below 5 µM.

Table 4.11. Formulation codes, formulation and production parameters of HPMC MPs

Formulation Codes	Formulation Parameters			Production Parameters
	Quantity of HPMC (gr.)	Quantity of Solvent (mL) d(H2O)	Concentration (w/v)	Pump Rate (%)
O1	0,3	100	0,3	20
O2	0,3	100	0,3	10
O3	0,3	200	0,15	10
O4	0,3	200	0,15	20
O5	0,3	400	0,075	10
O6	0,15	400	0,0375	10
O7	0,15	200	0,075	10

Pump rate parameter was optimized with formulations coded Q1-Q2 and Q3-Q4, solvent volume with formulations coded Q2-Q3 and Q6-Q7, and HPMC amount with formulations coded Q5 and Q6. Table 4.12 shows the particle size results for the relevant formulations.

Table 4.12. D-values and % production yield of 7 formulations of HPMC MPs

Formulation Codes	Dx (10) (µm)	Dx (50) (µm)	Dx (90) (µm)	% Production Yield (PY)
O1	3.381	7.462	17.752	26,33
O2	2.432	4.478	10.420	27,33
O3	2.205	3.835	9.862	25,83
O4	2.707	5.432	15.640	20,33
O5	2.329	5.143	42.678	17,33
O6	2.566	4.218	7.214	12,67
O7	2.266	4.370	22.892	18,00

If the results in table 4.12. are evaluated; as expected, a significant increase in particle sizes was observed as the pump rate was increased during spraying. Although it is thought that solvent volume has no direct effect on particle size, it was concluded that higher solvent volume leads to a decrease in particle size. This was thought to be related to the solids content in the solution as a result of the decrease in the concentration of the solution prepared for spraying. As the amount of HPMC and the amount and proportion of solids in the solution increased, an increase in the average

size was observed. It is known that the spray dryer used in the production works with a maximum efficiency of 60%. As the amount of dry powder produced increased, it was observed that the device worked more efficiently. 0.3 gr. HPMC used in the formulations resulted in similar production yields. As a result of optimization, the studies were continued with the formulation coded Q3 (0.3 gr. HPMC, 200 mL d(H2O), 10% pump rate) formulation was used.

4.6.2. Reproductibility Studies

The formulation (Q3) selected as a result of optimization studies was produced three more times and repeatability studies were carried out. Table 4.13 shows the particle size results for three dry powders produced under the same conditions for formulation Q3.

Table 4.13 D-values, mean and standard deviation values of the formulation coded Q3

Formulation Code	**Dx (10) (µm)**	**Dx (50) (µm)**	**Dx (90) (µm)**
R1	2.159	3.577	7.438
R2	2.364	4.236	10.309
R3	2.566	4.218	7.214
Mean of 3 results	2.363	4.010	8.320
Standart Deviation of 3 results	0.204	0.376	1.726

If the results in Table 4.13. are evaluated, the dimension results for the formulation coded Q3 were found to be very close to each other. It was concluded that the formulation was reproducible. The production of microparticles with average sizes below 5 µM targeted within the scope of the thesis was successfully realized. Figure 4.19.3 shows the overlayed particle size distribution for three formulations produced for reproducibility studies.

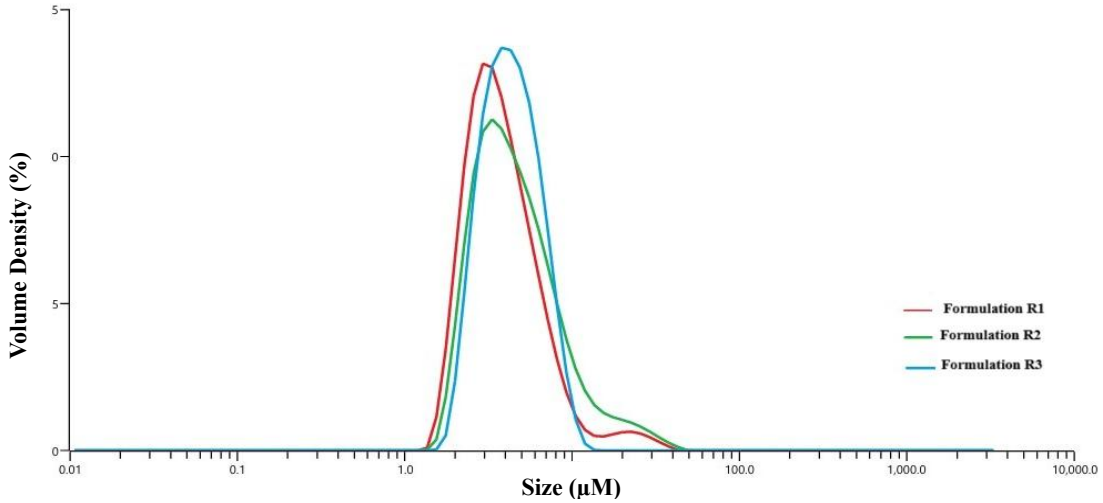

Figure 4.19. Size distribution graph of formulations; R1, R2 and R3

4.6.3. Optimization Studies of Lactose Monohydrate

Optimization studies were carried out for lactose used as an excipient in the formulation. Table 4.14. shows the particle size results for the dry powder lactose sample obtained from the aqueous solution of lactose.

Table 4.14. D-values and % production yield of lactose formulation

Amount of Lactose (gr.)	Dx (10) (µm)	Dx (50) (µm)	Dx (90) (µm)	Production Yield
0,9	3.547	8.495	22.432	%49

As expected, the particle sizes of dry powdered lactose were found to be larger than HPMC microparticles. The production efficiency showed a significant increase compared to the production efficiency of HPMC. It is known that the spray dryer device (Buchi, B-290) can operate with a maximum efficiency of 60%. (151).

Two different formulations prepared from aqueous solution of lactose and HPMC mixture were analyzed in terms of particle size and reaction efficiency and the values are shown in table 4.15.

Table 4.15. D- values and % production yield of lactose-containing HPMC formulations

Properties of Formulation		Particle Size			% Production Yield (PY)
Amount of HPMC (gr.)	Amount of Lactose (gr.)	Dx (10) (µm)	Dx (50) (µm)	Dx (90) (µm)	
0,3	0,9	3.547	8.495	22.432	37,5
0,3	0,3	2.385	5.190	49.354	26,33

If the values for the formulations produced are evaluated, an increase in the average particle size Dx (50) was observed as the lactose content increased. On the other hand, a remarkable increase in production efficiency was observed. It was decided to add 0.9 g of lactose to the formulation.

4.6.4. Characterization of PMs Integrared MPs

After integrating drug-free PMs (mPEG-PLA and COOH-PEG-PLA) and EVE-PMs (mPEG-PLA and COOH-PEG-PLA) into HPMC microparticles, they were characterized in terms of particle size. Finally, lactose was added to the HPMC formulation and EVE-mPEG-PLA micelles were integrated to prepare the final formulation and complete the characterization process.

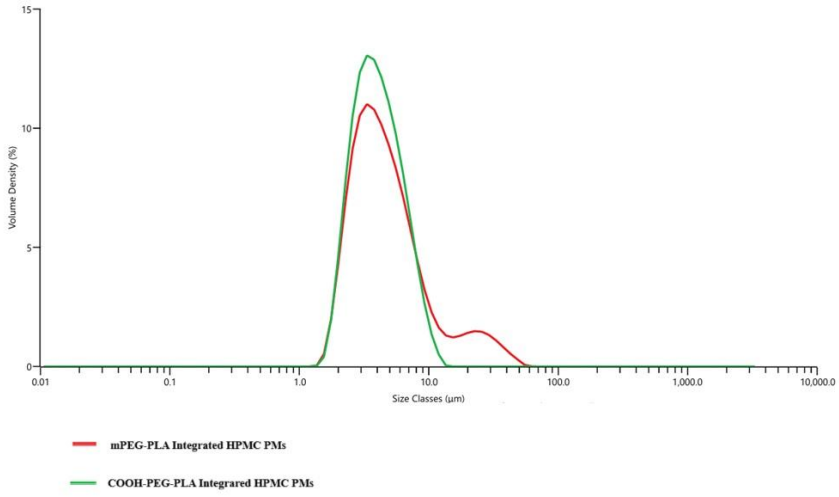

Figure 4.20. Size disturibiton graph of PMs Integrated MPs

Table 4.16. D-values of all of PMs integrated MPs

D-Values	Dx (10) (µm)	Dx (50) (µm)	Dx (90) (µm)
Drug Free PMs Integrated MPs			
mPEG-PLA Integrated HPMC MPs	2.351	4.277	13.035
COOH-PEG-PLA Integrated HPMC MPs	2.323	3.892	7.154
EVE-PMs Integrated MPs			
EVE-mPEG-PLA Integrated MPs	2.351	4.277	13.035
EVE-COOH -PEG-PLA-Integrated MPs	2.398	5.708	12.992
Final Formulation			
Lactose Containing HPMC MPs Integrated with EVE-mPEG-PLA	4.453	11.934	45.404

When the results in Table 4.16 are examined, it is seen that the encapsulation of EVE into micelles has no effect on MPs particle sizes as expected. In the final formulation containing lactose, significant particle size increase was realized at the expected rate. While 5 µM particles could be obtained as a result of the integration of the drug-loaded micelles targeted within the scope of the thesis into HPMC microparticles, the size target deviated significantly in the final formulation to which lactose was added.

4.7. Morphology of HPMC MPs

4.7.1. Light Microscopy

The images of HPMC microparticles were evaluated for shape in the light microscope and provided preliminary information to confirm the size results. Figure 4.21. shows the image of the micrograph taken from the light microscope.

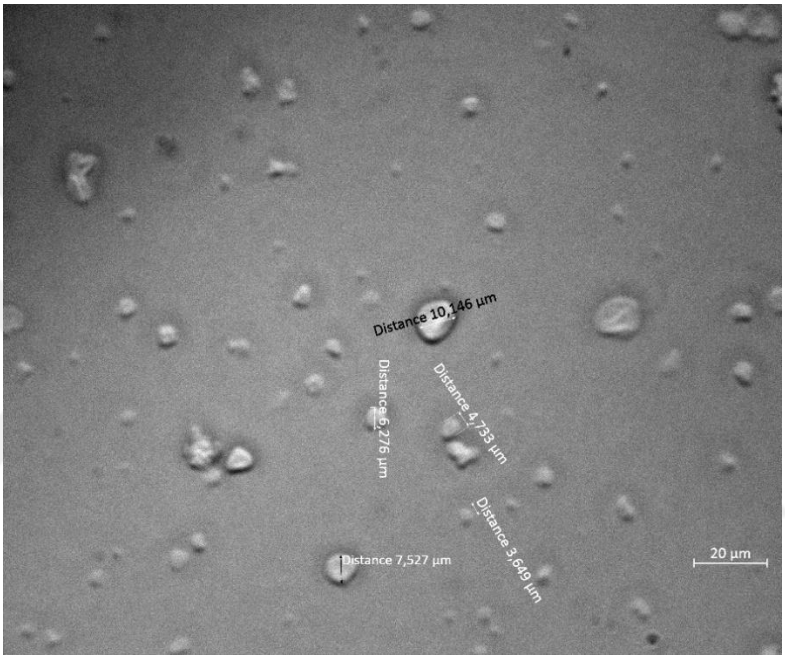

Figure 4.21. Light Microscopy micrograph of HPMC microparticles

Clear images of the particles show spherical shaped particles with uniform circumference, confirming the size results.

4.7.2. Scanning Electron Microscopy (SEM)

Images from scanning electron microscopy are shown in figure 4.22 and figure 4.23.

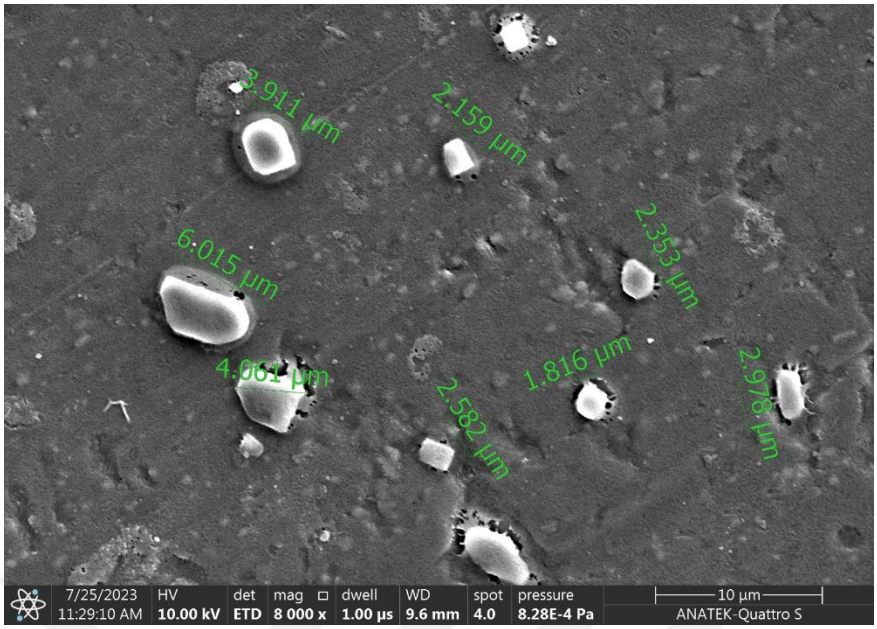

Figure 4.22. SEM Micrograph of HPMC MPs

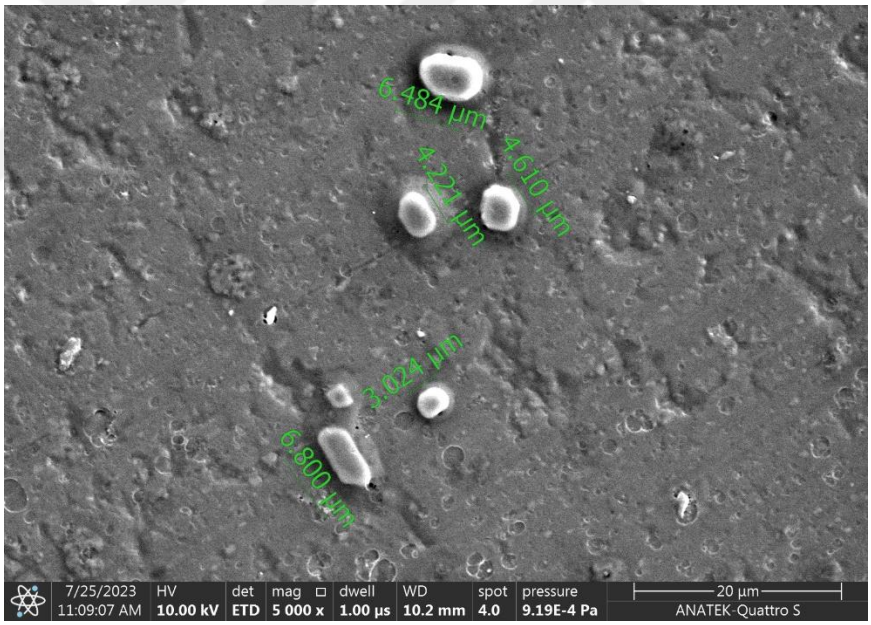

Figure 4.23. SEM Micrograph of HPMC MPs

In the micrographs obtained as a result of SEM analysis, microparticles have a morphology close to spherical structure and angular quadrilateral structures are also observed. In addition, the dimensions measured by SEM support the size measurements.

4.8. Swelling Ratio Tests

Swelling tests were performed on a single formulation containing only HPMC. The image of a single particle selected under the microscope was obtained at (0,15,30,60,120 and 240 min) and the diameter of the particle was measured with the "Measure Length" tool calibrated in the microscope software (Zen Blue Edition). Figure 4.24 shows the light microscope images taken at the specified minutes.

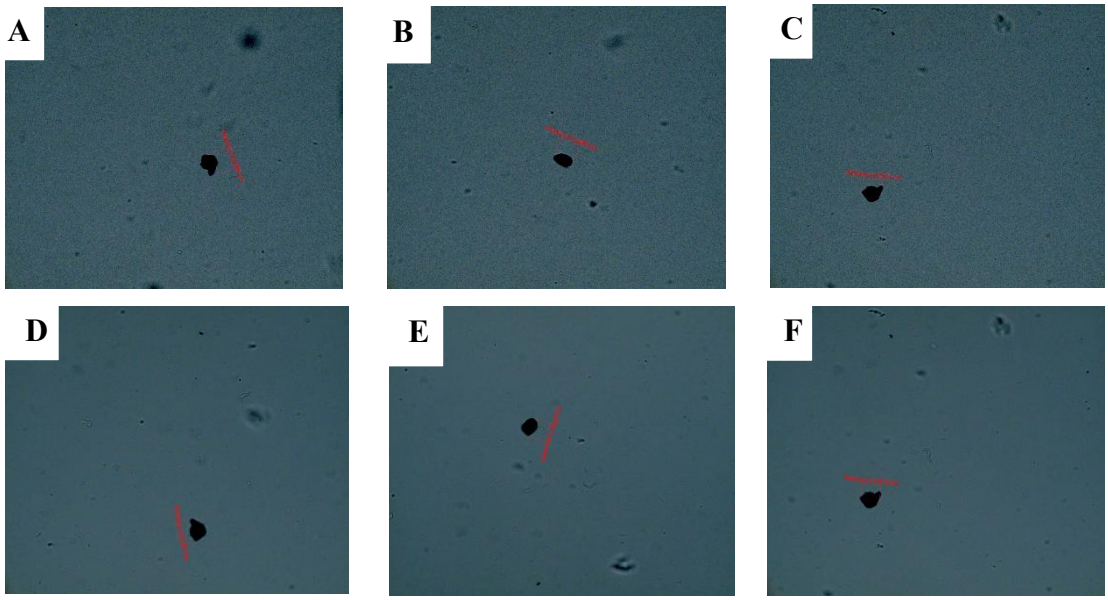

Figure 4.24. Light microscope images of a HPMC particle dispersed in d(H_2O) at six time points; A) 0.min, B) 15.min, C) 30.min, D) 60.min, E) 120.min, F) 240.min

Figure 4.25 shows the size of microparticles measured by light microscopy at six different time points in PBS and distilled water d(H_2O). According to graph, it is seen that the microparticle dispersed in PBS reaches maximum swelling in the first 15 minutes and then its size stabilizes. It was found that the microparticle grew by 57.25% between 0-15 min. On the other hand, the particle dispersed in water grew by approximately 19.51% in the first 15 minutes and reached its maximum size and then fluctuated in size during the time points.

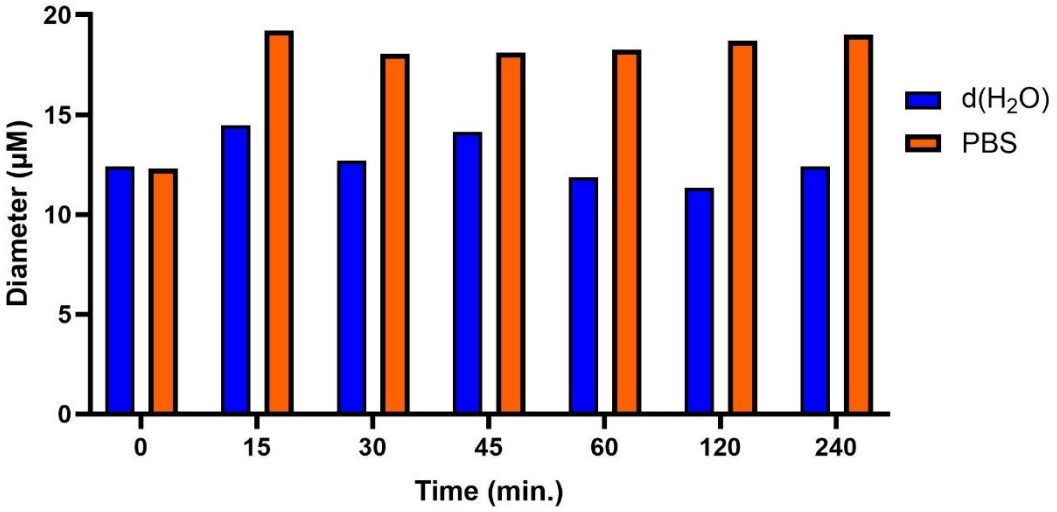

Figure 4.25. Variation of HPMC particle size in PBS and distilled water

4.9. Angel of Repose

In Image 4.1.the photograph of the formed pile related to the angle of repose measurements, along with the approximate measurement of the diameter using a ruler, is shown.

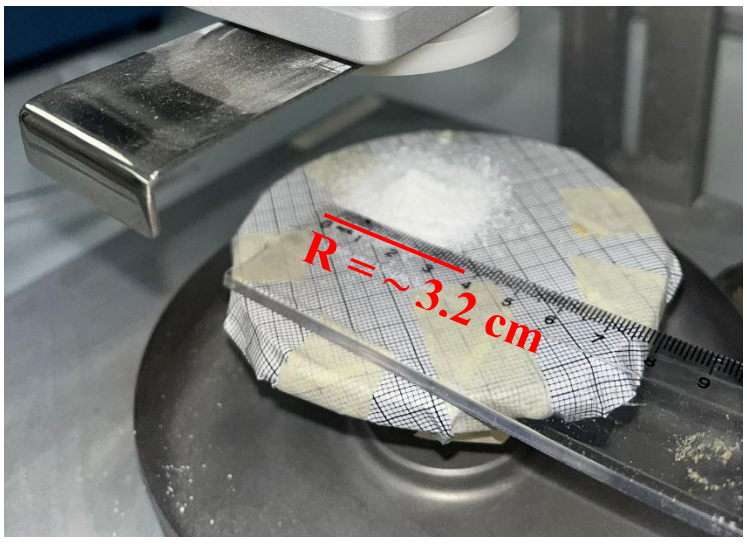

Image 4.1. Dust pile and measuring the diameter of the pile with a ruler

In Image 4.2. the photograph showing the height of the formed pile measured with a ruler is presented

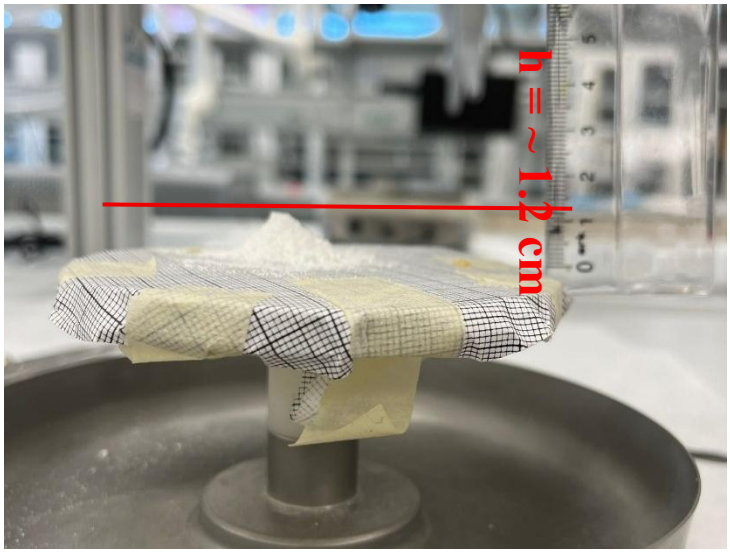

Image 4.2. Dust pile and measuring the height of the pile with a ruler

Based on the diameter and height information obtained from the photographs, the angle of repose was found to be approximately 36.87°. To ensure good powder flowability, an angle of repose below 30° was targeted.

4.10. Adhesion Tests

The values taken in two different ways, adhesive strength and adhesion, for adhesion tests performed on three different liquids are shown in Table 4.17. Four different samples were used in the measurement.

Table 4.17. Adhesive strength and adhesiveness values of the same samples in different dispersants

Type of Dispersant	Sample	Adhesive Force (g)	Adhesivness (mJ)
Distilled Water	Free HPMC MPs	93	0,4
	Lactose MPs	33	0,3
	Lactose + HPMC MPs	56	0,6
	PMs Integrated HPMC MPs	48	0,4
PBS	Free HPMC MPs	49	0,6
	Lactose MPs	9	0,1
	Lactose + HPMC MPs	118	0,4
	PMs Integrated HPMC MPs	49	0,4
Simulated Lung Fluid	Free HPMC MPs	31	0,3
	Lactose MPs	12	0,1
	Lactose + HPMC MPs	52	0,3
	PMs Integrated HPMC MPs	96	1,4

According to the results, it was shown that HPMC particles have adhesive properties and it was also observed that lactose particles alone have this property.

5.DISCUSSION

Everolimus, an mTOR inhibitor, is a potential therapeutic agent in the treatment of lung cancer. Encapsulation of the agent into RDG-conjugated polymeric micelles and integration into bioadhesive microparticles and inhaled administration of the agent with the advantages of active and passive targeting strategies were thought to increase patient compliance and treatment success. In addition, the high loading capacity and modifiability of polymeric micelles were utilized. Direct targeting was realized by conjugating the RGD peptide, which shows high affinity for cancer cells, to the polymeric micelles, and passive targeting was realized with the EPR effect brought by the nanosize of the polymeric micelles. With the integration of this system into bioadhesive microparticles and pulmonary application, a system that will provide the advantage of direct long-term release into cancer tissue has been designed.

First, measurements were performed with samples of various concentrations to determine the critical micelle concentration (CMC) of polymeric micelles. Critical micelle concentrations were calculated for all three polymer types to be used directly or indirectly in the study. CMC values close to each other were obtained for the three polymers and it was observed that the effect of the functional groups they carry on the CMC value was minimal. However, there was a significant difference between the critical micelle concentrations determined in the literature for micelles obtained with different molecular weights of the same polymers. In this direction, since approximately 25-fold dilution is expected in in-vivo drug delivery systems using micelles systems, three different surfactants (Pluronic F-127, Brij98 and Gelucire) were considered to be included in the polymeric micelle structure in order to reduce the CMC value of the micelles. It was also thought that these surfactants could improve the drug loading capacity within the system. CMC values were determined with the samples prepared for the three surfactants, but CMC values for the three surfactants were higher than the polymeric micelles (mPEG-PLA) or close to the CMC value of the polymeric micelles. When the CMC values of the surfactants were compared with the findings in the literature, very close results could be obtained especially for Brij98. Then, CMC values of the mixtures of polymeric micelles (mPEG-PLA) and surfactants

at a ratio of (1:2) were studied, but CMC values could not be reached in polymeric micelle mixtures added to brij98 and gelucire. The reason for this was thought to be that the polymeric micelle surfactant mixtures may not be suitable for the measurement of the surface tension-pendant drop method. In the mPEG-PLA blend containing Pluronic F-127, CMC value could be found, but since no significant decrease in CMC value was observed, surfactants were not included in further studies within the scope of the thesis.

In the characterization of polymeric micelles (mPEG-PLA, COOH-PEG-PLA and NHS-PEG-PLA), aggregates were observed even at low concentrations (5,10,15 μg/mL) in particle size measurements. After the samples were filtered with 0.45 μM filter, the size and PDI values targeted within the scope of the thesis were approached and completely reached in some samples. The targeted values were reached in the zeta potential measurements of the samples. It was thought that the functional groups on different polymer types, especially the -COOH carboxylic acid group, would provide more stability to the structure by providing a negative charge to the micelle structure. However, the zeta potential values of COOH-PEG-PLA micelles did not show a significant difference compared to other polymeric micelles (mPEG-PLA and NHS-PEG-PLA).

After the active substance everolimus (EVE) was encapsulated, centrifugation method was tried to optimize the purification method of the loaded micelles, but after the desired results were not obtained, GPC (Gel Permeability Chromatography) method was continued. EVE-loaded micelles purified and filtered by GPC could be produced in the targeted sizes in terms of size, PDI and zeta potential. In addition, the particle concentration of these samples was calculated and the number of particles in the sample was calculated.

In the SEM images of drug-loaded and drug-free micelles, spherical structures were determined and generally homogeneous distribution was detected. Size results were shown confirming the DLS results. However, it was thought that the negative pressure applied in the device due to the vacuum mode of the SEM device and the drying of the samples in the device may lead to a decrease in the particle size of the micelles. In the TEM images, the spherical structure was seen again and it was visualized as spherical particles with sharp lines, homogeneous distribution and separated from each other.

The FT-IR spectra of RGD-PEG-PLA micelles showed the presence of two peptide bond bands of RGD and the disappearance of the band related to the functional group on the NHS moiety of NHS-PEG-PLA, providing evidence of successful conjugation.

During the optimization of HPMC microparticles, the parameters were divided into two as formulation parameters and production parameters. According to the information obtained from the literature, for the formulation parameters, the amount of solids in the aqueous solution and the effect of the solids ratio on the particle size in the production carried out in spray dryer devices are known. For the production parameters, the effect of the pump rate parameter applied during the process on the size of the product obtained has been revealed. During the optimization, two parameters were optimized and the results obtained were in parallel with the literature. The size targets of Dx (50) $\leq$ 5 µM targeted within the scope of the thesis were achieved.

It was declared by the manufacturer that the device used during production can operate with a maximum efficiency of 60%. When spray drying was performed using only HPMC, the production efficiency was found to be significantly lower than the maximum efficiency. The reason for this was thought to be that HPMC has a sticky property and adheres to the glass columns where the drying process takes place during drying and the production scale realized in the device may be due to the smaller quantities compared to the production scale of the device. Therefore, it was considered to add lactose, which is frequently used as an excipient in formulations given using

dry powder inhalers, to the formulation content. In order to optimize the amount of lactose to be used, formulations were produced with different amounts and concentrations of lactose and the formulation with the highest production efficiency was continued. It was also considered that the addition of lactose to the formulation could lead to a significant change in particle size. Spray drying of the aqueous formulation of lactose was used for size characterization of the resulting product. However, it was observed that the dry powdered lactose quickly sedimented in the dispersant (isopropyl alcohol) used in the size measurement characterization of HPMC microparticles. Therefore, a suitable dispersant (ethylacetate) was chosen for the dispersion of lactose. In the size results for lactose, especially Dx (90) values were found to be considerably higher than the Dx (90) values of HPMC. It is thought that the reason for this situation is that the amount of lactose in the same volume of aqueous solution with HPMC is 3 times higher. In the characterizations carried out in HPMC mixtures containing lactose, 3-fold growth was observed in Dx (90) values, while Dx (50) values were close to 2-fold growth, as expected.

Deviations in the range of standard deviation values between measurements were observed in the results obtained after the integration of drug Free and drug-loaded polymeric micelles into microparticles and it is thought that the integration of micelles does not affect the size of microparticles.

In the determination of the morphological structure of HPMC microparticles, a more spherical structure was observed in the images obtained in the light microscope, while the structure was observed to have much sharper lines and square and rectangular-like structures in SEM images. This difference was thought to be the effect of the surface tension between IPA and HPMC on the formation or preservation of the spherical structure due to the dispersion of HPMC microparticles in IPA while obtaining images in the light microscope. Secondly, it is thought that the negative pressure applied from the SEM device during imaging may cause surface shrinkage in places. In addition, the higher resolution and zoom ratios in the SEM device may be effective in revealing that the particle shape, which gives the impression of spherical, is actually angular.

In the swelling experiments performed with HPMC microparticles, a size growth of approximately 19% was observed in the samples dispersed in distilled water, while in PBS it showed a growth of approximately 57%. The reason for this is thought to be that PBS solution contains various salts in its structure and allows diffusion by creating more osmotic pressure difference between HPMC and aqueous medium than distilled water.

The aimed angle of repose was ≤ 30 °. THowever, all of samples are determined in one experiment could be significant change for the results. Since there are not enough sample for angle of repose determination from one batch of production all of the samples which are only contains HPMC are used. The dry-powders has different properties such as size, humidity and morphology. Its need to be improved and re-test the angle of repose after the produce the all of the different conditonal samples product again.

The different dispersants did not affect the adhesional propeties of the samples. Expectedly, HPMC samples has adhesive properties and it showed. Also, only Lactose containing lactose powders show adhesive properties is remarkable.

6. CONCLUSION

Within the scope of the thesis study, the integration of everolimus-loaded RGD-conjugated PEG-PLA micelles into HPMC microparticles was targeted. The prepared structure was thought to be suitable for pulmonary delivery and a potential for the treatment of non-small cell lung cancer. Prolonged release was targeted thanks to the bioadhesion of HPMC microparticles. Active targeting strategy was applied with the affinity of the RGD peptide in the structure of RGD-PEG-PLA polymeric micelles integrated with HPMC to integrin αvβ5 receptors that are strongly expressed on cancer cells. Passive targeting strategy was applied by creating EPR effect due to the nanosize of polymeric micelles. Everolimus-loaded polymeric micelles were produced by thin film method and integrated into HPMC microparticles by in process spray drying method. RGD peptide was synthesized and reacted with NHS-PEG-PLA polymer to obtain RGD-PEG-PLA structure. The critical micelle concentrations of the polymeric micelles were calculated and everolimus was loaded above the critical micelle concentration. Surfactants were added to the study to change the critical micelle concentration and increase the loading capacity of the micelles. The critical micelle concentrations of the surfactants were calculated and the critical micelle concentrations of the micelle surfactant mixtures were calculated. Surfactants were not included in subsequent studies as no significant improvement was observed. The micelles produced were characterized in terms of size, PDI and zeta potential and particle concentration and the objectives of the study were generally achieved. Homogeneously distributed micelle structures with spherical structure were observed in SEM images, and structures with clear boundaries were detected in TEM images. Within the scope of the thesis, it was aimed to produce HPMC microparticles with an average size of less than 5 μM with low moisture content and good bioadhesive properties. In this direction, optimization studies were carried out and the formulation and production parameters that reached the targeted dimensions were proceeded. In order to improve the production efficiency rates determined in the formulations produced, lactose monohydrate was added to the formulation and optimization studies were carried out. As a result of the inclusion of lactose in the formulation, a significant improvement in production efficiency was observed, while particle sizes increased. In

the characterizations performed as a result of the integration of loaded and drug free micelles into HPMC microparticles, micelle integration did not change the size results as expected. In the swelling experiments performed on HPMC microparticles, the particles dispersed in PBS showed significantly more swelling behavior than those dispersed in distilled water.

7.REFERENCES

1. Siegel RL, Miller KD, Wagle NS, Jemal A. Cancer statistics, 2023. CA A Cancer J Clinicians.2023 ;73(1):17-48.
2. Bray F, Laversanne M, Sung H, Ferlay J, Siegel RL, Soerjomataram I, vd. Global cancer statistics 2022: GLOBOCAN estimates of incidence and mortality worldwide for 36 cancers in 185 countries. CA A Cancer J Clinicians
3. Rivera MP, editör. Lung cancer, part i, an issue of clinics in chest medicine, e-book. Amsterdam: Elsevier; 2020. 1 s.
4. Jiao Z, Pan Y, Chen F. The Metabolic Landscape of Breast Cancer and Its Therapeutic Implications. Molecular Diagnosis & Therapy 2023; 27: 349–369.
5. Dela Cruz CS, Tanoue LT, Matthay RA. Lung Cancer: Epidemiology, Etiology, and Prevention. Clinics in Chest Medicine [Internet]. 2011 Dec;32(4):605–4
6. Galateau-Salle F, Churg A, Roggli V, Travis WD. The 2015 World Health Organization Classification of Tumors of the Pleura: Advances since the 2004 Classification. Journal of Thoracic Oncology. 2016 Feb;11(2):142–54.
7. Travis WD, Brambilla E, Noguchi M, Nicholson AG, Geisinger KR, Yatabe Y, et al. International Association for the Study of Lung Cancer/American Thoracic Society/European Respiratory Society International Multidisciplinary Classification of Lung Adenocarcinoma. Journal of Thoracic Oncology. 2011 Feb;6(2):244–85.
8. Nicholson AG, Tsao MS, Beasley MB, Borczuk AC, Brambilla E, Cooper WA, et al. The 2021 WHO Classification of Lung Tumors: Impact of advances since 2015. Journal of Thoracic Oncology: Official Publication of the International Association for the Study of Lung Cancer [Internet]. 2021 Nov 19;17(3):S1556-0864(21)033165.
9. Le X, Heymach J. In Response. Journal of Thoracic Oncology. 2022 Mar;17(3):e39.
10. American Cancer Society. Lung Cancer. In: Cancer Facts & Figures 2023. American Cancer Society; 2023. p. 1–56. https://www.cancer.org/research/cancer-facts-statistics/all-cancer-facts-figures/2023-cancer-facts-figures.html. 2023.
11. J. Saller J, Boyle TA. Molecular Pathology of Lung Cancer. Cold Spring Harbor Perspectives in Medicine. 2021 Nov 8;12(3):5–16.
12. Drapkin BJ, Rudin CM. Advances in Small-Cell Lung Cancer (SCLC) Translational Research. Cold Spring Harbor Perspectives in Medicine. 2020 Jun 8;11(4):7–10.
13. Scott WJ, Howington J, Feigenberg S, Movsas B, Pisters K, American College of Chest Physicians. Treatment of non-small cell lung cancer stage I and stage II: ACCP evidence-based clinical practice guidelines (2nd edition). Chest. 2007 Sep 1;132(3 Suppl):234S-242S.
14. Peng L, Xu Q, Yin S, Zhang Y, Wu H, Liu Y, et al. The emerging nanomedicine-based technology for non-small cell lung cancer immunotherapy: how far are we from an effective treatment. Frontiers in Oncology. 2023 Apr 27;13.

15. Debela DT, Muzazu SG, Heraro KD, Ndalama MT, Mesele BW, Haile DC, et al. New Approaches and Procedures for Cancer treatment: Current Perspectives. SAGE Open Medicine [Internet]. 2021 Jan;9:18–21.

16. Horn L, Johnson DH. Evarts A. Graham and the First Pneumonectomy for Lung Cancer. Journal of Clinical Oncology. 2008 Jul 1;26(19):3268–75.

17. Arruebo M, Vilaboa N, Sáez-Gutierrez B, Lambea J, Tres A, Valladares M, et al. Assessment of the Evolution of Cancer Treatment Therapies. Cancers. 2011 Aug 12;3(3):3279–330.

18. Jaklitsch MT, Strauss GM, Healey EA, DeCamp MM, Liptay MJ, Sugarbaker DJ. An historical perspective of multi-modality treatment for resectable non-small cell lung cancer. Lung Cancer 1995; Suppl 2:S17-3

19. Hruba L, Das V, Hajduch M, Dzubak P. Nucleoside-based anticancer drugs: Mechanism of action and drug resistance. Biochemical Pharmacology. 2023 Sep 1;215:24.

20. Nussbaumer S, Bonnabry P, Veuthey JL, Fleury-Souverain S. Analysis of anticancer drugs: A review. Talanta. 2011 Oct 15;85(5):2265–89.

21. National Cancer Institute. Milestones in Cancer Research and Discovery [Internet]. National Cancer Institute. Cancer.gov; 2020. Available from: https://www.cancer.gov/research/progress/250-years-milestones

22. Guichard N, Guillarme D, Bonnabry P, Fleury-Souverain S. Antineoplastic drugs and their analysis: a state of the art review. The Analyst. 2017;142(13):2273–321.

23. Yin J, Yang Y, Li K, Zhang J, Shao B. Analysis of Anticancer Drugs in Sewage Water By Selective SPE and UPLC-ESI-MS-MS. Journal of Chromatographic Science. 2010 Nov 1;48(10):781–9.

24. Mandal MK, Mohammad M, Parvin SI, Islam MM, Rasid A. A Short Review on Anticancer Phytochemicals. Pharmacognosy Reviews/Bioinformatics Trends/Pharmacognosy review. 2023 Jan 5;11–23.

25. Wani MC, Taylor HL, Wall ME, Coggon P, McPhail AT. Plant antitumor agents. VI. Isolation and structure of taxol, a novel antileukemic and antitumor agent from Taxus brevifolia. Journal of the American Chemical Society. 1971 May;93(9):2325–7

26. Noble RL. The discovery of the vinca alkaloids—chemotherapeutic agents against cancer. Biochemistry and Cell Biology. 1990 Dec 1;68(12):1344–51.

27. Cragg GM, Newman DJ. Natural products: A continuing source of novel drug leads. Biochimica et Biophysica Acta (BBA) - General Subjects. 2013 Jun;1830(6):3670–95.

28. Todorov L, Kostova I. Recent Trends in the Development of Novel Metal-Based Antineoplastic Drugs. Molecules. 2023 Feb 18;28(4):1959.

29. Van Der Zanden SY, Qiao X, Neefjes J. New insights into the activities and toxicities of the old anticancer drug doxorubicin. The FEBS Journal. 2020 Oct 19;288(21):6095–111.

30. Kciuk M, Gielecińska A, Mujwar S, Kołat D, Kałuzińska Ż, Celik I, et al. Doxorubicin—An agent with multiple mechanisms of anticancer activity. Cells. 2023 Feb 19;12(4):659–9.

31. İnce E, Orhan HG. Estrogen-Induced Breast Cancer, Therapeutical Approaches and the Role of Melatonin in Treatment. HUJPHARM. 2019;39(2):113-28.

32. Hippokratis Kiaris, Ioulia Chatzistamou. Inhibition of tumor growth by agonists of growth hormone-releasing hormone. Proceedings of the National Academy of Sciences. 2018 Nov 7;115(47):11876–8.

33. Kim JG, Park MT, Heo K, Yang KM, Yi J. Epigenetics Meets Radiation Biology as a New Approach in Cancer Treatment. International Journal of Molecular Sciences. 2013 Jul 18;14(7):15059–73.

34. History.com Editors. German scientist discovers X-rays | November 8, 1895 | History [Internet]. History. 2009 [cited 2025 May 5]. Available from: https://www.history.com/this-day-in-history/november-8/german-scientist-discovers-x-rays?

35. Liu Y, Zheng C, Huang Y, He M, Xu WW, Li B. Molecular mechanisms of chemo- and radiotherapy resistance and the potential implications for cancer treatment. MedComm. 2021 Jun 10;2(3):315–40.

36. Koçak Uzel E. Radiotherapy in lung cancer: Current and future role. Şişli Etfal Hastanesi Tip Bulteni / The Medical Bulletin of Sisli Hospital. 2019;

37. Nakayama DK. Antisepsis and Asepsis and how They Shaped Modern Surgery. The American Surgeon. 2018 Jun;84(6):766–71.

38. Berardi R, Morgese F, Rinaldi S, Torniai M, Mentrasti G, Scortichini L, et al. Benefits and limitations of a multidisciplinary approach in cancer patient management. Cancer Management and Research. 2020 Sep;Volume 12:9363–74.

39. Montagne F, Guisier F, Venissac N, Baste JM. The Role of Surgery in Lung Cancer Treatment: Present Indications and Future Perspectives—State of the Art. Cancers. 2021 Jul 23;13(15):3711.

40. Jocham HR, Dassen T, Widdershoven G, Halfens R. Quality of life in palliative care cancer patients: a literature review. Journal of Clinical Nursing. 2006 Sep;15(9):1188–95.

41. Haun MW, Estel S, Rücker G, Friederich HC, Villalobos M, Thomas M, et al. Early palliative care for adults with advanced cancer. Cochrane Database of Systematic Reviews. 2017 Jun 12;6(6).

42. Huang M, Shen A, Ding J, Geng M. Molecularly targeted cancer therapy: some lessons from the past decade. Trends in Pharmacological Sciences. 2014 Jan 1;35(1):41–50.

43. Reynolds S. Alectinib Approved as an Adjuvant Treatment for Lung Cancer [Internet]. NIH (US NATIONAL CANCER INSTITUTE); 2024 [cited 2025 May 5]. Available from: https://www.cancer.gov/news-events/cancer-currents-blog/2024/fda-alectinib-lung-cancer-alk-positive

44. Ke X, Shen L. Molecular targeted therapy of cancer: The progress and future prospect. Frontiers in Laboratory Medicine. 2017;1(2):69-75.

45. Swayden M, Chhouri H, Anouar Y, Grumolato L. Tolerant/Persister Cancer Cells and the Path to Resistance to Targeted Therapy. Cells. 2020 Dec 4;9(12):2601.

46. Min HY, Lee HY. Molecular targeted therapy for anticancer treatment. Experimental & Molecular Medicine. 2022 Oct 12;54(10):1670–94.

47. Saxton RA, Sabatini DM. mTOR Signaling in Growth, Metabolism, and Disease. Cell. 2017 Mar;168(6):960–76.

48. Dann SG, Selvaraj A, Thomas G. mTOR Complex1–S6K1 signaling: at the crossroads of obesity, diabetes and cancer. Trends in Molecular Medicine. 2007 Jun;13(6):252–9.

49. Delgado A, Enkemann S. Three Layers of Personalized Medicine in the Use of Sirolimus and Its Derivatives for the Treatment of Cancer. Journal of personalized medicine. 2023 Apr 27;13(5):745–5.

50. Dancey JE. Inhibitors of the mammalian target of rapamycin. Expert Opinion on Investigational Drugs. 2005 Mar;14(3):313–28.

51. Conciatori F, Ciuffreda L, Bazzichetto C, Falcone I, Pilotto S, Bria E, et al. mTOR Cross-Talk in Cancer and Potential for Combination Therapy. Cancers. 2018 Jan 19;10(1):23.

52. Kirchner GI, Meier-Wiedenbach I, Manns MP. Clinical Pharmacokinetics of Everolimus. Clinical Pharmacokinetics. 2004;43(2):83–95.

53. Fingar DC, Blenis J. Target of rapamycin (TOR): an integrator of nutrient and growth factor signals and coordinator of cell growth and cell cycle progression. Oncogene. 2004 Apr;23(18):3151–71.

54. Houghton PJ. Everolimus. Clinical Cancer Research: An Official Journal of the American Association for Cancer Research. 2010 Mar 1;16(5):1368–72.

55. Kurdi A, De Doncker M, Leloup A, Neels H, Timmermans JP, Lemmens K, et al. Continuous administration of the mTORC1 inhibitor everolimus induces tolerance and decreases autophagy in mice. British Journal of Pharmacology. 2016 Oct 23;173(23):3359–71.

56. Kovarik JM. Everolimus: A proliferation signal inhibitor targeting primary causes of allograft dysfunction. Drugs of today. 2004 Jan 1;40(2):101–1.

57. Jang SW, Kang MJ. Improved oral absorption and chemical stability of everolimus via preparation of solid dispersion using solvent wetting technique. International Journal of Pharmaceutics. 2014 Oct;473(1-2):187–93.

58. Arena C, Maria Eleonora Bizzoca, Carlo V, Troiano G, Khrystyna Zhurakivska, Leuci S, et al. Everolimus therapy and side-effects: A systematic review and meta-analysis. International Journal of Oncology. 2021 Jun 15;59(1).

59. Everolimus (Afinitor) [Internet]. U.S. Food and Drug Administration. 2016 [cited 2025 May 5]. Available from: https://www.fda.gov/drugs/resources-information-approved-drugs/everolimus-afinitor?

60. D'Angelo SP, Janjigian YY, Ahye N, Riely GJ, Chaft JE, Sima CS, et al. Distinct Clinical Course of EGFR -Mutant Resected Lung Cancers: Results of Testing of 1118 Surgical Specimens and Effects of Adjuvant Gefitinib and Erlotinib. Journal of Thoracic Oncology. 2012 Dec;7(12):1815–22.

61. Wicki A, Witzigmann D, Balasubramanian V, Huwyler J. Nanomedicine in cancer therapy: Challenges, opportunities, and clinical applications. Journal of Controlled Release. 2015 Feb;200:138–57.

62. Buzea C, Pacheco I. Nanomaterials and their Classification. Advanced Structured Materials. 2016 Nov 10;3–45

63. Sahoo SK, Parveen S, Panda JJ. The present and future of nanotechnology in human health care. Nanomedicine: Nanotechnology, Biology and Medicine. 2007 Mar;3(1):20–31.

64. Parveen S, Misra R, Sahoo SK. Nanoparticles: a boon to drug delivery, therapeutics, diagnostics and imaging. Nanomedicine: Nanotechnology, Biology and Medicine. 2012 Feb;8(2):147–66.

65. Sezgin Z, Yüksel N, Baykara T. Preparatıon And Characterızatıon of Polymerıc Micelles As Drug Delıvery Systems. Ankara Universitesi Faculty Of Pharmacy Journal. 1974;125–42.

66. Chenthamara D, Subramaniam S, Ramakrishnan SG, Krishnaswamy S, Essa MM, Lin FH, et al. Therapeutic efficacy of nanoparticles and routes of administration. Biomaterials Research. 2019 Nov 21;23(1).

67. Jin Z, Lv Y, Cao H, Yao J, Zhou J, He W, et al. Core-shell nanocarriers with high paclitaxel loading for passive and active targeting. Scientific Reports. 2016 Jun;6(1).

68. Barenholz Y (Chezy). Doxil® — The first FDA-approved nano-drug: Lessons learned. Journal of Controlled Release. 2012 Jun;160(2):117–34.

69. Gabizon AA, Gabizon-Peretz S, Shadan Modaresahmadi, La-Beck NM. Thirty years from FDA approval of pegylated liposomal doxorubicin (Doxil/Caelyx): an updated analysis and future perspective. BMJ Oncology. 2025 Jan 1;4(1):e000573–3.

70. Jia Y, Jiang Y, He Y, Zhang W, Zou J, Magar KT, et al. Approved Nanomedicine against Diseases. Pharmaceutics. 2023 Feb 26;15(3):774**.**

71. Figueiras A, Domingues C, Jarak I, Santos AI, Parra A, Pais A, et al. New Advances in Biomedical Application of Polymeric Micelles. Pharmaceutics. 2022 Aug 15;14(8):1700.

72. Siyawamwaya M, du Toit LC, Kumar P, Choonara YE, Kondiah PPPD, Pillay V. 3D printed, controlled release, tritherapeutic tablet matrix for advanced anti-HIV-1 drug delivery. European Journal of Pharmaceutics and Biopharmaceutics. 2019 May 1;138:99–110.

73. Ugwoke M, Agu R, Verbeke N, Kinget R. Nasal mucoadhesive drug delivery: Background, applications, trends and future perspectives. Advanced Drug Delivery Reviews. 2005 Nov 3;57(11):1640–65.

74. Wang Y, Zhang H, Xiao W, Liu Y, Zhou Y, He X, et al. Unmasking CSF protein corona: Effect on targeting capacity of nanoparticles. Journal of Controlled Release. 2021 Apr 3;333:352–61.

75. Yunus M. An Insight into Polymeric Micelles Preparation Methods and Applications as Drug Delivery Approach: A Review. International Journal of Pharmaceutical Investigation. 2025 Apr 21;15(3):849–57.

76. Rey-Rico A, Cucchiarini M. PEO-PPO-PEO Tri-Block Copolymers for Gene Delivery Applications in Human Regenerative Medicine—An Overview. International Journal of Molecular Sciences. 2018 Mar 8;19(3):775.

77. Kulkarni RV, Inamdar SZ, Das KK, Biradar MS. Polysaccharide-based stimuli-sensitive graft copolymers for drug delivery. Polysaccharide Carriers for Drug Delivery. 2019 Jan 1;155–77.

78. Lund R, Willner L, Monkenbusch M, Panine P, Narayanan T, Colmenero J, et al. Structural Observation and Kinetic Pathway in the Formation of Polymeric Micelles. Physical Review Letters. 2009 May 5;102(18).

79. Brackman J, Engberts J. Polymer–micelle interactions: physical organic aspects. Chemical Society Reviews. 1993 Jan 1;22(2):85–92.

80. Ricceri R, Vila Romeu N, Taddei G. van der Waals Interactions in Nonionic Micelles. Langmuir. 1996 Jan;12(4):913–5.

81. Tanaka K, Kanazawa T, Ogawa T, Takashima Y, Fukuda T, Okada H. Disulfide crosslinked stearoyl carrier peptides containing arginine and histidine enhance siRNA uptake and gene silencing. International Journal of Pharmaceutics. 2010 Aug 3;398(1-2):219–24.

82. Onori G, Santucci A. Effect of temperature and solvent on the critical micelle concentration of sodium dodecylsulfate. Chemical Physics Letters. 1992 Feb;189(6):598–602.

83. Lu Y, Yue Z, Xie J, Wang W, Zhu H, Zhang E, et al. Micelles with ultralow critical micelle concentration as carriers for drug delivery. Nature Biomedical Engineering. 2018 May;2(5):318–25.

84. Aguiar J, Carpena P, Molina-BolívarJA, Carnero Ruiz C. On the determination of the critical micelle concentration by the pyrene 1:3 ratio method. Journal of Colloid and Interface Science. 2003 Feb 1;258(1):116–22.

85. Mohsen Ashjari, Sepideh Khoee, Mahdavian AR, Reza Rahmatolahzadeh. Self-assembled nanomicelles using PLGA–PEG amphiphilic block copolymer for insulin delivery: a physicochemical investigation and determination of CMC values. Journal of Materials Science Materials in Medicine. 2012 Feb 21;23(4):943–53.

86. Jamal A, Ali MI, Badshah M, Masood AB. Role of Biosurfactants in Agriculture Management. Springer eBooks. 2023 Jan 1;277–308.

87. Zhang YB, Xu D, Bai L, Zhou YM, Zhang H, Cui YL. A Review of Non-Invasive Drug Delivery through Respiratory Routes. Pharmaceutics. 2022 Sep 19;14(9):1974.

88. Cazzola M, Cavalli F, Usmani OS, Rogliani P. Advances in pulmonary drug delivery devices for the treatment of chronic obstructive pulmonary disease. Expert Opinion on Drug Delivery. 2020 Mar 16;17(5):635–46.

89. Pramanik S, Mohanto S, Manne R, Rajendran RR, Deepak A, Edapully SJ, et al. Nanoparticle-Based Drug Delivery System: The Magic Bullet for the Treatment of Chronic Pulmonary Diseases. Molecular Pharmaceutics. 2021 Sep 7;18(10):3671–718.

90. Siafaka PI, Özcan Bülbül E, Miliotou AN, Karantas ID, Okur ME, Üstündağ Okur N. Nano-based carriers for pulmonary drug delivery: A review on the available drug delivery

applications and toxicity issues. Journal of Drug Delivery Science and Technology. 2024 Feb 1;92:105381.

91. Newman SP. Drug delivery to the lungs: challenges and opportunities. Therapeutic Delivery. 2017 Jul;8(8):647–61.

92. Rathod HKK, A.Katekar V, Dhole YR, Nalinde PS, Rathod HKK, A.Katekar V, et al. Pulmonary drug delivery system: A review. GSC Biological and Pharmaceutical Sciences. 2023;25(3):149–58.

93. Maricoto T, Correia-de-Sousa J, Taborda-Barata L. Inhaler Technique Education in Elderly Patients with Asthma or COPD: Impact on Disease Exacerbations—a Protocol for a single-blinded Randomised Controlled Trial. BMJ Open. 2019 Jan;9(1):e022685.

94. Plaunt AJ, Nguyen TL, Corboz MR, Malinin VS, Cipolla DC. Strategies to Overcome Biological Barriers Associated with Pulmonary Drug Delivery. Pharmaceutics. 2022 Jan 27;14(2):302.

95. de Souza Carvalho C, Daum N, Lehr CM. Carrier interactions with the biological barriers of the lung: Advanced in vitro models and challenges for pulmonary drug delivery. Advanced Drug Delivery Reviews. 2014 Aug;75:129–40.

96. Shackleford DM, Jamsen KM. Quantifying Uncertainty in the Ratio of Two Measured Variables: A Recap and Example. Journal of Pharmaceutical Sciences. 2016 Sep 16;105(11):3462–3.

97. Francisco A, Rombolá CA, Atance PL. Aspectos técnicos del abordaje anterior transmanubrial en la cirugía de los tumores del estrecho torácico. Archivos de Bronconeumología. 2012 Jun 13;48(11):419–22.

98. Corrigan DO, Healy AM, Corrigan OI. The effect of spray drying solutions of polyethylene glycol (PEG) and lactose/PEG on their physicochemical properties. International Journal of Pharmaceutics. 2002 Mar;235(1-2):193–205.

99. Rahman M, Zhao M, Islam MS, Dong K, Saha SC. Aerosol Particle Transport and Deposition in Upper and Lower Airways of Infant, Child and Adult Human Lungs. Atmosphere. 2021 Oct 26;12(11):1402.

100. Abdelbary Elhissi, Elkhalifa D, Khan I, Ahmed W. Introduction: Pulmonary Drug Delivery and Inhalation Devices. Synthesis lectures on biomedical engineering. 2025 Jan 1;1–34.

101. Stein SW, Thiel CG. The History of Therapeutic Aerosols: A Chronological Review. Journal of Aerosol Medicine and Pulmonary Drug Delivery. 2017 Feb;30(1):20–41.

102. O'riordan TG, Greco MJ, Perry RJ, Smaldone GC. Nebulizer Function during Mechanical Ventilation. American Review of Respiratory Disease. 1992 May;145(5):1117–22.

103. Bhatt E, Malkin R. Errors in Metered Dose Inhaler Use Amongst Pediatric Asthma Patients. Journal of Asthma and Allergy. 2023 Nov 1;Volume 16:1259–65.

104. McCarthy SD, González HE, Higgins BD. Future Trends in Nebulized Therapies for Pulmonary Disease. Journal of Personalized Medicine. 2020 May 10;10(2):37.

105. Rahimpour Y, Hamishehkar H. Lactose engineering for better performance in dry powder inhalers. Advanced pharmaceutical bulletin. 2012;2(2):183–7.

106. Magramane S, Vlahović K, Gordon P, Kállai-Szabó N, Zelkó R, Antal I, et al. Inhalation Dosage Forms: A Focus on Dry Powder Inhalers and Their Advancements. Pharmaceuticals. 2023 Nov 28;16(12):1658.

107. Akdağ Çaylı Y, Şahin S, Öner L. Dry Powder Inhalers: Formulations and Aerodynamic Behaviours. HUJPHARM. 2018;38(1):39-52.

108. Price D, Summers M, Zanen P. Could interchangeable use of dry powder inhalers affect patients? International Journal of Clinical Practice. 2005 Nov 8;59:3–6.

109. Bale S, Khurana A, Reddy ASS, Singh M, Godugu C. Overview on Therapeutic Applications of Microparticulate Drug Delivery Systems. Critical Reviews™ in Therapeutic Drug Carrier Systems. 2016;33(4):309–61.

110. Lengyel M, Kállai-Szabó N, Antal V, Laki AJ, Antal I. Microparticles, Microspheres, and Microcapsules for Advanced Drug Delivery. Scientia Pharmaceutica. 2019 Aug 9;87(3):20.

111. Verma D, Bhatia A, Chopra S, Dua K, Parteek Prasher, Gupta G, et al. Advancements on microparticles-based drug delivery systems for cancer therapy. Elsevier eBooks. 2021 Jan 1;351–8.

112. Vinayak A. Katekar, Prafful P. Kothari, Aarti A. Nahar, Pooja A. Salve, Harsha H. Shendurkar, Shruti A. Adhau. A review on recent advantages and evaluation of microparticles and their applications. GSC Biological and Pharmaceutical Sciences. 2023 Aug 30;24(2):297–**307.**

113. Cook RO, Pannu RK, Kellaway IW. Novel sustained release microspheres for pulmonary drug delivery. Journal of Controlled Release. 2005 May;104(1):79–90.

114. Huang YC, Vieira A, Huang KL, Yeh MK, Chiang CH. Pulmonary inflammation caused by chitosan microparticles. Journal of Biomedical Materials Research Part A. 2005;75A(2):283–7.

115. Kumar M, Hilles AR, Almurisi SH, Bhatia A, Mahmood S. Micro and nano-carriers-based pulmonary drug delivery system: Their current updates, challenges, and limitations – A review. JCIS Open. 2023 Dec 1;12:100095.

116. Hasanain F, Guenther K, Mullett WM, Craven E. Gamma sterilization of pharmaceuticals--a review of the irradiation of excipients, active pharmaceutical ingredients, and final drug product formulations. PDA journal of pharmaceutical science and technology. 2014 Mar 1;68(2):113–37.

117. Sinha VR, Bansal K, Kaushik R, Kumria R, Trehan A. Poly-epsilon-caprolactone microspheres and nanospheres: an overview. International Journal of Pharmaceutics. 2004 Jun 18;278(1):1–23.

118. Park C, Lee C, Kwon O. Conducting Polymer Based Nanobiosensors. Polymers. 2016 Jun 30;8(7):249.

119. Saini L, Dubey A, Pal R, Pandey P, Mandal RK. Synthetic and Natural Polymers Enhancing Drug Delivery and Their Treatment: A Comprehensive Review. Journal of Drug Delivery and Therapeutics. 2024 Oct 15;14(10):153–65.

120. Satchanska G, Slavena Davidova, Petrov PD. Natural and Synthetic Polymers for Biomedical and Environmental Applications. Polymers. 2024 Apr 20;16(8):1159–9.

121. Díaz-Montes E. Polysaccharides: Sources, Characteristics, Properties, and Their Application in Biodegradable Films. Polysaccharides. 2022 Jun 27;3(3):480–501.

122. Kumar R, Sharma R, Singh A. Grafted cellulose: a bio-based polymer for durable applications. 2018 May 1;75(5):2213–42.

123. Lin Q, Gao M, Chang J, Ma H. Adsorption properties of crosslinking carboxymethyl cellulose grafting dimethyldiallylammonium chloride for cationic and anionic dyes. Carbohydrate Polymers. 2016 Oct;151:283–94.

124. Kenji Kamide. Cellulose and Cellulose Derivatives. Elsevier; 2005.

125. Bourges X, Weiss P, Daculsi G, Legeay G. Synthesis and general properties of silated-hydroxypropyl methylcellulose in prospect of biomedical use. Advances in Colloid and Interface Science. 2002 Dec 4;99(3):215–28.

126. Zarei Z, Kharaziha M, Karimzadeh F, Khadem E. Synthesis and biological applications of nanocomposite hydrogels based on the methacrylation of hydroxypropyl methylcellulose and lignin loaded with alpha-pinene. Carbohydrate Polymers. 2024 Dec;346:122642.

127. Kenji Kamide. Cellulose and Cellulose Derivatives. 1st Edition. Amsterdam: Elsevier Science; 2005:78-110

128. Dalmoro A, Sitenkov AY, Cascone S, Lamberti G, Barba AA, Moustafine RI. Hydrophilic drug encapsulation in shell-core microcarriers by two stage polyelectrolyte complexation method. International Journal of Pharmaceutics. 2016 Dec 26;518(1-2):50–8.

129. Gustafsson C, Nyström C, Lennholm H, Bonferoni MC, Caramella CM. Characteristics of Hydroxypropyl Methylcellulose Influencing Compactibility and Prediction of Particle and Tablet Properties by Infrared Spectroscopy. Journal of Pharmaceutical Sciences. 2003 Mar;92(3):494–504.

130. Li J, Wang Q, Xia G, Adilijiang N, Li Y, Hou Z, et al. Recent Advances in Targeted Drug Delivery Strategy for Enhancing Oncotherapy. Pharmaceutics. 2023 Sep 1;15(9):2233.

131. Zein R, Sharrouf W, Selting K. Physical Properties of Nanoparticles That Result in Improved Cancer Targeting. Journal of Oncology. 2020 Jul 13;2020:1–16.

132. Yhee JY, Son S, Son S, Joo MK, Kwon IC. The EPR Effect in Cancer Therapy. Cancer Targeted Drug Delivery. 2013;621–32.

133. Wu X, Chen J, Wu M, Zhao JX. Aptamers: Active Targeting Ligands for Cancer Diagnosis and Therapy. Theranostics. 2015;5(4):322–44.

134. Sun R, Xiang J, Zhou Q, Piao Y, Tang J, Shao S, et al. The tumor EPR effect for cancer drug delivery: Current status, limitations, and alternatives. Advanced Drug Delivery Reviews. 2022 Dec;191:114614.

135. Bandyopadhyay A, Das T, Nandy S, Synudeen Sahib, Subham Preetam, Abilash Valsala Gopalakrishnan, et al. Ligand-based active targeting strategies for cancer theranostics. Naunyn-Schmiedeberg's Archives of Pharmacology. 2023 Jul 19;396(12):3417–41.

136. Greenwald RB, Choe YH, McGuire J, Conover CD. Effective drug delivery by PEGylated drug conjugates. Advanced Drug Delivery Reviews. 2003 Feb;55(2):217–50.

137. Pearce AK, O'Reilly RK. Insights into Active Targeting of Nanoparticles in Drug Delivery: Advances in Clinical Studies and Design Considerations for Cancer Nanomedicine. Bioconjugate Chemistry. 2019 Aug 23;30(9):2300–11.

138. Sung Y, Choi Y, Kim ES, Ryu JH, Kwon IC. Receptor-ligand interactions for optimized endocytosis in targeted therapies. Journal of Controlled Release. 2025 Apr;380:524–38.

139. Pierschbacher MD, Ruoslahti E. Cell attachment activity of fibronectin can be duplicated by small synthetic fragments of the molecule. Nature. 1984 May;309(5963):30–3.

140. Stokes JM, Yang K, Swanson K, Jin W, Cubillos-Ruiz A, Donghia NM, et al. A deep learning Approach to Antibiotic Discovery. Cell. 2020 Feb 20;180(4):688–702.

141. Wu X, Chen J, Wu M, Zhao JX. Aptamers: Active Targeting Ligands for Cancer Diagnosis and Therapy. Theranostics. 2015;5(4):322–44.

142. Cheng X, Li C, Hong H, Zhou Z, Wu Z. Macrocyclic RGD-Peptides with High Selectivity for αvβ3 Integrin in Cancer Imaging and Therapy. RSC Medicinal Chemistry. 2025 Jan 1;

143. Cossu J, Thoreau F, Boturyn D. Multimeric RGD-Based Strategies for Selective Drug Delivery to Tumor Tissues. Pharmaceutics. 2023 Feb 4;15(2):525**.**

144. Majumdar S, Siahaan TJ. Peptide-mediated targeted drug delivery. Medicinal Research Reviews. 2010 Sep 2;32(3):637–58**.**

145. Yin L, Li X, Wang R, Zeng Y, Zeng Z, Xie T. Recent Research Progress of RGD Peptide–Modified Nanodrug Delivery Systems in Tumor Therapy. International Journal of Peptide Research and Therapeutics. 2023 May 16;29(4).

146. Hutanu D. Recent Applications of Polyethylene Glycols (PEGs) and PEG Derivatives. Modern Chemistry & Applications. 2014;02(02).

147. Zbicinski I, Ciesielski K, Ge B. Mechanism of Particle Agglomeration for Single and Multi-Nozzle Atomization in Spray Drying: A Review. Processes. 2022 Apr 9;10(4):727.

148. Boel E, Koekoekx R, Dedroog S, Babkin I, Vetrano MR, Clasen C, et al. Unraveling Particle Formation: From Single Droplet Drying to Spray Drying and Electrospraying. Pharmaceutics. 2020 Jul 4;12(7):625.

149. Zhou H, Pujales-Paradela R, Groppe P, Wintzheimer S, Mandel K. Tuning the Morphology of Spray-Dried Supraparticles: Effects of Building Block Size and Concentration. Particle & Particle Systems Characterization. 2022 Sep 12;39(11).

150. Khokhlova S, Burshtein AI. Screening of contact absorption by distant energy quenching. Chemical Physics. 2010 Aug 7;376(1-3):69–75.

151. BÜCHI Labortechnik AG. B-290 Mini Spray Dryer Operation Manual. Flawil, Switzerland: BÜCHI Labortechnik AG; 2018 Mar. p.49.

152. Vickovic D, Tomasz Pawel Czaja, Gaiani C, Søren Juhl Pedersen, Ahrné L, Anni Bygvrå Hougaard. The effect of feed formulation on surface composition of powders and wall deposition during spray drying of acidified dairy products. Powder Technology. 2023 Jan 31;418:118297–7.

153. Rao KK. Statics and Kinematics of Granular Materials. By R. M. Nedderman. Cambridge University Press, 1992. 352 pp. £50. Journal of Fluid Mechanics. 1995;286:405–405.

154. Hao T. Understanding empirical powder flowability criteria scaled by Hausner ratio or Carr index with the analogous viscosity concept. RSC Advances. 2015;5(70):57212–5.

155. Sigma-Aldrich. Pluronic® F-127 [Internet]. Product No: P2443 St. Louis (MO): Merck KGaA ;[cited 2025 27] Available from: https://www.sigmaaldrich.com/TR/en/product/sigma/p2443

156. Mariano, Gramosa NV, Ricardo, Morris GA, Adams RW, Nilsson M. Natural product mixture analysis by matrix-assisted DOSY using Brij surfactants in mixed solvents. RSC Advances. 2014 Jan 1;4(79):42029–34**.**

157. Gattefossé. Gelucire® 48/16 [Internet]. Lyon (France): Gattefossé; [cited 2025 May 27]. Available from: https://www.gattefosse.com/pharmaceuticals/product-finder/gelucire-4816

8.CURRICULUM VITAE

Personal Information

Name		**Surname**	
Place of Birth		**Date of Birth**	
Nationality		**Phone**	
E-mail			

Education

	Institution Name	**Graduation Year**
Doctor of Philosophy		
Master of Science		
Undergraduate		
High School		

Work Experience

Position	**Corporation**	**Duration**
1.		
2.		
3.		

Language	**Reading***	**Speaking***	**Writing***

*Evaluated as advenced, good, intermediate, beginner

Foreign Language Exam Results #

KPDS	ÜDS	IELTS	TOEFL IBT	TOEFL PBT	TOEFL CBT	FCE	CAE	CPE	OTHER

All Successful exams should be enrolled.

KPDS: Kamu Personeli Yabancı Dil Sınavı; ÜDS: Üniversitelerarası Kurul Yabancı Dil Sınavı; IELTS: International English Language Testing System; TOEFL IBT: Test of English as a Foreign Language-Internet-Based Test TOEFL PBT: Test of English as a Foreign Language-Paper-Based Test; TOEFL CBT: Test of English as a Foreign Language-Computer-Based Test; FCE: First Certificate in English; CAE: Certificate in Advanced English; CPE: Certificate of Proficiency in English

	Quantitative	Equally Weighted	Verbal
ALES Score			
(Other) Score			

Computer Skills

Program	*Ability to Use

*Evaluated as advenced, good, intermediate, beginner

National and International Publications/Posters/Certificates/Prizes/Others